ASE-2736

ERRATA SHEET

Contract NASW-2070 - Cover Page

FINAL DATA REDUCTION
AND ANALYSIS OF
THE AS&E OSO-IV
GRAZING INCIDENCE X-RAY
TELESCOPE EXPERIMENT

Change "Interim Report" to FINAL REPORT

No other changes on this Cover Page

ERRATA SHEET

Contract NASW-2070 - Title Page

FINAL DATA REDUCTION
AND ANALYSIS OF
THE AS&E OSO-IV
GRAZING INCIDENCE X-RAY
TELESCOPE EXPERIMENT

Change "Interim Report" to FINAL REPORT

No other changes on this Title Page

ERRATA SHEET

Substitude this page for Page 1-1 in ASE-2736

1.0 INTRODUCTION

This document is the Final Report for Contract NASW-2070 to perform the final data analysis of the AS&E grazing incidence X-ray telescope experiment on the pointed section of the OSO-IV satellite. The report covers the period of performance on the contract from 22 June 1970 to 31 March 1971. Eight monthly reports have been submitted as required for the contract during this period.

The OSO-IV X-ray experiment produced raster scans of the sun in the 2.5 to 12 Å waveband with a minimum time resolution of five minutes and a minimum angular resolution of one arc-minute. The spacecraft was launched on 18 October 1967 and the experiment has operated successfully throughout its lifetime. The general scientific objectives of the AS&E X-ray telescope experiment are to study individual solar X-ray sources in several wavebands over an extended period, and to study the relationship of these sources to problems of solar physics.

The reduction and anlysis of the OSO-IV data has taken place in several phases. Prior to launch of the spacecraft, computer programs for data reduction were developed and tested. This phase covered the period 30 June 1966 to 31 March 1967, and is reported in ASE-1921, the final report for contract NAS5-3569.

The second and third phases were reported in ASE-2432, the final report for contract NAS5-11106. Post-launch data reduction commenced 19 November 1967, one month after launch of the spacecraft, and continued until 30 June 1968. Preliminary data analysis commenced during this phase. The character and quality of the scientific results to be gained from the experiment were

Note: The only changes occur in the first paragraph.

ERRATA SHEET

Substitute this page for Page 1-2 in ASE-2736

defined during this phase of the analysis and preliminary results were reported to the scientific community. The prime data reduction and analysis phase began 1 July 1968 and was completed on 28 February 1970. During this phase routine data reduction was completed for all data received in the form of computer readable experimental data and spacecraft attitude magnetic tapes (essentially the period from experiment turn-on, 25 October 1967, to spacecraft tape recorder failure, 12 May 1968). Significant events for this period were selected, and these data were analyzed in detail.

Under contract NASW-2070, AS&E is to accomplish two overall goals. The first is the completion of the routine processing of Goddard Space Flight Center (GSFC)-supplied experimental data and spacecraft aspect magnetic tapes through the first year of the satellite's lifetime. Basically this covers the period from 12 May to 14 October 1968. Secondly, AS&E is to analyze the reduced data with direction towards the solution of particular problems in solar physics, some of which have only recently been revealed. This analysis involves the study of X-ray emitting active regions and their manifestations at other wavelengths. the study of the time variations of X-ray activity, and the study of the processes of solar x-ray emission with the subsequent derivation of a model X-ray spectra for solar X-ray emitting regions.

The routine processing and much of the data analysis, including the production of isothermal model spectra, was completed under this contract. Section...

Note: The only changes occur in the last paragraph.

ERRATA SHEET

Substitute this page for Page 4-1 in ASE-2736.

4.0 CONCLUSION

The OSO-IV pointed X-ray telescope experiment continues to return data. Since the failure of the second tape recorder on OSO-IV on 12 May 1968, only data transmitted during real-time passes over the receiving stations has been available. The amount of quick-look data received from GSFC has been greatly reduced, because of the telemetry overload on the Stadan network. At the time of tape recorder failure, the detector efficiency of the OSO-IV telescope was about 30% of its value on 27 October 1967. Since then it has stabilized at somewhat less than 20% of this value.

The instrument has been operated almost entirely in its most sensitive mode (2.35 μgm/cm^2 beryllium filter; 4 arc-minute aperture) since tape recorder failure. Occasionally it is commanded into the calibration mode for reference.

Routine computer processing of the spacecraft tapes has been completed through the first year of the satellite's lifetime. All of the original tapes have been returned to GSFC.

Most of the prime data has been analyzed, the results have been presented at various scientific meetings, and two papers have been accepted for publication in scientific journals.

Note: The only changes occur in the last paragraph.

AMERICAN SCIENCE AND ENGINEERING

11 CARLETON STREET, CAMBRIDGE,
MASSACHUSETTS 02142 (617) 868-1600

1 JUNE 1971

ASE-2736

INTERIM REPORT FOR

FINAL DATA REDUCTION AND ANALYSIS OF THE AS&E OSO-IV GRAZING INCIDENCE X-RAY TELESCOPE EXPERIMENT

BY
A. KRIEGER
W. TUCKER
G. VAIANA
D. WEBB

CONTRACT NO. NASW-2070
REPORT PERIOD: 22 JUNE 1970-31 MARCH 1971

PREPARED FOR
NATIONAL AERONAUTICS
AND SPACE ADMINISTRATION
NASA HEADQUARTERS
WASHINGTON, D.C. 20546

ASE-2736

INTERIM REPORT FOR
CONTRACT NASW-2070

FINAL DATA REDUCTION AND ANALYSIS OF THE AS&E OSO-IV GRAZING INCIDENCE X-RAY TELESCOPE EXPERIMENT

Prepared by:

A. Krieger, W. Tucker, G. Vaiana, D. Webb

American Science and Engineering, Inc.
11 Carleton Street
Cambridge, Massachusetts 02142

Prepared for:

National Aeronautics and Space Administration
NASA Headquarters
Washington, D.C. 20546

Report period: 22 June 1970 - 31 March 1971

1 June 1971

Approved: _____
H. Gursky, Vice President
Space Research Division

_____
G. S. Vaiana, Director
Solar Physics Research

CONTENTS

LIST OF ILLUSTRATIONS

LIST OF TABLES

1.0 INTRODUCTION

This document is an interim report for contract NASW-2070 to perform the final data analysis of the AS&E grazing incidence X-ray telescope experiment on the pointed section of the OSO-IV satellite. The report covers the period of performance on the contract from 22 June 1970 to 1 June 1971. Eight monthly reports have been submitted as required for the contract during this period. A modification to NASW-2070 is currently being negotiated to extend the contract.

The OSO-IV X-ray experiment produced raster scans of the sun in the 2.5 to 12 Å waveband with a minimum time resolution of five minutes and a minimum angular resolution of one arc-minute. The spacecraft was launched on 18 October 1967 and the experiment has operated successfully throughout its lifetime. The general scientific objectives of the AS&E X-ray telescope experiment are to study individual solar X-ray sources in several wavebands over an extended period, and to study the relationship of these sources to problems of solar physics.

The reduction and analysis of the OSO-IV data has taken place in several phases. Prior to launch of the spacecraft, computer programs for data reduction were developed and tested. This phase covered the period 30 June 1966 to 31 March 1967, and is reported in ASE-1921, the final report for contract NAS5-3569.

The second and third phases were reported in ASE-2432, the final report for contract NAS5-11106. Post-launch data reduction commenced 19 November 1967, one month after the launch of the spacecraft, and continued until 30 June 1968. Preliminary data analysis commenced during this phase. The character and quality of the scientific results to be gained from the experiment were

defined during this phase of the analysis and preliminary results were reported to the scientific community. The prime data reduction and analysis phase began 1 July 1968 and was completed on 28 February 1970. During this phase routine data reduction was completed for all data received in the form of computer readable experimental data and spacecraft attitude magnetic tapes (essentially the period from experiment turn-on, 25 October 1967, to spacecraft tape recorder failure, 12 May 1968). Significant events for this period were selected, and these data were analyzed in detail.

Under contract NASW-2070, AS&E is to accomplish two overall goals. The first is the completion of the routine processing of Goddard Space Flight Center (GSFC)-supplied experimental data and spacecraft aspect magnetic tapes through the first year of the satellite's lifetime. Basically this covers the period from 12 May to 24 October 1968. Secondly, AS&E is to analyze the reduced data with direction towards the solution of particular problems in solar physics, some of which have only recently been revealed. This analysis involves the study of X-ray emitting active regions and their manifestations at other wavelengths, the study of the time variations of X-ray activity, and the study of the processes of solar X-ray emission with the subsequent derivation of a model X-ray spectra for solar X-ray emitting regions.

The routine processing and much of the data analysis, including the production of isothermal model spectra, has been completed. In a letter proposal, (ASE-2723) we have outlined additional work to be done under this contract. This work was suggested by the results of the model spectrum analysis and the high resolution X-ray photographs obtained by sounding rockets. This report summarizes the work completed thus far on the contract. Section

2.0 describes the routine data processing. Section 3.0 summarizes the results to date of the scientific data analysis of the contract. Appendix A contains a list of the publications generated under this contract, Appendix B and C are two papers that have been accepted for publication by technical journals, and Appendix D is a printout of three computer programs used in the data analysis.

2.0 ROUTINE DATA PROCESSING

The data analysis and reduction programs for the OSO-IV solar X-ray experiment are used at AS&E's in-house IBM System 360/40 Data Processing Facility. The program formats are mostly written in PL/1 language and may be read from PL/1, assembly language, or COBOL. Detailed descriptions and print-outs of the basic data reduction programs are contained in ASE-2432.

Data processing commenced at AS&E when compatible magnetic data and spacecraft attitude tapes were received from GSFC. The original 7-track data, or telemetry tapes, were converted to 9-track tapes called Telemetry so that they would be compatible with AS&E's computer. GSFC attitude tapes were converted to tapes called Aspect-Ephemeris. This routine tape processing has now been completed for data obtained through the first year of the satellite's lifetime (from 18 October 1967 to 24 October 1968). Table I is a list of the AS&E processed tapes with dates and times of coverage. All of the original tapes through number 155 have been returned to GSFC.

Magnetic tapes covering the period from the start time of the experiment's routine scanning, 25 October 1967, to the time of the failure of OSO-IV's second tape recorder, 12 May 1968, have been sent to the National Space Science Data Center (NSSDC) for potential use by interested members of the scientific community. These tapes consist of raw rasters and background rasters which then can be merged to produce corrected solar X-ray spectroheliograms.

TABLE I

TIME COVERAGE OF OSO-IV SOLAR X-RAY DATA

TELEMETRY TAPE NO.	ATTITUDE TAPE NO.	COVERAGE PERIOD (TIMES ARE U.T.)
		(1967)
000	100	18 - 25 October
001	101	25 October (0713) - 31 October (2155)
002	102	1 November (0021) - 7 November (1252)
003	103	7 November (1302) - 14 November (0335)
004	104	14 November (0414) - 20 November (1846)
005	105	20 November (1759) - 27 November (1120)
006	106	27 November (1135) - 4 December (0215)
007	107	4 December (0255) - 10 December (1716)
008	108	10 December (1912) - 17 December (0747)
009	109	17 December (1144) - 24 December (0013)
010	110	24 December (0138) - 30 December (1543)
		(1968)
011	111	30 December (1559) - 6 January (0708)
012	112	6 January (0723) - 12 January (2004)
013	113	13 January (0001) - 19 January (1230)
014	114	19 January (1245) - 25 January (2357)
015	115	26 January (0538) - 1 February (2002)
016	116	1 February (2018) - 8 February (0710)
017	117	8 February (1105) - 15 February (0146)
018	118	15 February (0230) - 21 February (1820)

TABLE I

TIME COVERAGE OF OSO-IV SOLAR X-RAY DATA

(Continued)

TELEMETRY TAPE NO.	ATTITUDE TAPE NO.	COVERAGE PERIOD (TIMES ARE U.T.)
019	119	21 February (1840) - 28 February (0847)
020	120	28 February (0932) - 5 March (2356)
021	121	6 March (0056) - 12 March (1152)
022	122	12 March (1515) - 19 March (0541)
023	123	19 March (0620) - 25 March (2227)
024	124	25 March (2243) - 1 April (1350)
025	125	1 April (1405) - 8 April (0230)
026	126	8 April (0626) - 14 April (1903)
027	127	14 April (1923) - 21 April (0748)
028	128	21 April (1154) - 28 April (0216)
029	129	28 April (0306) - 2 May (1939)
030	130	2 May (1929) - 12 May (2327)
031	131	13 May (1453) - 18 May (0047)
032	132	18 May (0156) - 24 May (1542)
033	133	24 May (1723) - 31 May (0522)
034	134	31 May (0838) - 6 June (2123)
035	135	7 June (0039) - 12 June (1829)
036	136	No data - bad telemetry tape
037	137	20 June (0908) - 26 June (1934)

TABLE I

TIME COVERAGE OF OSO-IV SOLAR X-RAY DATA

(Continued)

TELEMETRY TAPE NO.	ATTITUDE TAPE NO.	COVERAGE PERIOD (TIMES ARE U.T.)
038	138	26 June (2044) - 2 July (0704)
039	139	3 July (1145) - 10 July (0212)
040	140	10 July (0242) - 16 July (1742)
041	141	16 July (1913) - 23 July (0857)
042	142	23 July (0937) - 29 July (2354)
043	143	30 July (0027) - 5 August (1511)
044	144	5 August (1536) - 12 August (0452)
045	145	12 August (0730) - 18 August (2122)
046	146	No data - bad telemetry tape
047	147	25 August (1314) - 1 September (0354)
048	148	1 September (0404) - 7 September (1919)
049	149	7 September (2015) - 14 September (1007)
050	150	14 September (1138) - 21 September (0128)
051	151	21 September (0223) - 27 September (1613)
052	152	27 September (1646) - 4 October (0728)
053	153	4 October (0753) - 10 October (2248)
054	154	11 October (0018) - 17 October (1407)
055	155	17 October (1438) - 24 October (0449)

3.0 SCIENTIFIC DATA ANALYSIS

3.1 Introduction

The OSO-IV X-ray telescope experiment was the first instrument capable of identifying the sources of solar soft X-ray emission, and of monitoring individual sources for periods on the order of their lifetimes. The analysis of the OSO-IV data has followed three major lines: (1) the angular resolution characteristics of the instrument have been used to determine the spatial dimensions of X-ray emitting regions; (2) time histories of the X-ray activity of individual, selected active regions have been studied in order to determine the temporal characteristics of these regions; and (3) the data has been compared with observations made at radio and optical wavelengths. The important initial results of this analysis are included in a paper which has been accepted for publication in Solar Physics. This paper is presented in Appendix B of this report.

An important portion of the scientific analysis of the data has been a detailed study of the processes of solar X-ray emission, and the construction of a theoretical model of the X-ray spectrum of the solar corona. Model spectra for isothermal regions have been constructed. The assumptions, calculations, and results of this study are presented in a paper which has been accepted for publication by the Astrophysical Journal. This paper is included as Appendix C of this report.

The model spectrum was convolved with the spectral response characteristics of the OSO-IV telescope experiment to yield filtered model spectra. These spectra were compared with the observed OSO-IV data in an attempt to gain information about the emission characteristics of solar active regions, and to serve as

a check on the detector response of the instrument. The computer programs used in the production and interfacing of these studies are presented in the form of computer listings in Appendix D.

The results of the above activities are detailed in this section.

3.2 Cataloging of Events

During the initial period of performance of this contract, several gaps in the processed data for the interim before 12 May 1968 were filled. These gaps existed because some tapes sent to us by GSFC were unreadable and required replacement. As these gaps became filled and subsequently studied, several new X-ray events were found and added to the general catalogue of X-ray events observed by the OSO-IV telescope experiment. The general catalogue lists all statistically significant X-ray events as observed by the OSO-IV instrument through 12 May 1968. It now contains about 1000 such events.

For convenience in the analysis, we chose to divide these X-ray events arbitrarily into three classes on the basis of their durations. Events of duration less than 8 hours were termed "flares", or "impulsive events". Events of duration greater than 24 hours were called "slow variations". Events with intermediate duration were termed "long enduring brightenings". Although the bounds of these classes were established arbitrarily, it is plausible to expect that at least two, and possibly three, different physical mechanisms are involved in producing these three classes of events. In general, the time scales of flare-associated soft X-ray events are sufficiently short that such events might be regarded as the dissipation of energy "dumped" in the lower corona by some impulsive process. On the other hand, slow variations lasting several days require a more gradual energy input. The intermediate class was established to accommodate

events of duration longer than flares but short compared to the slow variations.

The following three tables are updated lists of major X-ray events of the types described above. Dates, observed times and durations, associated McMath plage numbers, and counting rates are shown for each type of event. Table II lists all well-observed X-ray "flares" with peak fluxes in the 2.5 to 12 Å waveband greater than or equal to 2.5×10^6 photons/cm^2 - sec. The peak X-ray counting rates were extrapolated from the observed time behavior of the event. The total number of observed counts in the detector passband was obtained by numerical integration of the event time profile. These latter two quantities are derived from observations made with the 2.35 μgm/cm^2 beryllium filter (2.5 - 12 Å) and the four arc-minute aperture mode, unless otherwise specified. A few other large X-ray flares are known to have occurred. However, if the observations were not sufficient to permit a detailed characterization of an event, it was not included in Table II.

Tables III and IV list major long enduring bursts and slow variations respectively for which sufficient data was obtained to permit characterizing these events in detail. The combination of satellite operations, a fluctuation toward reduced solar activity, and the gradual decline in instrumental sensitivity made these longer events more difficult to include after January 1968.

The list of active regions used for the calculation of the vertical extent of active regions was reevaluated and several new regions were added to make the list complete through 12 May 1968. All of the regions used were examined with the intent of avoiding confusion at the limb caused by closely spaced transiting regions of similar heliographic latitude. The criterion for noting when a

TABLE II

LARGE IMPULSIVE X-RAY EVENTS

DATE	McMATH PLAGE NO.	OBSERVED TIMES (U.T.) START	MAX.	END	DURATION (min.)	PEAK COUNTING RATE (cnts/140 msec) **
29 October 1967	9034	0124	0341	0417	173	7.1×10^3 *
29 October 1967 - 30 October 1967	9034	2324	2344 - 0054	0215	171	$> 3.6 \times 10^3$ *
11 November 1967	9073	<1127	1132	1454	>207	3.2×10^4
12 November 1967	9073	<1403	1408	>1544	>101	3.1×10^4
16 November 1967	9073	<2145	2206	>2226	> 41	1.3×10^5
1 December 1967	9091	<0448	0534	0805	>197	4.4×10^3 *
1 December 1967	9091	<1308	1308	1438	> 90	4.7×10^3 *
1 December 1967	9091	1449	1459	1630	101	6.1×10^4
1 December 1967	9091	<2358	2358	>0205	>127	2.9×10^4
2 December 1967	9091	0325	0330	0506	101	3.2×10^4
2 December 1967	9091	0511	0652	>0848	>217	6.5×10^4
11 December 1967	9101	2158	2219	2354	156	8.5×10^4
13 December 1967	9101	0056	0101	0306	130	2.7×10^4
16 December 1967	9118	0240	0301	>0612	>332	4.9×10^3 *
15 January 1968	9146	<2357	0007	>0053	> 56	4.3×10^4
17 January 1968	9146	0513	0523	>0539	> 26	1.2×10^5
28 January 1968	9184	<0844	0858-1045	>1115	>151	$> 4.2 \times 10^4$
10 February 1968	9204	1918	1923	>1948	> 30	3.7×10^4

* = One arc-minute aperture

** = Through 2.35 $\mu gm/cm^2$ Be filter and 4 arc-minute aperture

TABLE III

LONG ENDURING X-RAY BRIGHTENINGS

DATE	McMATH PLAGE NO.	OBSERVED TIMES (U.T.) START	MAX.	END	DURATION (hrs.)	ESTIMATED** PEAK COUNTING RATE (cnts/140 msec)	TOTAL OBSERVED† COUNTS (10^9)
29 October 1967	9034	0104	~ 0600	1806	17.1	2.75×10^3 *	2.7 - 3.7
29 October 1967- 30 October 1967	9034	1806	~ 0230	0722	13.4	1.5×10^3 *	3.3
30 October 1967- 31 October 1967	9034	1504	1948	0116	10.2	2.2×10^3 *	2.2
31 October 1967- 1 November 1967	9034	1456	1828	0026	9.5	1.5×10^3 *	2.1
10 November 1967- 11 November 1967	9073	1602	1950	0444	12.7	1.6×10^4	2.4
11 November 1967	9073	0449	1132	1458	10.15	1.05×10^4	4.05
11 November 1967	9047	$<$0825	1307	$>$1910	$>$10.75	8×10^3	3.4
11 November 1967- 12 November 1967	9047	1722	0208	0520	12.0	2.5×10^3	0.6
12 November 1967- 13 November 1967	9073	0942	1756	0149	16.1	6.3×10^3	--
26 November 1967- 27 November 1967	9082	0847	1536	$>$0558	$>$21.2	5×10^3	--
26 November 1967- 27 November 1967	9073	0658	$>$1000	$>$1000	$>$27.0	$>4.5 \times 10^3$	--
1 December 1967	9091	0207	0453	1630	14.4	1.8×10^3 *	--
8 December 1967- 9 December 1967	9115	$<$1558	0646	0907	$>$17.15	6.6×10^2	0.35

TABLE III (Continued)

DATE	McMATH PLAGE NO.	OBSERVED TIMES (U.T.) START	MAX.	END	DURATION (hrs.)	ESTIMATED** PEAK COUNTING RATE (cnts/140 msec)	TOTAL OBSERVED† COUNTS (10^9)
11 December 1967- 12 December 1967	9108	2353	0002	0906	9.2	8.3×10^3	--
13 December 1967- 14 December 1967	9115	2349	0938	2133	21.7	7.3×10^3	4.6 - 5.3
16 January 1968- 17 January 1968	9146	< 2110	~0500	0939	>12.65	6.0×10^3	--

* = One arc-minute aperture

** = Through 2.35 $\mu gm/cm^2$ Be filter and 4 arc-minute aperture

† = 2.5 - 12 Å waveband

TABLE IV

SLOW X-RAY VARIATIONS

DATE	McMATH PLAGE NO.	APPROXIMATE OBSERVED TIMES (U.T.) START	MAX.	END	DURATION (hrs.)	ESTIMATED PEAK** COUNTING RATE (cnts/140 msec)	TOTAL OBSERVED† CNTS (10^9)
28 October 1967- 1 November 1967	9034	2050	0100 (31 Oct)	0020	75	3.6×10^2 *	--
10 November 1967- 12 November 1967	9047	0000	0000 (11 Nov)	1850	66	8.1×10^3	4.6
10 November 1967- 14 November 1967	9073	1600		0800	87	--	--
14 November 1967- 15 November 1967	9073	0800		0600	22	2.5×10^3	--
15 November 1967- 16 November 1967	9073	0600		>2215	>40	--	--
14 November 1967- 16 November 1967	9062	0320		1850	61	--	--
26 November 1967- 4 December 1967	9091	0250		0850	165	--	--
8 December 1967- 10 December 1967	9110	2200	1830 (9 Dec)	>0420	>30.5	5.15×10^2	0.5
8 December 1967- 10 December 1967	9115	<1600	0910 (9 Dec)	0410	>36	8.1×10^2	2.8 - 3.6
9 December 1967- 11 December 1967	9108	0730	0000 (10 Dec)	0720	48	7.9×10^2	2.0
10 December 1967- 11 December 1967	9115	1040	0300	2020	33	6.2×10^2	2.0
11 December 1967- 12 December 1967	9108	0720	2030	1830	35	8.2×10^2	2.6

TABLE IV (Continued)

DATE	McMATH PLAGE NO.	APPROXIMATE OBSERVED TIMES (U. T.) START	MAX.	END	DURATION (hrs.)	ESTIMATED PEAK** COUNTING RATE (cnts/140 msec)	TOTAL OBSERVED † CNTS (10^9)
12 December 1967- 16 December 1967	9108	2030		> 2200	> 97	--	--
12 December 1967- 19 December 1967	9115	1830	0420 (18 Dec)	1800	168	3.4×10^2 *	5.2 - 8.2
2 January 1968- 5 January 1968	9146	2330	2040 (4 Jan)	1240	61.5	2.9×10^3	3.4
5 January 1968- 10 January 1968	9146	1240		0350	111	--	--
10 January 1968- 13 January 1968	9146	0540		0650	73	--	--
13 January 1968- 19 January 1968	9146	0650	1210 (14 Jan)	0740	145	2.6×10^3	8.75

* = One arc-minute aperture.

** = Through 2.35 μgm/cm^2 Be filter and 4 arc-minute aperture.

† = 2.5 - 12 Å waveband

region appeared on the east limb or disappeared on the west limb was made more restrictive, and the previously analyzed regions were reevaluated using this criterion.

The relationships of X-ray fluxes from active regions to the equivalent emission at other wavelengths was reexamined after the inclusion of the new OSO-IV data. Primarily this involved comparisons with data taken at the H_α line and at 9.1 cm. For instance, a detailed comparison had been made between X-ray events and H_α flares whose maxima occurred within 10 minutes of each other. Also the correspondence of solar X-radiation with the 9.1 cm peak brightness temperatures of active regions had been examined. The listings of these correlations were expanded, significantly improving the statistical validity of the results.

3.3 Model Solar X-ray Spectrum

Details of the study and construction of the solar X-ray spectrum are contained in the paper in Appendix C. Briefly, the analysis included input data typical of a high temperature, low density plasma covering the spectral range 0.5 - 70 Å and a temperature range of $6 \times 10^5 - 10^8$ °K. Twenty-three discrete temperatures were included, one for every 0.1 interval in the logarithm. Elemental abundances characteristic of either the solar corona or stellar material can be included in the program. Only solar abundances have been considered for this report.

The model spectrum included radiation contributions arising from both line emission and the continuum. The importance of line radiation to coronal X-ray emission has only recently been appreciated. Consequently a detailed study of the processes of line emission following electron collisional excitation was made, and some 459 lines were included in the model. Continuum radiation processes included were recombination, bremsstrahlung, and

two-photon decay following the excitation of the meta-stable 2S state in hydrogenic and helium-like ions. Mainly because of the large number of lines considered, this model differs from older ones both with regard to the relative importance of line versus continuum radiation, and the detailed shape of the spectrum.

The calculations producing the spectrum are made with a computer program called MKOREN, presented in Appendix D. The output of this program, which is the spectrum itself, is both printed out and deposited on a magnetic tape. The tape is then used on AS&E's Calcomp plotter to yield plots of power versus wavelength for specific temperatures. The tape is also used as input for other AS&E programs, such as OSOINT described in the next section.

Figure 3-1 shows Calcomp plots of the model spectrum for temperatures representative of the quiescent corona (1.6×10^6 ^oK) and of active regions (5×10^6 ^oK). Curves are drawn individually for the three continua processes, and for the total continuum (dotted line), with the lines shown summed over 0.2 Å wavelength intervals. Figure 3-2 shows the relative contributions of the individual processes contributing to the spectrum power integral.

3.4 OSOINT and FILGEN Computer Programs

A program called OSOINT (see Appendix D) uses as input the model spectrum as contained on the tape just described, and filter transmission data, which represent the spectral response characteristics of the OSO-IV X-ray telescope experiment. It then produces a theoretical filtered spectrum. This filtered spectrum can then be compared with the actual OSO-IV raster data to gain information about the emission characteristics of solar active regions, and to serve as a check on the detector response of the instrument.

For each temperature the OSOINT program takes 0.2 Å bins of the continuum input data, multiplies each bin by the interpolated

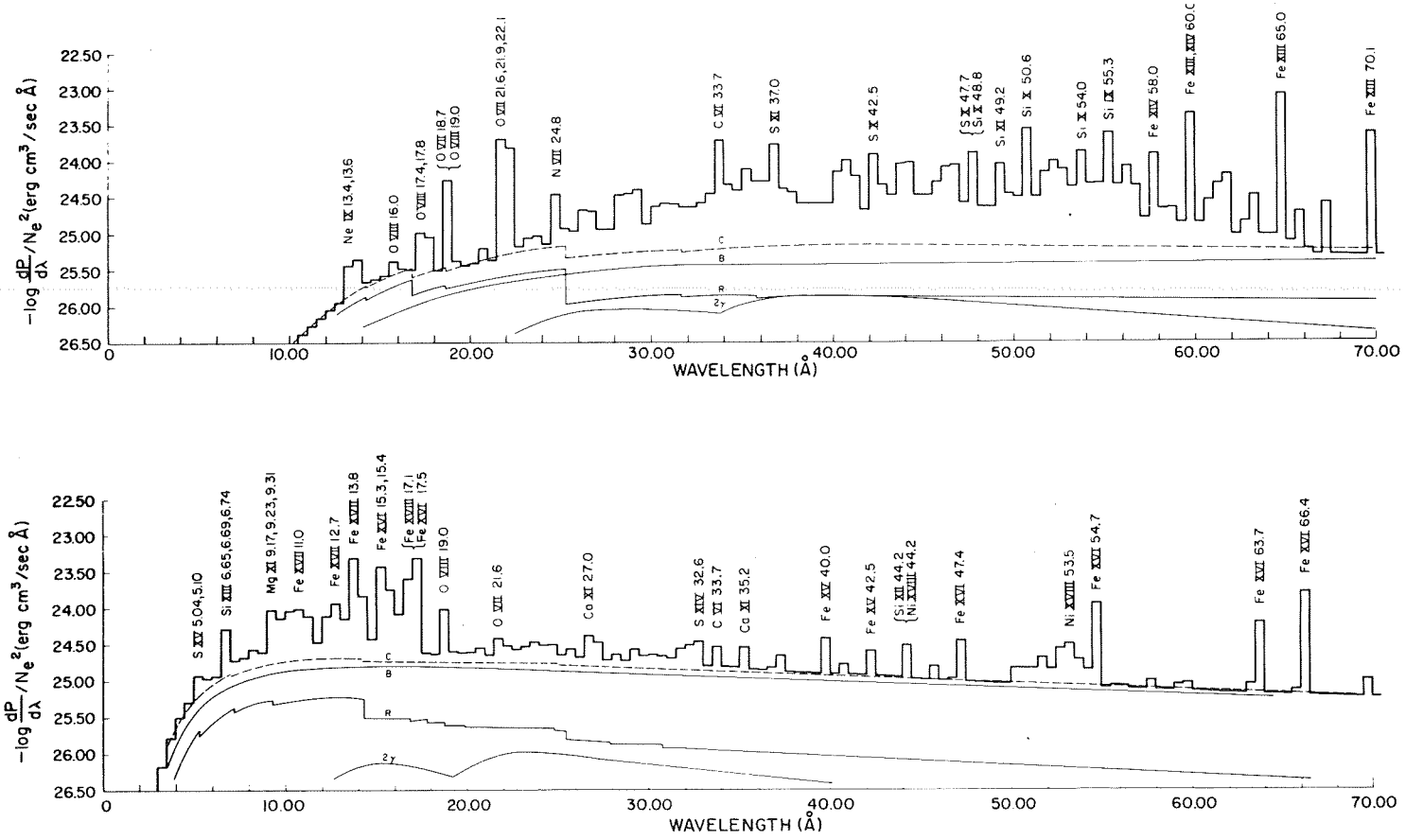

Figure 3-1 The model solar X-ray spectrum for temperatures of 1.6×10^6 °K (upper) and 5×10^6 °K (lower). These temperatures are representative of the quiescent corona and of active regions respectively. The abcissa has units of log power per unit emission measure, a form convenient for analysis.

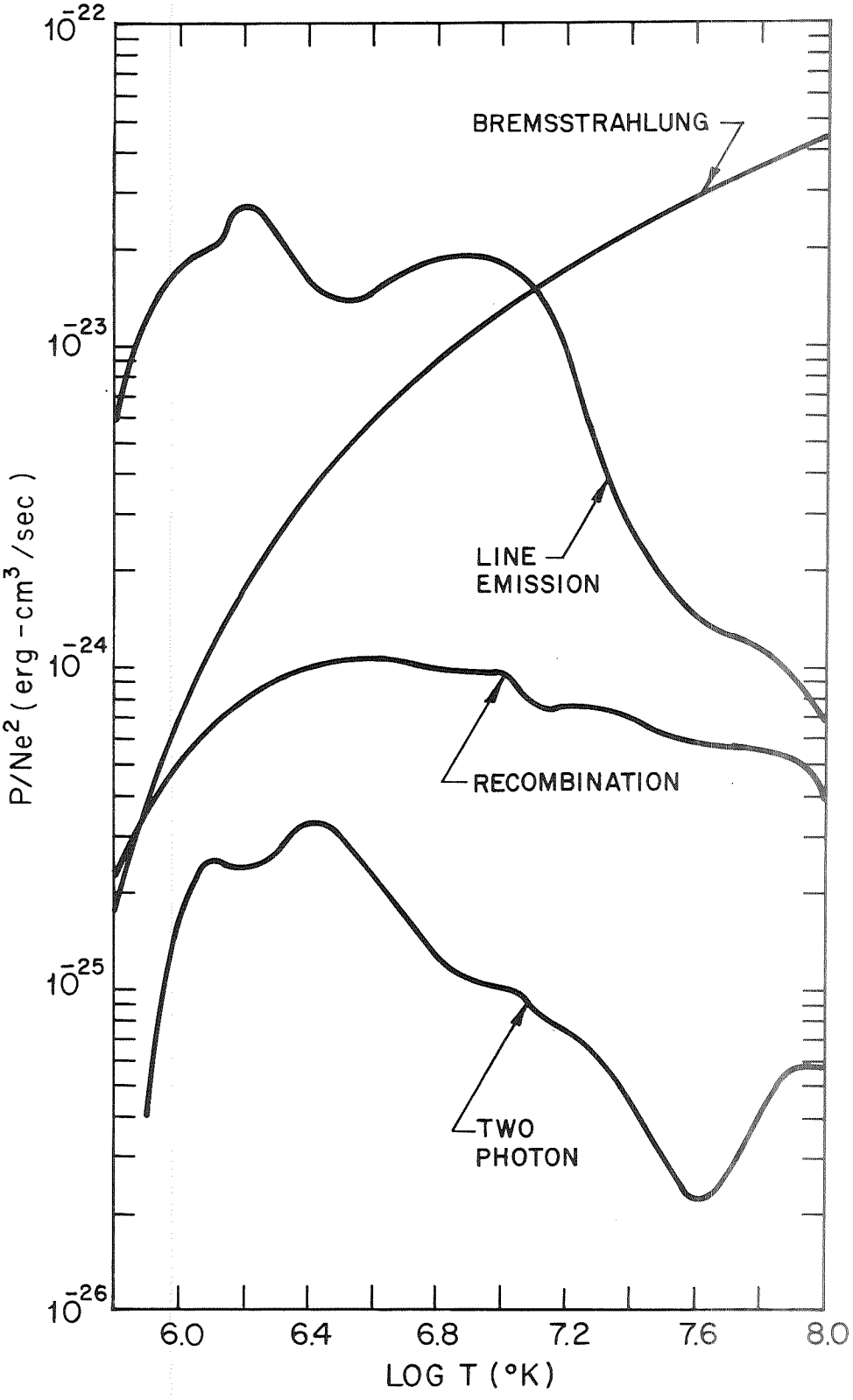

Figure 3-2 The temperature dependence of the individual processes used in the construction of the model spectrum. Note the importance of line emission to the spectrum at lower temperatures.

filter transmission at the midpoint of the bin, adds the counting rate contributed by any lines in the bin, and prints out the wavelength at the beginning of the bin and the filtered counting rate contributed by the bin. This bin counting rate is then added to a cumulative sum over the whole spectrum; the final filtered integral is printed at the end of the spectrum along with the final input integral. Absorption edges are taken into account by dividing the affected 0.2 Å bin into two smaller bins at the edge. Each smaller bin is then treated exactly like a 0.2 Å bin, then recombined as a 0.2 Å bin for printing. Any combination of filter data and temperatures (within the limits on the input tape) can be used. The OSOINT program is actually a modified version of a program called TEMPINT. The essential difference between the two programs is that OSOINT converts the input spectral power to counts during the bin calculations, while TEMPINT produces results in energy units.

Calcomp plots are produced as output from the OSOINT and TEMPINT programs, and are similar to those produced from the MKOREN tape discussed in the previous section. For OSOINT the plots have axes of counts vs wavelength for specific temperatures. For TEMPINT the units are power vs wavelength.

The filter transmission data, used as input to both the TEMPINT and OSOINT programs, are the output of a program called FILGEN (see Appendix D). FILGEN uses information specifying the density and thickness of each element contained in an X-ray filter, and the X-ray mass absorption coefficients of the filter material, to calculate the filter transmission at one Å intervals. At an absorption edge, two additional transmissions are computed, one each at the top and bottom of the edge. The output consists of a series of cards for each filter giving the transmission versus λ from 3 to 60 Å. Filters can be combined in the program to produce a

series of output filter transmissions. For the OSO-IV experiment, the filter transmissions from FILGEN for the three filters must be combined with the spectral response characteristics of the instrument to produce final "filters" that are used as input data for OSOINT.

3.5 OSO-IV Detector Response Analysis

The observed counting rate of the OSO-IV detector is related to the flux of solar radiation at the spacecraft through the collection area of the telescope and the instrument's detection efficiency function. Details of the detector design can be found in ASE-2432. Briefly, the detection efficiency function, F, is comprised of three wavelength-dependent quantities: r, the telescope reflectance, q, the photocathode quantum efficiency, and x, the filter transmission. The time-dependent part of the photocathode efficiency is known from in-flight calibration.

The precise characteristics of the function F are unknown. This uncertainty is primarily because the calibration techniques in use at the time of the construction of the OSO-IV experiment were not sufficient for detailed knowledge of the spectral response. There are two major reasons for this: (1) both the telescope reflectance and the filter transmissions were calibrated using only one X-ray emission line, the 8.3 $\mathring{A}$ K_α line of aluminum, and (2) the exact strength of the Fe^{55} source used for in-flight calibration was essentially unknown at launch time, allowing only relative calibration of the detector sensitivity with respect to the first day of usable data from the experiment. Concerning item (1) above, significant improvements in filter calibration techniques, both in the number of lines used and the measurement sensitivity, have been made recently. These methods are outlined in ASE-2665-I. We have found that large errors in determination of the

transmission integral of a filter can be made if one relies entirely on measurements made at just the 8.3 Å line. Also, manufacturing tolerances at the present time are not sufficient to allow reliance on the thickness specifications of filters. These known effects indicate that the true transmission characteristics of the OSO-IV flight filters, and likewise the function, F, were probably poorly determined.

During the course of the Solar Astronomy Program at AS&E, we have found that the two major sources of solar soft X-ray emission, the quiescent corona and active regions, are characterized by fairly consistent, specific temperature ranges. For the OSO-IV data we form what is called a Spectral Hardness Index (SHI) by taking the percentage ratios of the three filters at closely spaced intervals in time. The three independent ratios are calibration independent, and are characteristic of the emitting region. If we assume that the emission in the waveband of the OSO detector is produced thermally, the SHI will be a measure of the temperature of the emitting region. By assuming a reasonable model for X-ray regions, one can construct expected SHI vs temperature curves for each of the three ratios. Figure 3-3 shows such curves for the OSO filters convolved with the model spectrum described in Section 3.3. We then use observed SHI data to determine the expected temperatures. For any single X-ray event, the three SHI values should yield similar temperatures, and be consistent with known values. Using this technique for the OSO data and with the original detector response, we found that the derived temperatures differed from each other and were far too high.

Consequently during the initial period of this contract, an iteration method was used whereby values for the detector response were varied depending upon assumed values for the

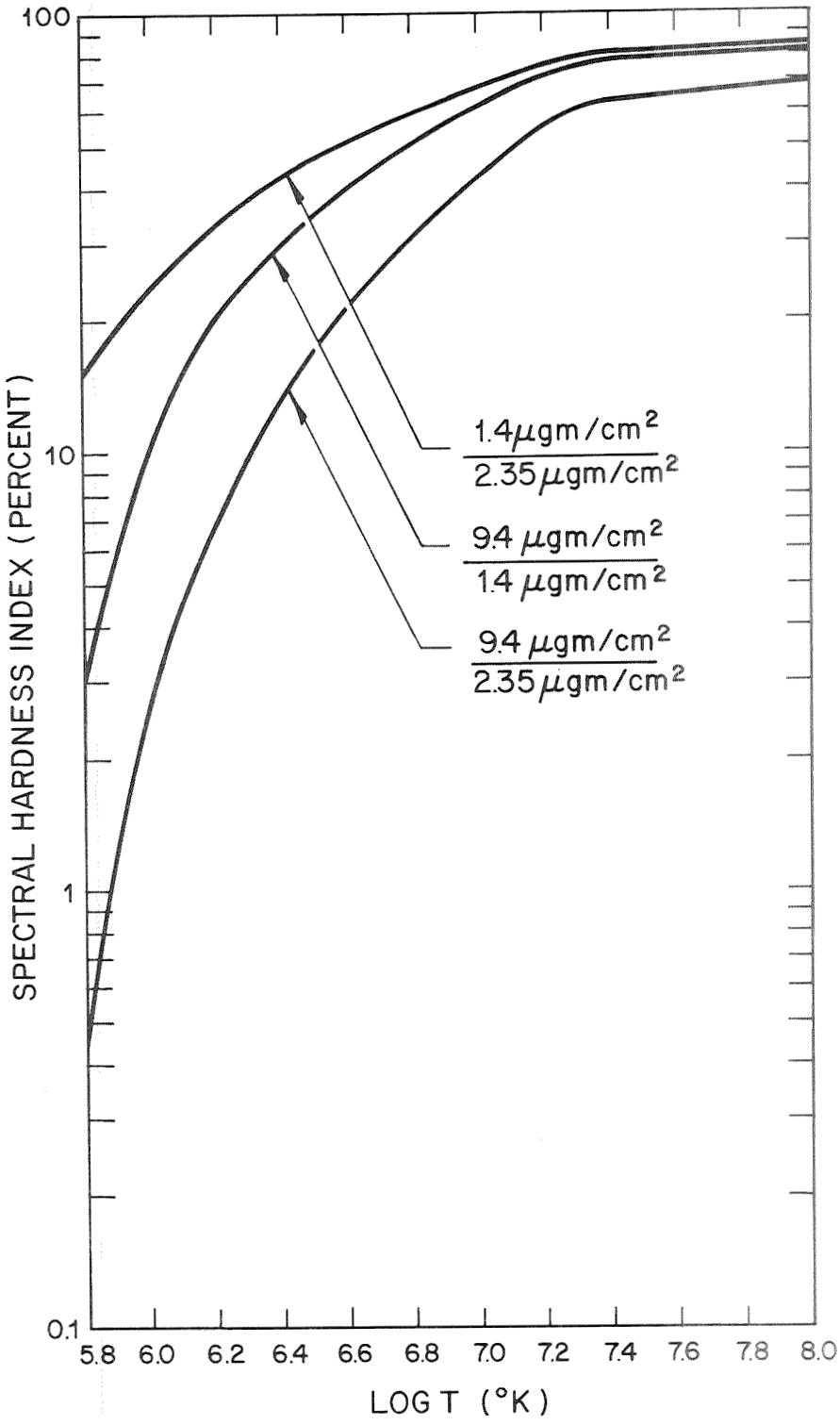

Figure 3-3 Theoretical spectral hardness index (SHI) vs. temperature curves for the OSO-IV detector response convolved with the model spectrum. The SHI's are plotted for the independent ratios of the three OSO filters, and are derived from the filtered integrals of Figure 3-9.

thicknesses of the filters and the CsI photocathode. Figure 3-4 is a family of curves showing the changing spectral response of the function, F, for these various assumptions. All the curves utilize the most sensitive filter mode: 2.35 μgm/cm^2 Be. The uppermost curve is the one which gives the most consistent agreement with expected temperatures. This curve assumes a flat response for the CsI photocathode, and implies that effective loss of this material (through possibly contamination or disintegration) may have occurred early in the experiment's lifetime.

Figures 3-5 through 3-8 are graphs of the output of the OSOINT program, using the 2.35 μgm/cm^2 Be filter + the flat detector response assumption, for four temperatures. Comparing these figures to Figure 3-1, it is obvious that at lower temperatures the dominant contribution to the OSO counting rate is from line emission, since continuum radiation is shifted to longer wavelengths. At higher temperatures, the continuum becomes a more important contributor (and finally dominates the spectrum in Figure 3-8) in the OSO passband.

Figure 3-9 shows curves of the counting rate of the OSO instrument as a function of temperature for each of the OSO filters which result from plotting the output of the OSOINT program for the flat detector response assumption. Each curve is produced by plotting the calculated filtered spectrum integral (3 - 60 Å) for each temperature value. The abscissa units are in counts per unit emission measure per unit time and wavelength, a form convenient for analysis. The Spectral Hardness curves of Figure 3-3 are produced by taking ratios of the appropriate filtered integrals and plotting them for each temperature value. Again these curves assume flat detector response.

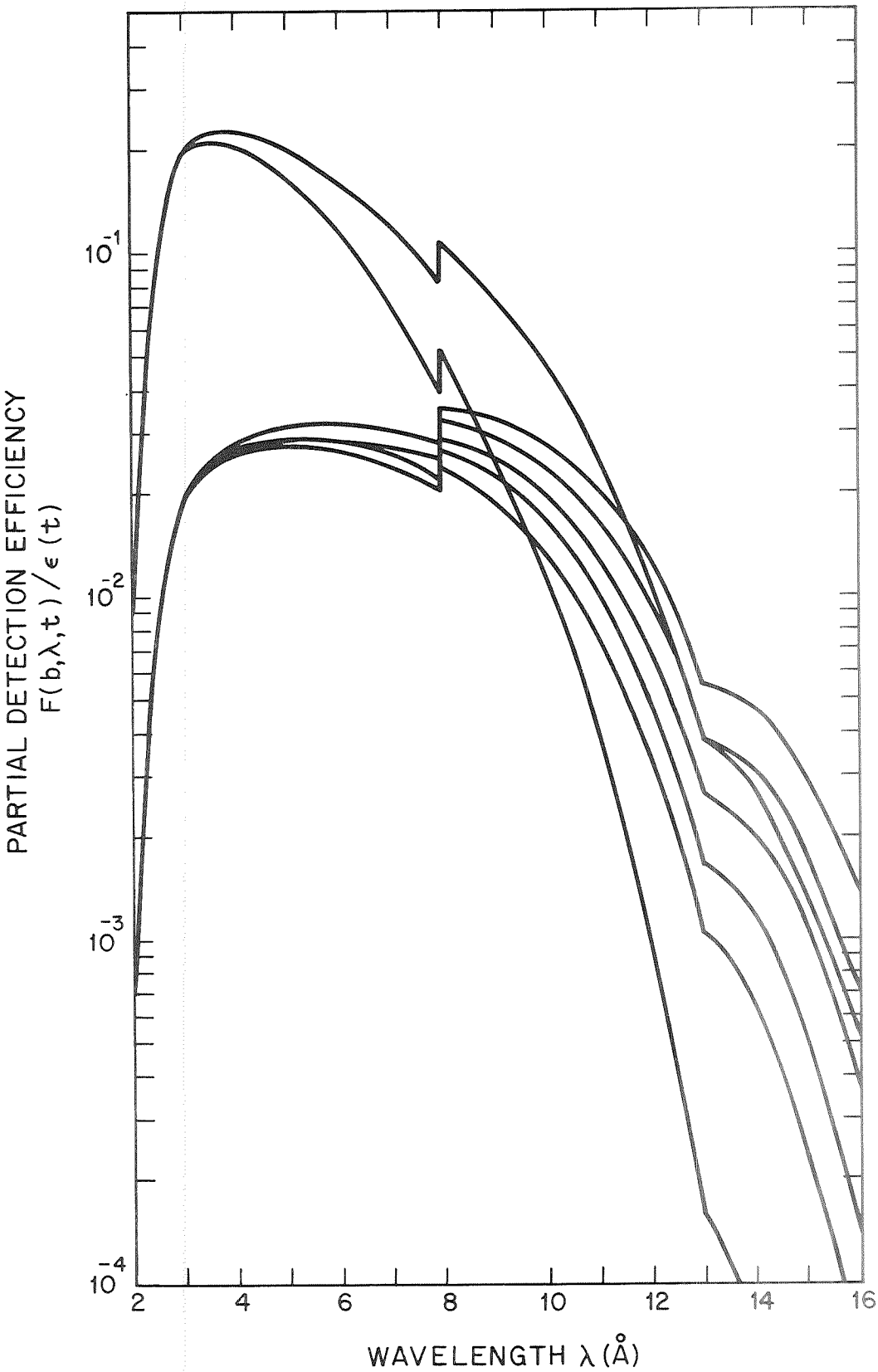

Figure 3-4 Curves showing the changing spectral response of the OSO-IV detector for different assumptions. The uppermost curve, assuming a flat photocathode response, has been adopted for the present calculations.

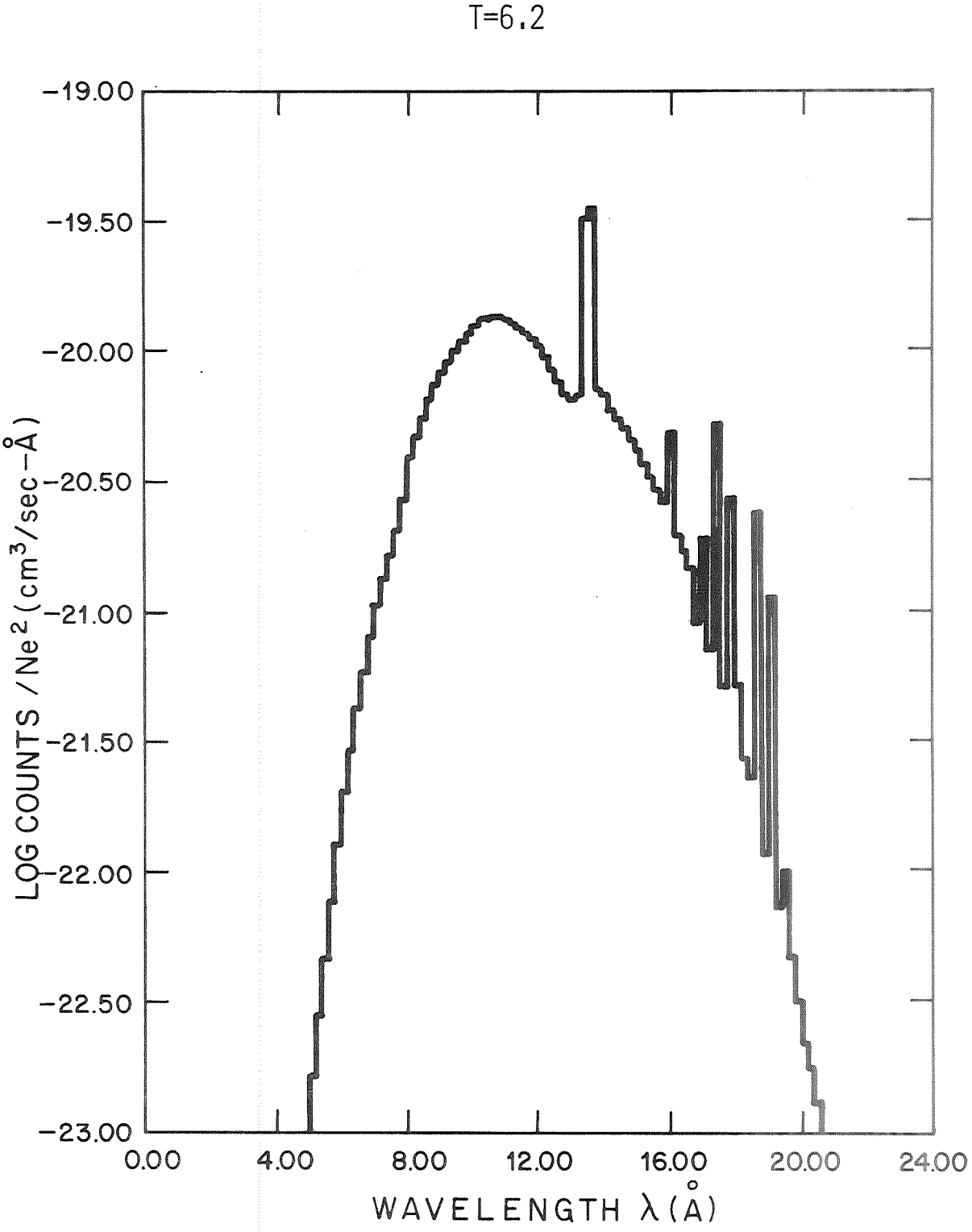

Figure 3-5 Curve resulting from the OSOINT program. This graph is the result of convolving the model spectrum with the OSO-IV flat detector response assumption. It is for a temperature of 1.6×10^6 °K.

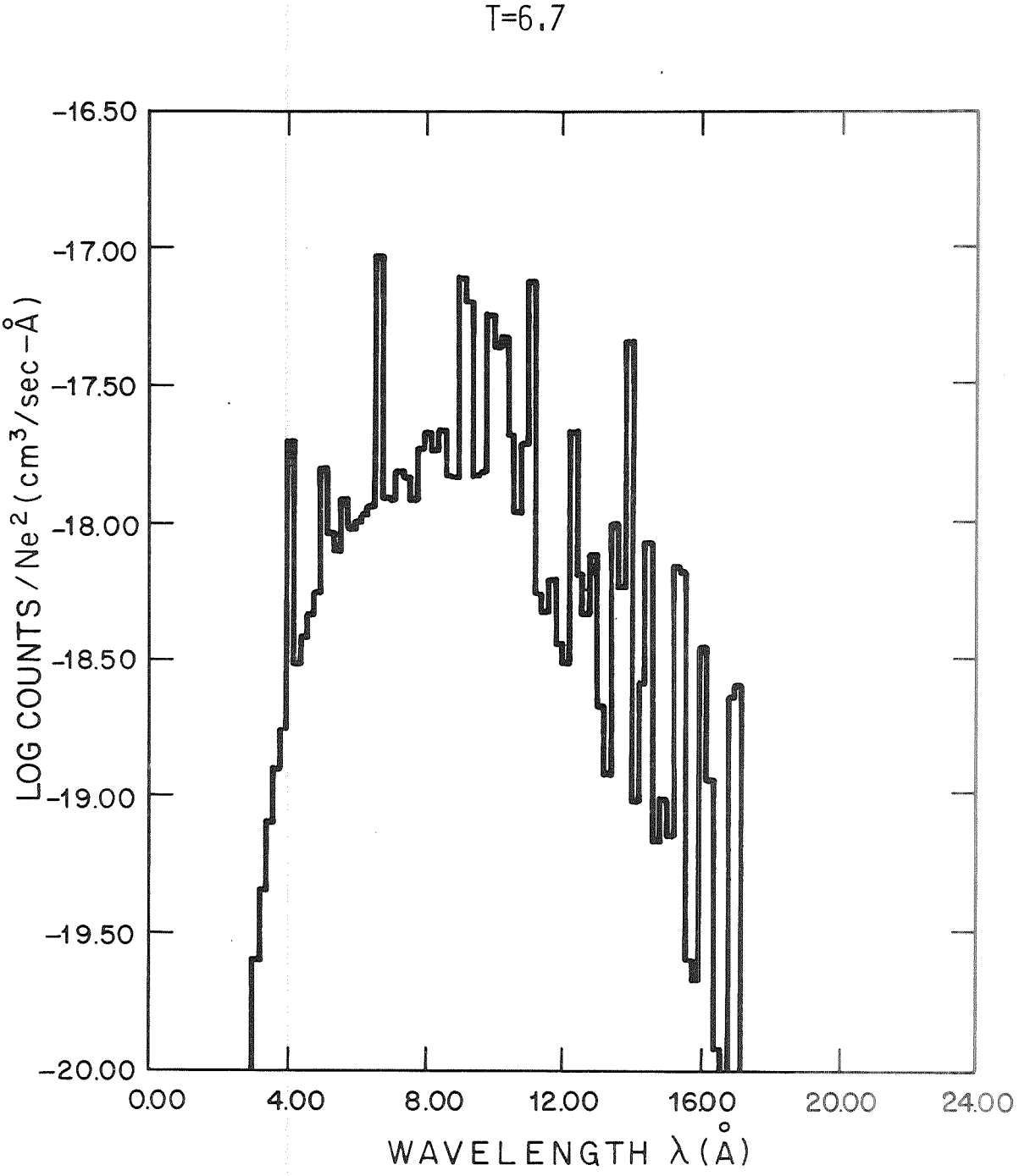

Figure 3-6 Curve resulting from the OSOINT program. This graph is the result of convolving the model spectrum with the OSO-IV flat detector response assumption. It is for a temperature of 5×10^6 °K.

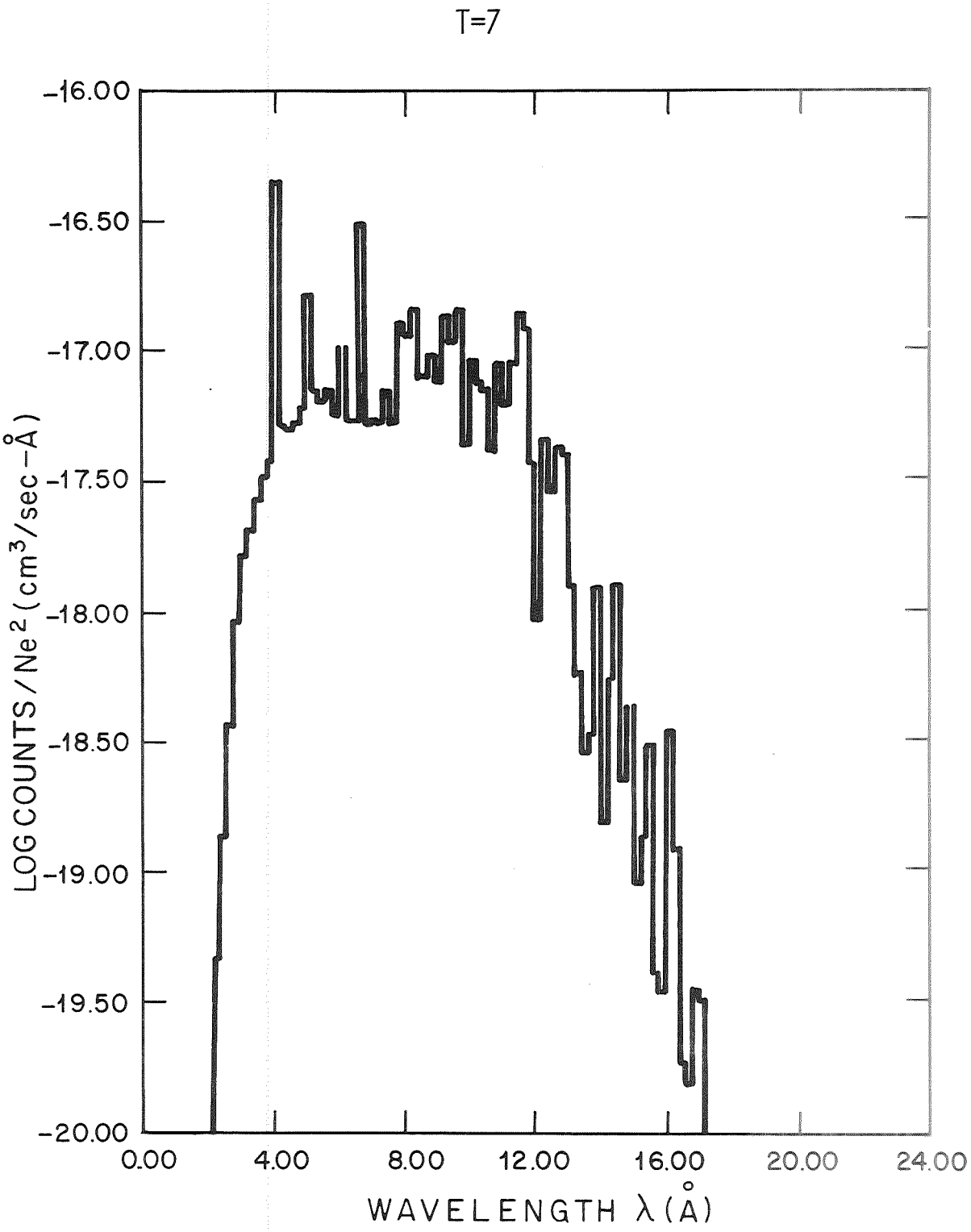

Figure 3-7 Curve resulting from the OSOINT program. This graph is the result of convolving the model spectrum with the OSO-IV flat detector response assumption. It is for a temperature of 10^7 °K.

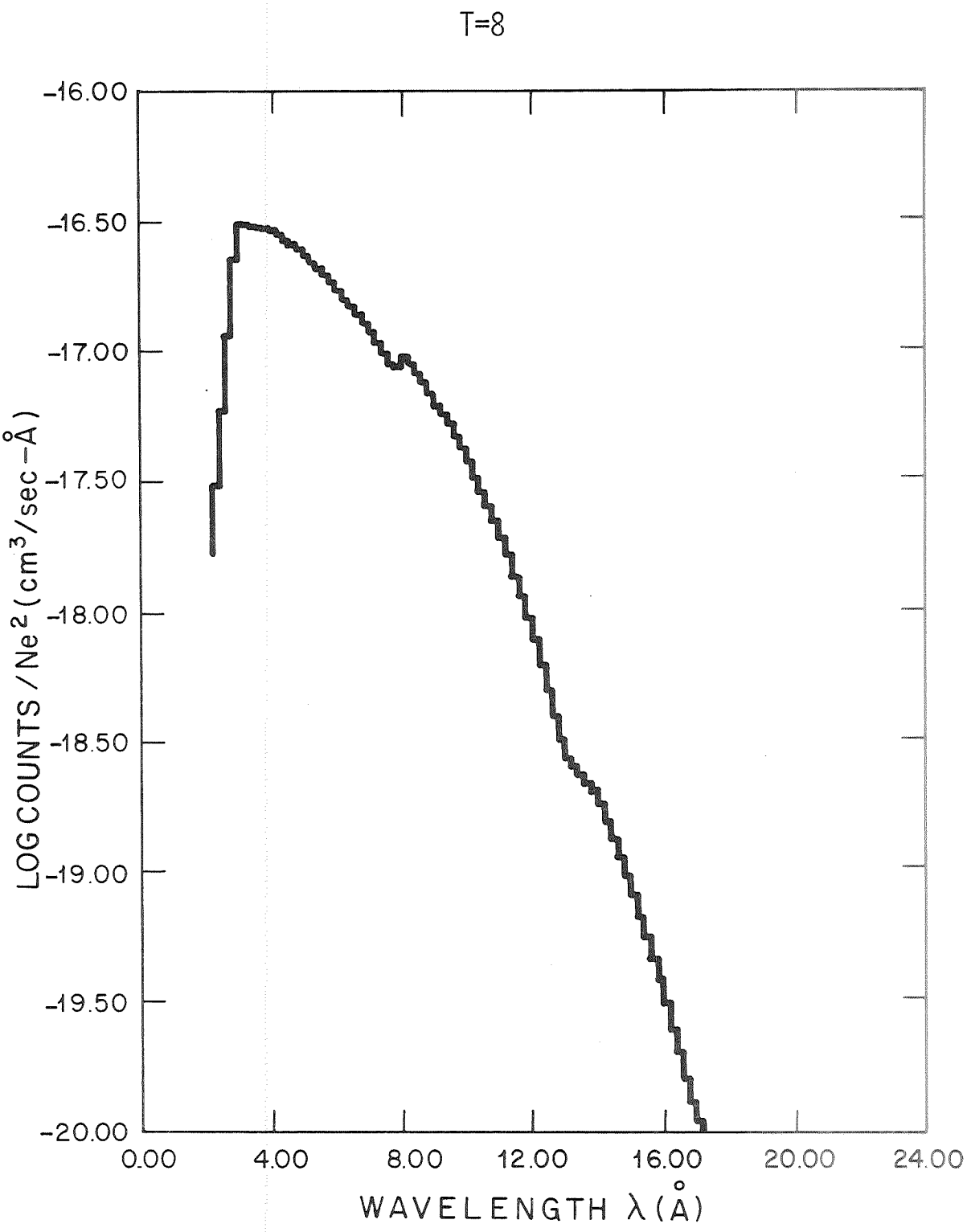

Figure 3-8 Curve resulting from the OSOINT program. This graph is the result of convolving the model spectrum with the OSO-IV flat detector response assumption. It is for a temperature of 10^8 °K.

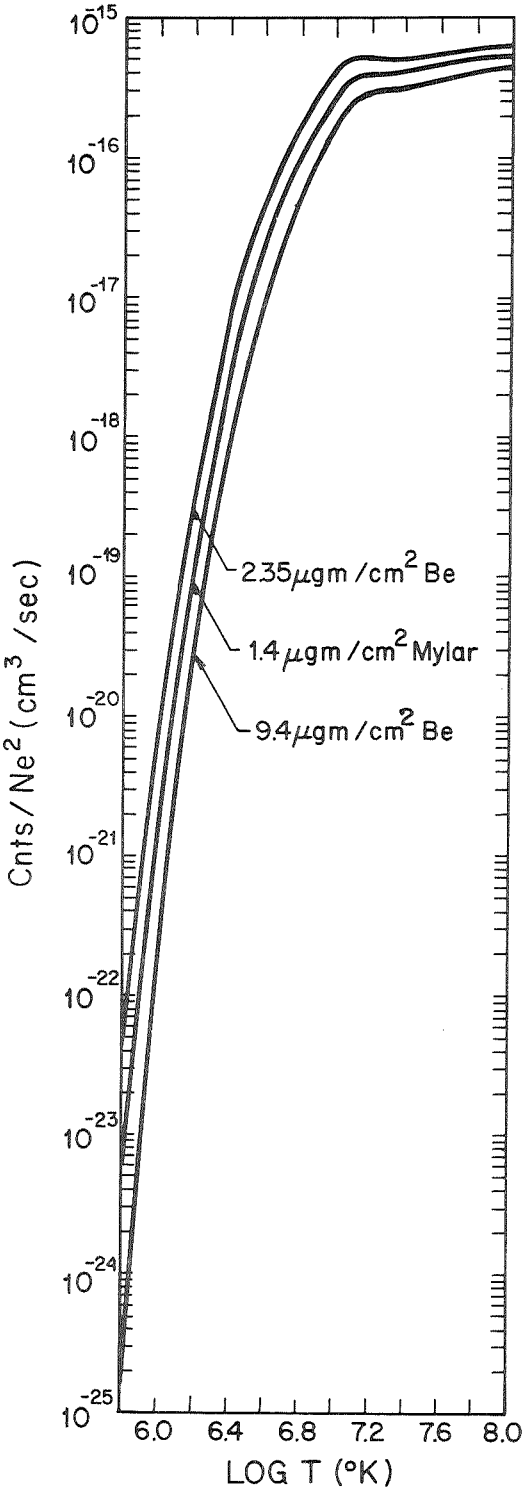

Figure 3-9 Curves of the counting rate integrals of the OSO-IV detector as a function of temperature for the three filters. The integrals are calculated by the OSOINT program. Flat detector response is assumed. The SHI ratios of Figure 3-3 are produced from these integrals.

4.0 CONCLUSION

The OSO-IV pointed X-ray telescope experiment continues to return data. Since the failure of the second tape recorder on OSO-IV on 12 May 1968, only data transmitted during real-time passes over the receiving stations has been available. The amount of quick-look data received from GSFC has been greatly reduced, because of the telemetry overload on the Stadan network. At the time of tape recorder failure, the detector efficiency of the OSO-IV telescope was about 30% of its value on 27 October 1967. Since then it has stabilized at somewhat less than 20% of this value.

The instrument has been operated almost entirely in its most sensitive mode (2.35 μgm/cm^2 beryllium filter; 4 arc-minute aperture) since tape recorder failure. Occasionally it is commanded into the calibration mode for reference.

Routine computer processing of the spacecraft tapes has been completed through the first year of the satellite's lifetime. All of the original tapes have been returned to GSFC.

Most of the prime data has been analyzed, the results have been presented at various scientific meetings, and two papers have been accepted for publication in scientific journals. Further analysis effort on contract NASW-2070 will be devoted to the determination of the physical state of X-ray emitting structures, and to the relationship between the detailed structures observed by our solar sounding rockets and the dynamical phenomena observed by our OSO-IV experiment.

APPENDIX A

List of publications supported in part or in full by NASA contract NASW-2070:

Krieger, A., Paolini, F., Vaiana, G. S. and Webb, D., "Results From OSO-IV: The Long Term Behaviour of X-ray Emitting Regions". Accepted for publication in Solar Physics.

Tucker, W. H. and Koren, M., "Radiation From a High Temperature, Low Density Plasma: The X-ray Spectrum of the Solar Corona". Accepted for publication in the Astrophysical Journal.

APPENDIX B

ASE-2654
Revision A

RESULTS FROM OSO-IV: THE LONG TERM BEHAVIOUR OF X-RAY EMITTING REGIONS

A. Krieger, F. Paolini, * G. S. Vaiana, D. Webb
American Science and Engineering
Cambridge, Massachusetts

ABSTRACT

A grazing incidence X-ray telescope on board the OSO-IV spacecraft obtained images of the sun in the 2.5 to 12 Å waveband nearly continuously from 27 October 1967 to 12 May 1968. The instrument had sufficient spatial resolution (one to four arc-minutes) and temporal resolution (5 to 20 minutes) to estimate the spatial characteristics of X-ray emitting regions and to monitor the temporal behaviour of individual active regions. Variations in the absence of flares of as much as a factor of 10 in the X-ray output of individual regions were observed, with typical durations ranging from several hours to several days. The X-ray time variations are related to observations at optical and radio wavelengths. The results are interpreted under the assumption that the X-ray time variations are caused by temperature changes in the coronal portions of active regions. The contribution of radiative losses to the energy budget of the coronal active region is estimated.

Accepted for publication by Solar Physics

*Present Address: Philips Electronic Instruments, Mt. Vernon, N. Y.

1. Introduction

The OSO-IV satellite was successfully launched into earth orbit on 18 October 1967. AS&E's grazing incidence X-ray telescope on board the spacecraft obtained solar images in the 2.5 to 12 Å waveband, nearly continuously from 27 October 1967 to 12 May 1968 when the satellite tape recorder failed. Intermittent data was received thereafter.

The OSO-IV X-ray telescope had sufficient spatial resolution (one and four arc-minutes) to locate and identify the sources of solar soft X-ray emission. The temporal resolution (five to 20 minutes) of the instrument was sufficient to resolve the time variations in X-ray flux (except during impulsive flares), and the duration was sufficient to monitor active regions for periods on the order of their lifetimes. Because of its spatial resolution, the instrument could measure the X-ray emission from a particular active region even while the majority of the total solar X-ray flux was being produced by other regions. Consequently, the X-ray telescope was able to follow the temporal behavior of individual active regions for several solar rotations.

The analysis of the OSO-IV telescope data has followed three major lines: (1) the angular resolution characteristics of the instrument have been used to determine the spatial dimensions of X-ray emitting regions; (2) time histories of the X-ray activity of individual, selected active regions have been studied in order to determine the temporal characteristics of these regions; and (3) the data has been compared with observations made at radio and optical wavelengths. The results of this analysis follow a brief description of the instrumentation and our experimental procedure.

2. Description of Experiment

a) Instrumentation

The grazing incidence X-ray telescope is a two-mirror, image forming system of optics. Incident X-rays reflect off the first mirror, which is a paraboloid of revolution, onto the second mirror, which is a confocal hyperboloid of revolution. The radiation reflected off the second mirror subsequently forms a true image of the source in the focal plane of the system. For X-radiation of wavelengths greater than 2 Å, angles of incidence are less than the critical angle necessary for total external reflection; reflection efficiency is therefore high. A detailed description of grazing incidence X-ray telescope design and application has been given by Giacconi et al. (1969).

The telescope on OSO-IV (shown mounted into the instrument in Figure 1) was fabricated of electroformed nickel; it was approximately 7.6 cm in diameter by 16 cm long; its collecting area was 2.01 cm^2; and its focal length was 83.6 cm. Its inherent resolution was 20 arc-seconds. The grazing angle of reflection for rays incident parallel to the axis was 40 arc-minutes for both reflections.

The reflection efficiency of the X-ray telescope was measured at the 8.3 Å aluminum line. The reflection efficiency on axis was found to be 28%. The theoretical reflection efficiency (Zehnpfennig et al., 1967) at 8.3 Å for two reflections from nickel surfaces pitched at equivalent angles to the X-ray beam (that is, 40 arc-minutes for both reflections) is approximately 65%. This difference between the theoretical and actual efficiencies is considered typical of X-ray telescopes fabricated by the electroforming technique. The computed reflection efficiency is shown in Figure 2.

Transmission as a function of wavelength for all filters was calculated from the values of the mass absorption coefficients tabulated by Henke et al. (1967) and the measured areal densities ($gm\text{-}cm^{-2}$) of the filter materials used. Their transmissions to 8.3 Å Al-$K\alpha$ X-radiation were then experimentally measured and were found to be consistent with calculations. Besides the wheel-mounted filters, there was a fixed filter in the optical path of 0.00038 cm Mylar with 2000 Å evaporated aluminum, adding primarily 0.53 mg/cm^2 of carbon.

The detector was a "photoemission-scintillation" detector. Lincke and Wilkerson (1962) have described its use in the extreme ultraviolet. The detector consisted of an external photocathode and a scintillation detector. The photocathode was a conical shell of nickel substrate, the interior of which was coated with CsI. This substance has been found by Lukirskii et al. (1960) to have an extremely high photoelectric quantum efficiency for X-radiation. The photocathode was held at a potential of -10 kV. The scintillation detector used a plastic scintillator mounted on a lucite light pipe, and viewed by a 14-stage photomultiplier. The scintillator was coated with a film of vacuum-deposited aluminum; the aluminum film was at ground potential.

Incident X-radiation struck the interior of the conical cathode causing, with high probability, the emission of one or more photoelectrons. The conical shape of the photocathode substrate structure and the planar shape of the aluminum filter over the scintillator formed an electrostatic lens which directed the photoelectrons into the scintillator. This produced enough scintillation light to be detected by the photomultiplier with reasonable efficiency.

b) Experimental Procedure

A schematic representation of the AS&E grazing incidence X-ray telescope experiment is shown in Figure 3. The instrument used a grazing

incidence system of mirrors (an X-ray telescope) which formed an image of the sun on the Aperture Wheel in the focal plane of the telescope. The wheel contained four apertures of two different sizes (one arc-minute and four arc-minutes) which determined the spatial resolution of the optical system. The Aperture Wheel was programmed to step automatically between complete scans of the sun, or to stay at any desired position. As the OSO-IV pointed section scanned the sun, the solar image moved over the Aperture Wheel. Only X-radiation from that region of the sun at which the instrument was pointed passed through the aperture for further analysis.

The X-radiation from a single picture element subsequently passed through one of three filters in the Filter Wheel located immediately behind the Aperture Wheel. The filters, together with a fixed filter in the optical path of the X-ray telescope and the reflection properties of the telescope itself, permitted analysis of X-radiation in three wavelength bands. These were approximately: (a) 2.5 to 12 Å, (b) 2.5 to 11 Å, and (c) 2.5 to 9 Å. The Filter Wheel could be programmed to step automatically between complete scans of the sun. It cycled through four positions: three filter positions and a calibration position. It could also be programmed to stay at any desired fixed position. Beyond the filters, transmitted X-ray quanta struck the photocathode where photoelectrons were emitted and were then accelerated into the scintillator viewed by a photomultiplier tube. The counts accumulated between data sample times were thus proportional to the number of X-rays emitted from the corresponding picture element of the sun. A total of 1920 such sets of accumulated counts comprise the data from one complete scan of the sun.

The pulses from the photomultiplier were subsequently counted and the result telemetered to the ground. These sets were reconstructed on the ground into an array of 48 by 40 numbers which constitute an X-ray

map of the sun. The position of a given number in the array corresponds to a unique position on the sun and the magnitude of the number corresponds to its brightness in X-radiation. Data accumulation time was 0.14 seconds at each raster position. Due to readout delay time, the actual time interval required to accumulate the data for one X-ray filtergram was 5.12 minutes. Thus, if the filter Wheel was cycling (as was usually the case), 20.5 minutes elapsed between consecutive filtergrams through the same filter. Table 1 lists the instrumental characteristics of the OSO-IV telescope experiment.

The initial output "raw raster" consisted of solar X-rays, background counts due to spacecraft generated noise (a function of raster position), and energetic charged particle counts. The latter counts depend upon spacecraft orbital position and time, but are independent of raster position. To determine the number of true counts due to solar X-rays, N, as a function of raster position, one must subtract from the raw raster an "average background raster," which contains the spacecraft generated noise and the average charged particle counting rate.

The average background raster was generated from raster scans utilizing an Fe^{55} calibration source, instead of the X-ray filters, in the optical path of the telescope. Rasters obtained when the spacecraft was passing through the South Atlantic Anomaly were removed entirely from data processing.

The number of true counts, N, accumulated during the 0.14 second live time interval between data words is related to the spectral distribution function, ϕ, at the spacecraft by the expression:

$$N(a,b,t,T) = 0.14\,A \int_0^\infty F(b,\lambda,t)\,\phi(a,t,T,\lambda)\,d\lambda \qquad (1)$$

where a = Aperture Wheel index, indicating the angular resolution mode of the experiment;

b = Filter Wheel index, indicating the transmission filter in position, and thus specifying an effective wavelength passband;

t = Time;

T = Spectral parameter indicating the nature of the source spectrum;

A = Sensitive collection area of the telescope aperture;

λ = Independent variable, wavelength, in Å;

ϕ = Spectral distribution function of radiation at the spacecraft (units are photons/cm^2-sec Å); and

F = Instrument detection efficiency function.

TABLE 1

OSO-IV INSTRUMENTAL CHARACTERISTICS

SPECTRAL RANGE:*	2.5 - 12 Å	(2.35 μgm/cm^2 beryllium filter)
	2.5 - 11 Å	(1.4 μgm/cm^2 Mylar filter)
	2.5 - 9 Å	(9.4 μgm/cm^2 beryllium filter)
SPATIAL RESOLUTION:	1 arc-minute	
	4 arc-minute	
TIME RESOLUTION:	5.12 minutes	
	20.48 minutes	
MINIMUM SENSITIVITY:	2×10^3 photons/cm^2-sec	

* The wavelengths presented represent the nominal passbands for these filters. The actual wavelengths to which the instrument responds are a function of the form of the incident X-ray spectrum.

The function of $F(b,\lambda,t)$ is expressed by

$$F(b,\lambda,t) = r(\lambda)\ \epsilon(t)\ \ q(\lambda)\ \ x(b,\lambda)$$

where r = Telescope reflectance;

ϵ = Time-varying part of the photocathode detection efficiency, calculated from the in-flight calibration mode;

q = Photocathode detection efficiency i.e., the probability that one count will be recorded upon irradiation by a single photon of wavelength λ; and

x = Filter transmission function

The function $F(b,\lambda,t)$ for the three filters used in this experiment appear in Figure 4. Details of construction, calibration procedures, and computer analysis of the OSO-IV telescope instrument are available elsewhere (Giacconi et al. 1968: Giacconi et al. 1970).

3. Location and Size of X-ray Emitting Regions

a) X-ray Emitting Regions

A typical raster scan of the sun (Figure 5) shows eight different regions as sources of solar X-ray emission. The 9.1 cm and CaK spectroheliograms of the same date are presented for comparison. As was originally noted by Chubb et al. (1961), the X-ray emitting regions are associated with solar active regions, and can be identified with their CaK counterparts. All active regions visible on the 9.1 cm spectroheliogram are apparent on the X-ray filtergram. No extra radiation is observed from the general corona at the limb other than that attributable to active regions. Therefore, the X-ray brightness of the coronal limb in the instrumental passband* is less than 150 photons/cm^2-sec-$(arc\text{-}min)^2$.

*When no filter passband is specified the results refer to the 2.35 $\mu g/cm^2$ Be filter.

There is a substantial range in the X-ray emission of individual active regions. The total photon flux observed from region 9034, the brightest region shown in Figure 5, is $(4.6 \pm .2) \times 10^4$ photons/cm^2-sec. The flux observed from region 9035 is only $(3.8 \pm .8) \times 10^3$ photons/cm^2-sec. Thus the range in X-ray flux in the detector passband is at least a factor of 12. Moreover, several of the active regions observed in CaK are below the threshold of sensitivity of the X-ray experiment at this time (approximately 2×10^3 photons/cm^2-sec). The physical conditions in the various active regions must differ for this to be the case. The ratio of the areas observed in CaK for regions 9034 and 9035 is only 2.2 (Solar-Geophysical Data Bulletins); therefore, unless the vertical structures of these active regions are very different, either the temperatures or densities of the X-ray emitting portions of these two active regions must be different.

b) Vertical Extent of Active Regions

High resolution solar X-ray images (Vaiana et al., 1968; Vaiana and Giacconi, 1969 ; Van Speybroeck et al., 1970) obtained with a rocket-borne telescope indicate that the X-ray emitting regions extend to substantial heights in the corona. The resolution of the OSO-IV telescope is insufficient for a direct measurement of the vertical extent of an active region. However, the vertical extent of an active region can be estimated by observing the time at which the region becomes completely occulted by the solar limb due to rotation. The vertical extent is then calculated geometrically. In general, the time at which the X-ray intensity from the active region drops below the threshold sensitivity of the X-ray telescope is known to $\pm$ 20.5 minutes. The uncertainty is never larger than 95.8 minutes. The vertical extent of the emitting region is calculated from the heliographic coordinates of the center of the underlying CaK region and the solar rotation rate $\omega = 13.39 - 2.7 \sin^2 \lambda$ (degrees/day)(Allen, 1964), where λ is the heliographic latitude. Closely spaced regions of similar heliographic latitude, but

different heliographic longitudes, are difficult to distinguish at the limb. Consequently, we have eliminated such cases from consideration for this analysis.

Using data obtained between October 1967 and March 1968, we were able to determine the time of first appearance at the east limb of 6 X-ray emitting active regions and the time of disappearance at the west limb of 11. Measured vertical extensions ranged from 19,000 km to 193,000 km. The results are tabulated in Table 2.

Wende (1969), on the basis of Explorer XXXV and Mariner V data, derives a half height of 7.6×10^4 km for region 9034 at the west limb. This is in reasonable agreement with our value of 11.8×10^4km for the full height of the X-ray emitting region.

Two major sources of error are present in our estimates. First the X-ray output of active regions is highly variable. Therefore, the possibility exists that the X-ray emission of the active region could drop below the threshold of detectability because of time variations before the point of geometrical occultation is reached. This would result in an underestimate of the height of the active region. We have attempted to minimize the possibility of this error by considering only the brightest X-ray emitting regions. In four cases, where activity observed later might be attributed to the region assumed occulted we have listed our observed value as a lower limit estimate of the height of the region. Second, we have assumed that the top of the X-ray emitting region is located directly above the center of the CaK plage. An uncertainty in the height estimate proportional to the longitudinal extent of the active region is thus introduced.

In Table 2 we have listed the CaK area of the active regions as observed near central meridian passage. If we assume that the outline of

TABLE 2

VERTICAL EXTENT OF ACTIVE REGIONS

McMath Plage No.	Appearance Date	Time (UT)	Disappear-ance Date	Time (UT)	Latitude	Appearance to CMP (days)	CMP to Disappear-ance (days)	θ (Degrees behind limb)	Height (10^3 km)	CaK Area* (at CMP)
	(1967)		(1967)							
9034			2 Nov	0825	N12		9.3	31.30	118	3700
9041			6 Nov	1121	N18		9.1	29.24	102	2700
9047			13 Nov	0816	S21		9.8	37.82	185	(6200)
9048			11 Nov	1448	N23		8.6	21.61	53	2500
9073			28 Nov	>2153	N14		>9.0	>29.09	>100	(7800)
9088	20 Nov	0042			S18	8.3		19.00	40	3100
9091			5 Dec	>1547	S28		>9.8	>35.39	>159	1400
9092			10 Dec	0001	S19		9.4	33.18	136	2300
9108	2 Dec	0004			S18	8.5		21.62	48	(3700)
9115			26 Dec	1642	N14		9.7	38.35	193	7500
9118	12 Dec	<0634			N21	>9.7		>36.52	>171	9100
9120	14 Dec	0740			S27	9.4		30.64	114	4300
	(1968)		(1968)							
9145			18 Jan	0508	S21		8.8	24.78	71	(9000)
9196			14 Feb	2229	N14		7.8	13.21	19	5200
9204			23 Feb	1454	N20		8.8	25.05	73	6100
9214	11 Feb	1907			S14	8.3		19.83	44	2400
9244	26 Feb	<2058			S26	>9.5		>32.28	>128	3600

*Millionths of a Solar Hemisphere

the base of the X-ray emitting region conforms, in general, to the outlines of the CaK plage (as observed by Vaiana et al., 1968), that the topologies of all X-ray emitting regions are similar, and that the region does not change in size between the center of the disk and the limb, then the vertical extent of a region should be proportional to the square root of its CaK area. It is evident that this relationship does not hold. It would therefore appear that the topology of the X-ray emitting portions of active regions differ from region to region as would be expected if the structure of the X-ray emitting region is dependent on the detailed configuration of the magnetic field. VanSpeybroeck et al., (1970) have shown this to be the case.

c) Size of Flares

One can estimate the size of X-ray flares observed on the disk by comparing the observed X-ray intensity profiles with the expected response of the telescope to sources of various sizes. We have examined the intensity profiles of 42 bright X-ray flares observed between 27 October 1967 and 3 December 1967. For each of these events the diameter of the telescope field stop was one arc-minute. We have compared these intensity profiles with those calculated from the response of the telescope for circular sources of various diameters (Zehnpfennig et al., 1967). Figure 6 is a histogram of the relative frequency of occurrence of the measured full widths at half maximum intensity (FWHM). The mean value of the FWHM is 1.51 arc-minutes, which corresponds to a source diameter of 1.24 arc-minutes. The standard deviation of the distribution is 0.30 arc-minutes. We have compared the measured FWHM of the X-ray intensity distributions with the corresponding values of the measured area in Hα for the 24 X-ray events from this sample which were listed as Hα events in the Solar-Geophysical Data Bulletins. There is no apparent relationship between the measured area in Hα and the observed width of the X-ray distribution. If the jitter in the OSO-IV pointing control (about 0.25 arc-min) is taken into account, the observed X-ray intensity distributions are consistent with source dimensions of one arc-minute of less.

In a similar manner we have examined the intensity profiles of 10 bright X-ray flares observed at the limb. The mean value of the observed FWHM is 1.64 arc-minutes which corresponds to a source diameter of 1.35 arc-minutes. The standard deviation of the observed distribution of limb flare FWHM is 0.38 arc-minutes. Therefore, the vertical extent of the X-ray flares observed by the OSO-IV telescope would also appear to be on the order of one arc-minute.

From the OSO-IV results, it would appear that the majority of the soft X-ray flux from flares is emitted from regions whose characteristic dimensions are less than one arc-minute. We can therefore set an upper limit on the volume of the X-ray emitting region for the observed flares of about 10^{29} cm^3.

4. Time Variations in X-ray Emission from Active Regions

a) The Range of Variations in the X-ray Emission of an Active Region

The magnitude and variety of the changes in the instantaneous X-ray emission observed from an individual active region can be noted by examining a plot of the time history of such a region over a period of several days (Figure 7). Each point on the plot is the integrated number of X-ray counts received from the active region during a raster scan, taking the telescope response function into account. The rates are normalized in order to compensate for temporal changes in the detector efficiency. Table 3 lists the 32 active regions whose time histories were followed. The most notable features of the time history plots are the existence of significant variations in X-ray counting rate in the absence of flares, and the extreme range of variability in the instantaneous X-ray counting rate. Even if flares are not considered, the X-ray counting rate for an individual active region varies considerably during a single passage across the disk. The non-flare X-ray counting rate of region 9073, for example, (shown in Figure 7) rose by a factor of twenty in a period of four hours and then slowly

TABLE III

ACTIVE REGION TIME HISTORIES LIST

McMath Plage No.	Approximate Period Followed (1967)
9034	28 Oct., 9^h - 1 Nov., 9^h
9047	27 Oct., 6^h - 12 Nov., 19^h
9062	10 Nov., 0^h - 16 Nov., 21^h
9073	10 Nov., 0^h - 27 Nov., 11^h
9082	17 Nov., 16^h - 4 Dec., 0^h
9088	24 Nov., 15^h - 4 Dec., 0^h
9091	24 Nov., 15^h - 4 Dec., 0^h
9101	1 Dec., 15^h - 14 Dec., 14^h
9107	5 Dec., 11^h - 6 Dec., 21^h
9108	2 Dec., 11^h - 17 Dec., 0^h
9110	8 Dec., 16^h - 12 Dec., 8^h
9115	8 Dec., 16^h - 23 Dec., 23^h
9118	12 Dec., 5^h - 17 Dec., 0^h
9128	25 Dec., 5^h - 31 Dec., 6^h

McMath Plage No.	Approximate Period Followed (1968)
9132/3	2 Jan., 23^h - 6 Jan., 6^h
9146	2 Jan., 23^h - 19 Jan., 12^h
9184	26 Jan., 6^h - 1 Feb., 20^h
9188	29 Jan., 23^h - 11 Feb., 5^h
9204	8 Feb., 11^h - 22 Feb., 23^h
9222	18 Feb., 8^h - 28 Feb., 8^h
9224	21 Feb., 0^h - 28 Feb., 9^h
9225	22 Feb., 18^h - 28 Feb., 9^h
9267	10 Mar., 21^h - 22 Mar., 6^h
9273	23 Mar., 3^h - 1 Apr., 6^h
9281	21 Mar., 10^h - 27 Mar., 0^h
9285	19 Mar., 2^h - 3 Apr., 15^h
9286	24 Mar., 0^h - 6 Apr., 3^h
9313	8 Apr., 8^h - 23 Apr., 2^h
9337	24 Apr., 13^h - 30 Apr., 10^h
9358	30 Apr., 21^h - 9 May, 20^h
9364	27 Apr., 10^h - 12 May, 23^h
9372	3 May, 1^h - 10 May, 11^h

fell back to approximately twice its original value over a period of four days. In fact, the rise in the counting rate of region 9073 was larger than is indicated in the figure. Region 9073 was unresolved from the adjacent weaker regions, McMath 9066 and 9067, until the latter regions rotated away from the east limb on 11 November. The rise in X-ray counting rate is attributed to region 9073 which was actually behind the limb in $H\alpha$, because (1) no $H\alpha$ event was observed in conjunction with the X-ray event from either region 9066 or 9067, and (2) the later X-ray time history of region 9073 showed it to be substantially more active than the other two regions. Variations of a factor of ten in the non-flare X-ray counting rate of an active region over a disk passage are typical of the active regions which we observed.

When flares are included, the total variation between the highest counting rate shown in the figure (15.6 minutes after the X-ray peak of the importance 3b flare of 2130 UT on 16 November) and the lowest rate shown (0513 UT on 10 November) is 160. In order to extrapolate back to the peak of the X-ray flare, we use the fact that the X-ray intensity of the 16 November flare fell exponentially with a time constant of 17.5 minutes. This would indicate a maximum range in the 2.5 to 12 $\mathring{A}$ X-ray intensity of a factor of 400 in a seven day period. This range is typical of that exhibited by solar active regions during periods of flare activity. For the period 27 October 1967 to 6 January 1968, the maximum range of X-ray flux variation exhibited by an individual active region during a passage across the disk was shown by the region corresponding to McMath-Hulbert Plage No. 9091. This region was below the threshold of detectability, 3.8×10^3 photons/cm^2-sec, until 24 November 1967. On 2 December 1967, 0652 UT, we observed a flare with a peak X-ray flux of 6.5×10^6 photons/cm^2-sec. Thus, the range in X-ray flux was at least a factor of 1700.

b) Time Behavior of Active Regions

The time history of an individual active region (Figure 7) is comprised of variations in X-ray intensity whose durations range from several minutes to several days. The shortest of these are associated with solar flares. The longest duration events presumably contribute to the slowly varying component of the solar X-ray emission in spatially unresolved observations. The intermediate time scale events are less noticeable in measurements of the total solar X-ray flux, however, such enhancements are quite noticeable in the spatially resolved data from the OSO-IV X-ray telescope. Intense, X-ray flares are immediately obvious on the plot of the time history of the X-ray emission of an active region (Figure 7). Such events appear as a sequence of a few points with substantially higher X-ray flux than the mean level of emission from the active region immediately before or after. During a six-month period commencing in late October 1967, more than 1,000 statistically significant events were recorded by the OSO-IV detector. Because the interval between comparable measurements (20.5 minutes) is of the same order of magnitude as the duration of these flare events (see, for example, the data of Teske, 1969), the probability of observing the peak of an event is relatively low. Consequently, the flare enhancement in X-ray emission observed by this experiment is less than the actual enhancement.

In general, the time profiles determined from the OSO-IV data are affected by the presence of unresolved rapid fluctuations in X-ray brightness caused by flares. Figure 8 illustrates this point. The time history of the X-ray emission in the three OSO-IV wavebands is shown for two active regions. Also shown are higher time resolution, 2 to 12 Å total solar X-ray flux measurements for this period (Drake et al., 1969), and 2800 MHz radio flux measurements (Covington, private communication). One effect of the low time resolution of the OSO-IV instrument is to increase the apparent duration of the impulsive X-ray flares. However, the X-ray images allow the identificiation with only small

ambiguity of the active regions responsible for the flare X-rays. Moreover, by comparison with high time resolution data, it is easy to distinguish those portions of the OSO-IV data which are affected by the impulsive X-ray bursts. By means of comparisons between the OSO-IV data and higher time resolution total solar X-ray flux measurements, we have been able to distinguish periods in which the time history of a particular active region is relatively unaffected by unresolvable fluctuations.

For convenience in analysis, we have chosen to divide observed X-ray events arbitrarily into three classes on the basis of their durations. Events of duration less than 8 hours are termed "flares". Events of duration greater than 24 hours are called "slow variations". Events with intermediate duration are termed "long enduring brightenings". Although, the bounds of these classes are established arbitrarily, it is plausible to expect that at least two, and possibly three, different physical mechanisms are involved in producing these three classes of events. In general, the time scales of flare-associated soft X-ray events are sufficiently short that such events might be regarded as the dissipation of energy "dumped" in the lower corona by some impulsive process (see for example, the analysis of Hudson et al., 1969). On the other hand, slow variations lasting several days require a more gradual energy input. The intermediate class was established to accommodate events of duration longer than flares but short compared to the slow variations. Four such events are depicted in Figure 9 (the X-ray time history of region 9034 from 28 October to 1 November 1967). Large X-ray flares are superimposed on two of these events. The relationship between long enduring brightenings of the active region and the occurrence of large X-ray flares tends to justify our classification. We have selected the 18 impulsive X-ray events with peak-observed flux in the 2.5 to 12 Å waveband ($2.35 \mu gm/cm^2$ beryllium filter) greater than or equal to 2.5×10^6 photons/cm^2 -sec which were observed during the period 27 October 1967 to 12 May 1968. Three of these events occurred at times when the non-flare level of X-ray emission from the active region was below the threshold of sensitivity of our detector. The time behavior of the

active region before and after the 15 remaining events was examined. In all 15 cases, the large flare occurred during the course of an X-ray brightening of duration between 16 and 18 hours. Smaller X-ray flares, however, are less well associated with the long enduring brightenings.

We have also examined 16 easily identifiable long enduring X-ray brightenings. Of these, only 9 produced major X-ray flares with peak flux greater than 2.5×10^6 photons/cm^2-sec. In fact, no impulsive X-ray events were observed at all in the case of three of these gradual X-ray brightenings. An examination of the fast time resolution total solar X-ray flux records of Explorer XXXV (Drake et al., 1969) in the 2 to 12 Å band and OSO-III in the 1 to 1.6 Å band (Hudson et al., 1969) confirm these results. Therefore, we conclude that the existence of a long-enduring X-ray brightening seems to be required for the occurrence of large impulsive X-ray flares, however, the existence of such a gradual X-ray brightening does not necessarily imply that such a flare or indeed any X-ray flares will occur. The observations of long enduring brightenings which are not associated with X-ray flares rules out the possibility that such events represent the post flare state of the active region.

In Table 4 we list some of the observed characteristics of the three event classes. The quantities listed are typical of the range of measurements made on 49 flares, 16 gradual events, and 18 slow variations. The ranges of duration of the three classes are defined. The peak X-ray counting rates, are extrapolated from the observed time behavior of the event. The total number of observed counts in the detector passband is obtained by numerical integration of the event time profile. The rise and decay times are the time constants of exponential fits to the event counting rate profiles observed through the 2.35μgm/cm^{2}beryllium filter. The peak spectral hardness index is the percentage ratio of the counting rate measured through the 9.4μgm/cm^{2}beryllium filter to the rate measured through the 2.35μgm/cm^{2}beryllium filter at the peak of the event. The spectral hardness index increases as the X-ray spectrum becomes enhanced in shorter wavelength photons, i.e., as the effective temperature of the X-ray spectrum increases.

TABLE 4

TYPICAL CHARACTERISTICS OF THREE EVENT CLASSES: OBSERVED QUANTITIES

	Flares	Long Enduring Enhancements	Slow Variations
Duration	<5 min. - 8 hr.	8 - 24 hrs.	1-9 days
Peak Counting Rate (cnts/140 msec)	$4 \times 10^3 - 10^5$	$7 \times 10^2 - 3 \times 10^4$	$3 \times 10^2 - 8 \times 10^3$
Total Observed Counts (2.5 - 12 Å)	$10^7 - 10^9$	$3 \times 10^8 - 4 \times 10^9$	$5 \times 10^8 - 10^{10}$
Rise Time	<20 min.	1 - 14 hrs	1/2 - 5 days
Decay Time	<20 min. - 1 hr.	1.5 - 12 hrs.	1/2 - 5 days
Spectral Hardness Index*	>50	45	30

* Spectral Hardness Index is the relative X-ray intensity observed in two wavebands. It is a measure of the effective temperature of the emitting regions.

Examination of Table 4 shows that the total number of photons observed in the detector passband for each of the three event classes is roughly comparable. The lower peak fluxes of the longer time scale events are compensated by their longer durations. The peak spectral hardness for the event classes decreases as the duration increases, implying higher temperatures for the more impulsive events, but there is substantial overlap.

c) Spectral Behavior of Active Regions

We have attempted to fit the rising and falling portions of long enduring X-ray events and slow variations to exponential curves. This was done independently for the three different X-ray filters. In general, the exponential rise and decay times are found to be shorter for the same event observed through the thicker filters than through the thinnest. For example, in the case of the long enduring event observed at the east limb from region 9073 at 1630 UT, 10 November 1967 (Figure 8) the rise time as observed through the 2.35μgm/cm^2 beryllium filter (2.5 to 12 Å) is 73 $\pm$ 5 minutes. The rise time measured for the 9.4μgm/cm^2 beryllium filter data (2.5 to 9 Å) is 51 $\pm$ 7 minutes. Similarily, the decay times are 325 $\pm$ 25 mintues for the thinner filter and 260 $\pm$ 20 minutes for the thicker filter. Thus, the X-ray spectrum becomes enhanced in higher energy photons as the event rises toward maximum intensity, i.e., the effective temperature of the active region increases. During the decay phase the spectrum softens. This behavior has been noted for nine cases in which there is a statistically significant difference in the characteristic times for the two beryllium filters. In one case, the characteristic rise times in the two filters were equal within the statistical uncertainties. In 12 other cases, the statistical uncertainties in the counting rates through the thicker filter prevented measurement of a meaningful difference in the characteristic times. No events were observed in which the spectrum softened towards the peak of the event.

In Figure 10 we plot the relationship between the counting rates measured through the 2.35 gm/cm^2 beryllium filter and the spectral hardness index for the slow variation of the bright active region shown in Figure 7.

The relationship between spectral hardness and X-ray counting rate is monotonic within the experimental errors. If we assume that 2.5 - 12 Å X-rays are produced by thermal mechanisms, the spectral hardness index will be related to the temperature distribution of the emitting plasma. The exact form of this relationship depends on the shape of the X-ray spectrum as a function of temperature including the effect of emission lines. The spectral hardness index will always increase with increasing temperature. The X-ray counting rate, on the other hand, is a function not only of the temperature distribution, but also of the total emission measure. In the temperature range between one and 10 million degrees, the counting rate in the OSO-IV passband varies at least as strongly as the second power of temperature. The counting rate from an active region is linearly proportional to the emission measure of the region. This implies that the OSO-IV instrument is more sensitive to changes in temperature than to changes in emission measure. The monotonic relationship between the counting rate in the OSO-IV passband and the spectral hardness index shown in Figure 10 implies that, for the six-day period plotted in Figure 7, the variations in the X-ray counting rate of the active region were associated with variations in its temperature distribution. In fact, most of the variation in the counting rate can be accounted for by the temperature variation. Because of uncertainties in the spectral response of the instrument in orbit, and the lack of exact knowledge of the form of the X-ray spectrum, it is difficult to determine the exact variation in emission measure of an active region during a non-flare X-ray increase. A change in the emission measure of the region of more than a factor of three would, however, be inconsistent with the data shown in Figure 7 and 10.

Thus, both measurement of relative time constants in two wavebands and direct spectral hardness measurements indicate that most non-flare variations in active region X-ray emission in the 2.5 - 12Å band are associated with changes in the average temperature of the emitting plasma. In a similar manner Culhane and Phillips (1970) have interpreted the decay phase of X-ray flares as a cooling of the emitting coronal plasma. It would appear then that the average temperature of the coronal active region can change over characteristic time scales ranging from minutes to days.

The differences in 2.5 - 12 Å X-ray counting rate between one active region and another are due both to spectral differences and to differences in the total emission measure of the regions. For example, during the period on 10 November 1967, shown in Figure 8, the X-ray counting rates observed from region 9047 were a factor of five higher than the rates observed from region 9073 at the same value of the spectral hardness index. Since equality of spectral hardness implies equality of average temperature, the total emission measure of region 9047 must have been a factor of five larger than that of region 9073 at the time of the measurements.

5. Relationship between X-rays and Other Solar Emissions

a) X-ray and Hα Flares

In general, individual X-ray impulsive events are associated with individual Hα flares. Teske and Thomas (1969) have shown that, with only one possible exception, all Hα flares of importance one or greater are accompanied by an impulsive soft X-ray event. Most, if not all, subflares are also accompanied by detectable X-ray emission.

The reverse correlation is not quite as obvious. Many X-ray events occur in active regions which are at or beyond the limb in Hα. Thus the Hα event, if any, accompanying a particular X-ray event may be unobservable. We have selected a set of X-ray events for which there was a high probability that any accompanying Hα event could be observed. The center of intensity of the X-ray event was assumed to overlie the center of its CaK region. The center of the CaK region was required to be within 75° of the central meridian. The maximum X-ray counting rate observed from the central 1 arc-minute of the flare image was required to be above a threshold which (for a typical flare image) would correspond to a photon flux integrated over the flare image of 6.3×10^{5} photons/cm^{2}-sec. The time of the X-ray peak was required to be within a period of Hα flare patrol. Between 27 October 1967 and 12 May 1968, 97 impulsive X-ray events were observed which satisfied these conditions. A search was then made of the solar flare listings in the Solar-Geophysical Data Bulletins. An X-ray event was considered to have an Hα counterpart if an Hα flare or subflare was found in the active region producing the X-ray event, with the time of Hα maximum occurring within 10 minutes of the X-ray maximum. Hα counterparts were identified for 92

X-ray events. These Hα events varied in importance from -f to 3b.

In Figure 11 we have plotted the peak observed X-ray intensity integrated over the flare image as a function of Hα importance classification. Although there may be a tendancy for large X-ray events to be associated with Hα flares of greater importance, a large range of Hα importance classifications can be covered at moderate X-ray intensities. It should be noted that the actual X-ray peaks of these flares may in some cases be larger than the values plotted because of the time resolution of the OSO-IV telescope. However, the magnitude of the underestimate of the X-ray flux introduced is substantially less than the range of X-ray fluxes covered by a single Hα importance classification.

It would appear that virtually all X-ray events with intensity at 1 a.u. in the detector passband greater than 6.3×10^5 photons/cm^2-sec are accompanied by Hα flares. However, these results show that the importance classification of Hα events and the peak X-ray emission associated with a particular event are not well correlated. This lack of correlation cannot be explained entirely by the time resolution of the OSO-4 instrument. A more quantitative index of Hα emission is required before chromospheric and coronal flare phenomena can be compared.

b) X-ray Active Regions and the Slowly Varying Component of the Radio Flux

The general correlation between solar soft X-ray emission and microwave emission is well known (Kundu, 1965). We have already mentioned the correspondence in location between the X-ray emitting regions and the sources of the 9.1 cm radio flux. Several observers (Reidy et al., 1968; Chubb et al., 1961) have noticed the general correlation between the peak radio brightness temperature, T_b, of a solar active region and its X-ray flux.

We have compared the 9.1 cm peak brightness temperature of active regions measured by the Stanford Radio Astronomy Institute (Solar Geophysical Data Bulletins) with the value of the X-ray photon flux measured by the OSO-IV telescope at the same time. Figure 12 shows this comparison. Measurements made during impulsive X-ray flares have been omitted. There is a strong tendancy for high X-ray flux to be accompanied by high T_b; however, there is a significant scatter in this relationship. One could conjecture that this

scatter is due to the variations between active regions. On the other hand, it is easily shown that even for a single active region, the relationship between 2.5 to 12 Å photon flux and 9.1 cm T_b is not monotonic. Figure 13 shows the trajectories on the N_x, T_b plot of individual regions of high activity. In Figure 13a, the X-ray flux of region 9073 actually decreases as the radio brightness temperature increases. The trajectory of another active region (McMath 9091) is shown in Figure 13b. Here in general, the X-ray counting rate is proportional to the radio brightness temperature; however, there appears to be a large jump in the constant of proportionality over a one day time interval.

Although the behavior of these two regions is different, both types of behavior may be understood, at least qualitatively, in terms of a model in which both X-rays and microwaves are emitted thermally from the same plasma. The behavior of other active regions was intermediate between these two extreme cases.

During the period between 10 November 1967 and 15 November 1967 spectral hardness data was obtained for region 9073. This data implies in the context of a thermal model that the emission integral of the region remained relatively constant while the electron temperature decreased. If the emitting region is considered optically thin to 9.1 cm radiation and if this radiation is emitted by the thermal bremsstrahlung process, the radio brightness temperature should increase as the X-ray intensity decreases, $T_b \sim T^{-1/2}$ (Kundu, 1965). This is the behavior shown. On the other hand, the generally linear relationship between T_b and X-ray intensity for region 9091 might indicate that the temperature of this region remained constant while the emission measure increased. The jump in X-ray intensity at constant radio brightness temperature might indicate an increase in temperature, accompanying a continued increase in emission measure. The ensuing decrease in both T_b and X-ray intensity might indicate a drop in emission measure at constant temperature. Unfortunately, spectral hardness information was not obtained during this period and so the temperature behavior

of the region is unknown. The region was born on the disk on 24 November and the interpretation of the X-ray and radio behavior is consistent with slow emergence of the coronal region through 28 November, a sudden rise in temperature, and then the gradual occultation of the region as it passed the limb on 1 December.

The behavior observed for region 9073 is inconsistent with a model in which the region is optically thick to 10 cm radiation. If the region were optically thick, the observed decrease in both the spectral hardness and X-ray flux would have been accompanied by a decrease rather than an increase in radio brightness temperature.

c) X-ray Events and Microwave Bursts

Several observers (Teske and Thomas, 1969; Wende, 1969; Donnelly, 1968; Neupert et al., 1969) have studied the relationship between soft X-ray flux increases and microwave radio bursts. Detailed correlation for any but the largest events has been hindered by the lack of spatial resolution and also the concomitant low signal-to-noise ratios. This problem is alleviated by imaging X-ray detectors, such as that of OSO-IV, in that the region responsible for the X-ray emission can be identified and analyzed independent of the X-ray flux from other active regions.

As a preliminary step, we have established the statistical relationship between reported 10 cm radio bursts and the soft X-ray events observed by the OSO-IV telescope. During the period 27 October to 3 December 1967, 62 distinct outstanding events of all classes at 2700 and 2800 MHz were reported by Covington, Gagnon and Moore (1968). For this analysis, we have considered complex events as single events. Fifteen events occurred while the spacecraft was either within the earth's shadow or passing through regions of high trapped particle flux. X-ray brightenings of at least two standard deviations in the flux from an individual active

region were observed in conjunction with 43 of the remaining 47 outstanding events at 10 cm. Three of the four radio bursts that were not observed to be X-ray events were of duration less than the 307 seconds necessary to complete a solar scan. None of the radio bursts which were unobserved in X-rays exceeded 4×10^{-22} watts-m^{-2}-Hz^{-1} in peak flux at 2800 MHz. Thus, of the 39 centimeter-wave radio bursts of duration longer than five minutes, 38 produced noticeable X-ray brightenings. Similarly, 37 of the 38 centimeter radio bursts with peak flux greater than 3×10^{-22} watts-m^{-2}-Hz^{-1} produced noticeable X-ray brightenings regardless of duration. We therefore consider it to be reasonably certain that any radio event of longer duration than 5 minutes and greater peak flux than 4×10^{-22} watts-m^{-2}-Hz^{-1}, has an observable X-ray counterpart.

Kawabata (1960) has pointed out the statistical correlation between long enduring microwave radio bursts (both gradual rise and fall bursts and post burst increases) and soft X-ray flux enhancements. We have examined the relationship between a specific long enduring microwave burst at 2800 MHz and the corresponding X-ray event.

During the period 1650 UT to 2030 UT on 10 November 1967 (shown in Figure 8), Covington, Gagnon and Moore (1968) distinguish two separate radio events at 2800 MHz. One is a complex event which we associate with the impulsive X-ray bursts observed by the solar X-ray flux monitors on Explorer XXXV. Most of these impulsive bursts can be attributed to region 9047. The second microwave event is a gradual rise and fall radio burst (simple 3A) which we associate with the X-ray brightening of region 9073.

In Figure 14 we show the time histories of the 2800 MHz simple 3A burst (Covington, private communication) and the X-ray brightening of region 9073. If the association of the radio event with the X-ray event is correct, we see that the X-ray brightening begins slightly earlier than the

radio burst and continues for much longer. The X-ray intensity rises to two standard deviations above the previous mean level at 1640 UT. The radio burst is listed as starting at 1650 UT (Covington et al., 1968). The duration of the radio burst is given as 220 minutes. The time of the peak of the X-ray event is somewhat uncertain, but it is clear that the peak of the radio burst occurs 20 to 40 minutes before the peak of the X-ray event. The presence of this substantial time delay would appear to argue against models in which the long enduring radio burst and long enduring X-ray burst are produced by the same mass of plasma by a thermal process.

6. Discussion

The time histories of individual active regions indicate that even in the absence of flares, the 2.5 - 12 Å X-ray output of a region can vary by as much as an order of magnitude. The X-ray spectrum of an active region becomes harder as its X-ray flux increases and softer as its X-ray flux decreases. Thus, not only flares but slower active region changes as well, involve variations in the temperature distribution of the emitting plasma. Comparison of the X-ray flux and 9.1 cm radio brightness of individual active regions is generally consistent with this interpretation.

The OSO-IV X-ray telescope observations contribute to a crude estimate of the energy budget of the coronal portions of an active region. The majority of the energy radiated by the corona is emitted in the form of X-ray lines and continuum radiation. Therefore, the OSO-IV telescope observations are measurements of the radiative losses of individual coronal active regions. It is consistent with the observations reported here to consider a typical quiescent active region as having a temperature of 3×10^6 K and an emission measure on the order of 10^{48} cm^{-3}. A region might be expected to remain in this state for approximately three rotations. Some active regions were observed by OSO-IV for as much as 5 rotations, while other were observed for only one rotation. Using the results of a recent calculation of

the coronal X-ray spectrum by Tucker and Koren (1971), we find that a coronal active region with the parameters estimated above will radiate 2.2×10^{25} ergs/sec. Thus, the total energy radiated by the coronal portion of the active region excluding flares and long enduring bursts will be on the order of 10^{32} ergs. Noyes et al. (1970), have estimated the conductive flux in the transition zone below quiescent active regions to be approximately 3×10^{6} ergs/cm^{2}-sec. Higher resolution solar X-ray photographs from rockets (Vaiana et al., 1968; Vaiana and Giacconi, 1969; Van Speybroeck et al., 1970; Krieger et al., 1970) show that the general outline of coronal active regions observed on the disk resembles that of the corresponding Hα and CaK plages. Therefore, using the average CaK area from Table 2, and ignoring the effects of possible unresolved details in the structure of the bases of coronal active regions, the power conducted downward would be typically about 5×10^{26} ergs/sec. If these assumptions are realistic, the energy losses in the coronal portions of quiescent active regions are dominated by conduction.

During a typical long enduring X-ray event (for example, Figure 7 or 9) the X-ray counting rate from an active region in the OSO-IV telescope waveband is increased by a factor of 5 to 10 above its quiet level. If there is no change in emission measure, this would correspond to a peak temperature during a large event of about 7×10^{6}K, using the spectra computed by Tucker and Koren folded into the OSO-IV spectral response shown in Figure 4. However, the total power radiated by such an event at all wavelengths would only increase to 3×10^{25} ergs/sec. Most of the increased counting rate observed by OSO-IV is produced by the shift in the X-ray spectrum toward shorter wavelengths. An examination of active region X-ray time histories indicates that an active region may be undergoing a long enduring X-ray brightening approximately 10% of the time. Therefore the total energy radiated by the active region in the absence of flares is increased by only about 5% by long enduring X-ray brightenings. However, if the conductive power is roughly proportional to $T^{7/2}$, an increase in temperature from 3 to 7×10^{6}K results in an increase in conductive

loss rate by a factor of 20 and, if long enduring X-ray brightenings take 10% of the total lifetime of the active region, the total energy requirements of the coronal active region are tripled.

The contribution of impulsive X-ray flares to the total energy loss from the coronal portion of active regions is probably small with the possible exception of the giant flares which are observed only a few times in each solar cycle. In order to estimate the energy radiated in flares, we note that over the 18 days of observation of region 9073, between 25 and 50% of the total counts observed in the OSO-IV telescope passband were emitted during flares, where the uncertainty is primarily due to the time resolution of the instrument. On the other hand,if we assume that the peak temperature of flare events is on the order of 20×10^6K, reference to the X-ray spectra of Tucker and Koren (1971) and the OSO-IV telescope spectral response (Figure 4) indicates that flares are detected approximately 25 times as efficiently as quiescent active regions. Thus only about 2% of the total radiated energy appeared in the form of flares. The contribution from unresolved flares of duration less than 20 minutes is probably no greater than the same magnitude.

The total energy radiated by the coronal portion of the active region during its lifetime is not much greater than the energy radiated in the absence of flares and long enduring bursts, a few times 10^{32} ergs. The total energy conducted downward during the lifetime of the region can be estimated to be an order of magnitude larger, although the detailed configuration of the magnetic field could either increase or decrease this figure substantially. These energy losses must be balanced by energy inputs. Mechanical heating by wave dissipation is generally considered to be the major source of energy input to both the quiet corona and active regions, excluding flares. One can ask whether the slow dissipation of

the magnetic field in the coronal portion of the active region might also contribute. It appears that from the point of view of energetics, the radiative losses of the coronal active region could be accounted for by the dissipation of a field of 50 gauss filling a nominal volume given by the average vertical extent, 10^{10} cm, and the Ca K area, 10^{20} cm^2. However, if the conductive losses are as large as we have estimated, then considerably more energy is required.

ACKNOWLEDGEMENTS

We wish to thank Dr. Riccardo Giacconi and Dr. Herbert Gursky for their interest in and contributions to the OSO-IV project since its inception. We are indebted to Michael Bate, Paul Burstein, and Steven Perrenod for their assistance in the data analysis. This work has been supported by the National Aeronautics and Space Administration under Contracts NAS5-11106 and NASW-2070. We would like to especially thank NASA's Goddard Space Flight Center, which has supported our efforts through the OSO Project Office.

References

Allen, C. W.: 1964, Astrophysical Quantities, Athlone Press, 2nd Ed. University of London.

Chubb, T. A., Friedman, H., Kreplin, R. W. and Unzicker, A. E.: 1961, Mem. Soc. Roy. Sci. Liege, 4, 228.

Covington, A. E., Gagnon, H. P. and Moore, J. D.: 1968, Observations of Solar Flux at the Algonquin Radio Observatory on 2800 MC/S and at the Dominion Radio Astrophysical Observatory on 2700 MC/S: National Research Council of Canada, Radio and Electrical Engineering Division Report ERB-780, Ottawa, Canada.

Culhane, J. L. and Phillips, K. J. H.: 1970, Solar Phys. 11, 117.

Donnelly, R. F.: 1968, ESSA Technical Report ERL-81-SDL2.

Drake, J. F., Gibson, J. and Van Allen, J.: 1969, Iowa Catalog of Solar X-ray Flux (2 - 12 Å), University of Iowa, No. 69-36.

Gabriel, A. H. and Jordan, C.: 1969, Mon. Not. R.A.S., 145, 241.

Giacconi, R., Gursky, H., Krieger, A. S., Naranan, S., Paolini, F. R., Vaiana, G. S. and Webb, D. F.: 1970, Final Report for Prime Data Reduction and Analysis of the AS&E OSO-IV Pointed and Wheel Experiments, ASE-2432.

Giacconi, R., Gursky, H., Paolini, F. R. and Rockwell, C.: 1968, Final Report for AS&E OSO-IV X-ray Pointed Telescope and Rotating X-ray Wheel Experiments, ASE-1921.

Giacconi, R., Reidy, W. P., Vaiana, G. S., Van Speybroeck, L., Zehnpfenning, T.: 1969, Space Science Reviews, 9, 3.

Henke, B. L., Elgin, R. L., Lent, R. E. and Ledingham, R. B.: 1967, Norelco Reporter, 14, 112.

Hudson, H. S., Peterson, L. E. and Schwartz, D. A.: 1969, Astrophys. J., 157, 389.

Kawabata, K.: 1960, Rept. Ionsph. Space Science, Japan, 14, 405.

Krieger, A. S., Vaiana, G. S. and Van Speybroeck, L. P.: 1970, Proc. IAU Symp. No. 43, in Paris (ed. by R. Howard), in press.

Kundu, M. R.: 1965, Solar Radio Astronomy, Interscience, New York.

Lincke, R. and Wilkerson, T. D.: 1962, Rev. Sci. Instr., 33(9), 911.

Lukirskii, A. P., Rumsh, M. A. and Karpovich, I. A.: 1960, Optics and Spectroscopy, 9, 343.

Neupert, W. M., White, W.A., Gates, W.J., Swartz, M. and Young, R. M.: 1969, Solar Phys., 6, 183.

Noyes, R. W., Withbroe, G. L., and Kirshner, R. P.: 1970, Solar Phys., 11, 388.

Reidy, W. P., Vaiana, G. S., Zehnpfennig, T. and Giacconi, R.: 1968, Astrophys. J., 151, 333.

Solar-Geophysical Data Bulletins: Published monthly by National Oceanic and Atmospheric Administration, Boulder, Colorado.

Teske, R. G.: 1969, Solar Phys., 6, 193.

Teske, R. G. and Thomas, R. J.: 1969, Solar Phys., 8, 348.

Tucker, W. H. and Koren, M.: 1971, Radiation From a High Temperature Low Density Plasma: The X-ray Spectrum of the Solar Corona, ASE-2597.

Vaiana, G. S. and Giacconi, R.: 1969, Plasma Instabilities in Astrophysics, D. G. Wentzel and D. A. Tidman, Editors ; Gordon and Breach, Publishers.

Vaiana, G. S., Reidy, W. P., Zehnpfennig, T., Van Speybroeck, L. and Giacconi, R.: 1968, Science, 161, 564.

Van Speybroeck, L. P., Krieger, A. S., and Vaiana, G. S.: 1970, Nature, 227, 818.

Wende, C. D.: 1969, J. Geophys. Res., 74, 4649.

Zehnpfennig, T., Giacconi, R., Haggerty, R., Reidy, W. P. and Vaiana, G. S.: 1967, A Laboratory Program to Develop Improved Grazing Incidence X-ray Optics, NASA CR-717.

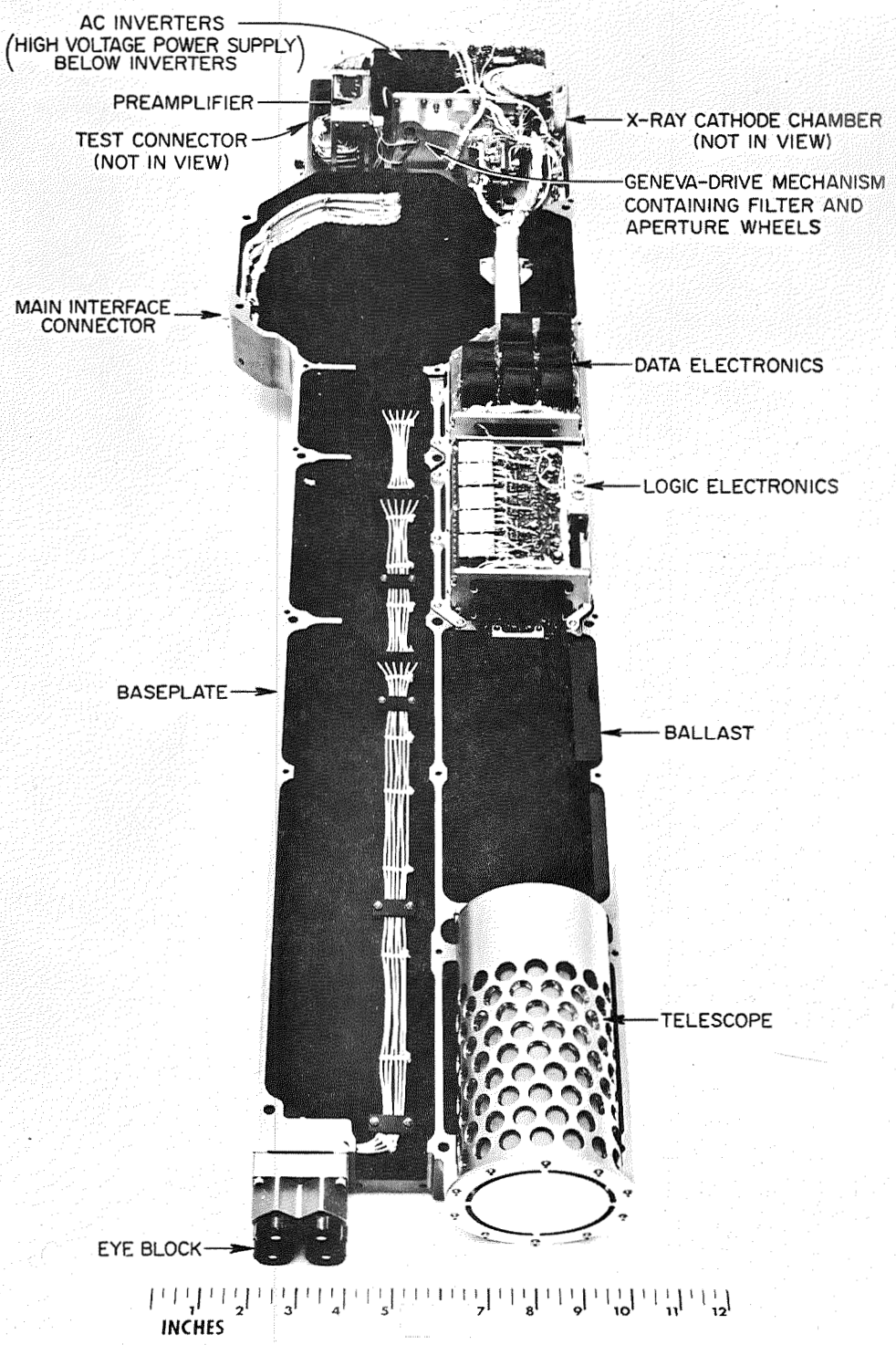

CD - 123A

Figure 1. AS&E pointed X-ray telescope experiment.

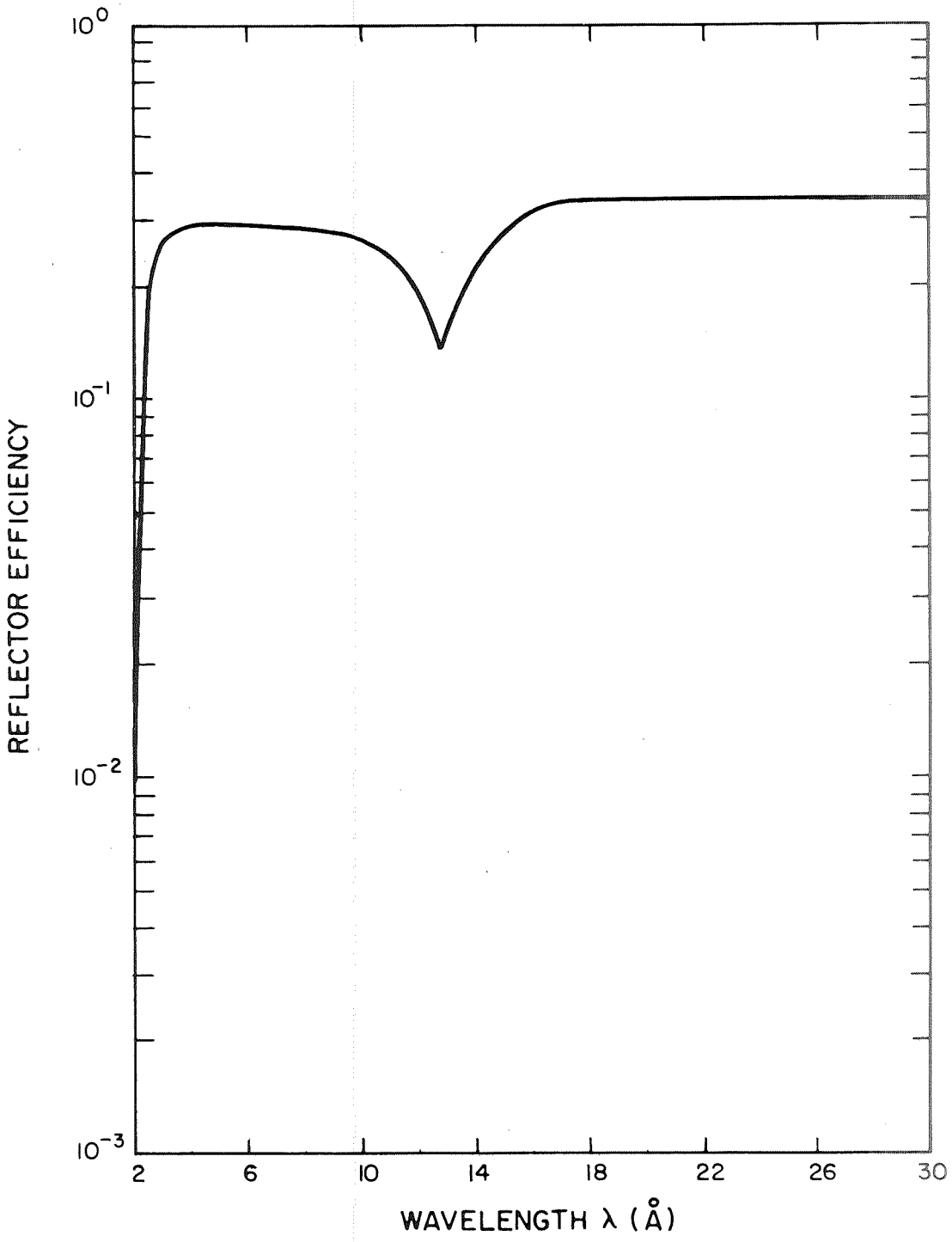

Figure 2. Computed telescope reflection efficiency normalized to the value measured at 8.3 Å.

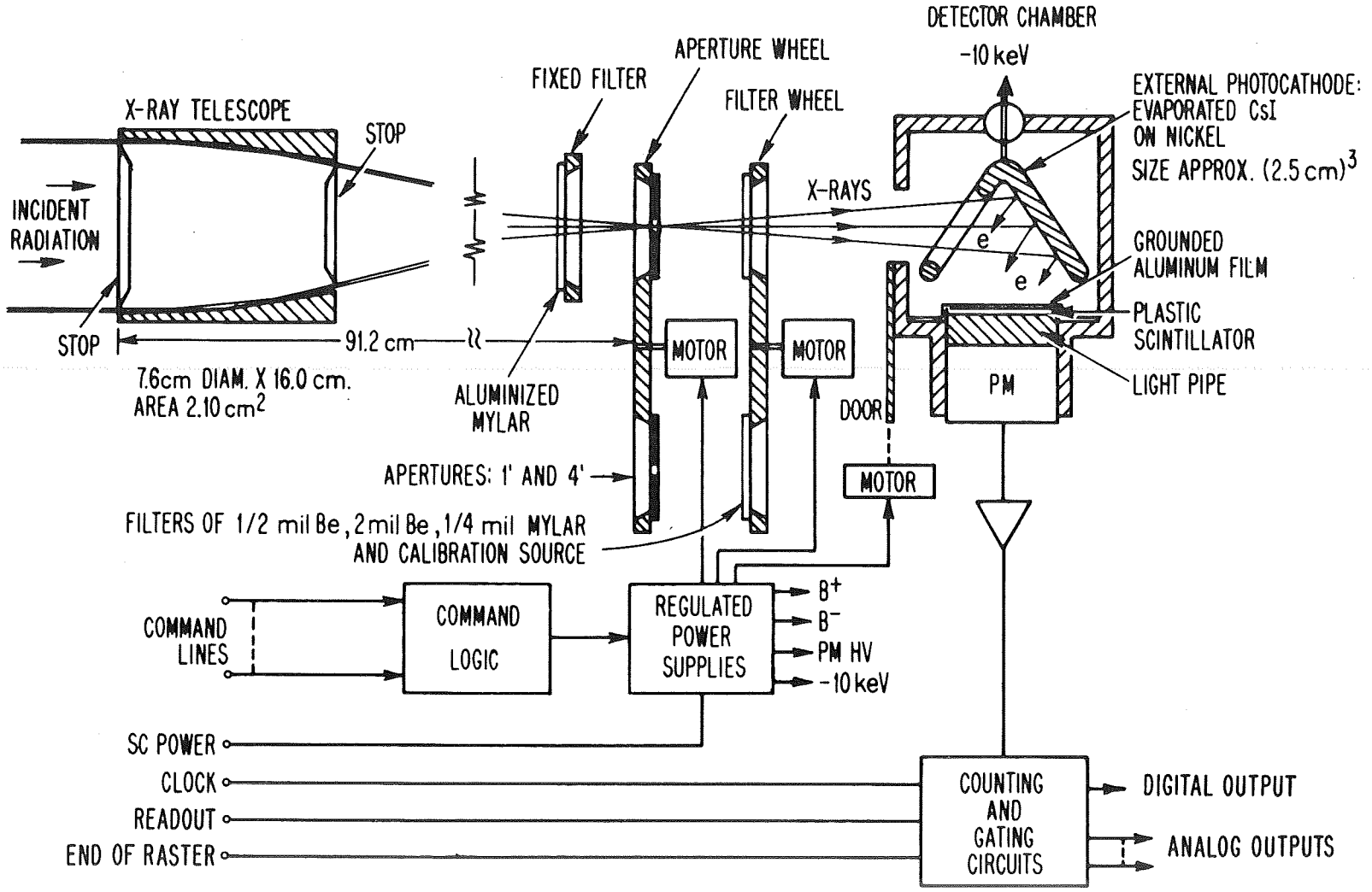

Figure 3. Schematic drawing of the grazing incidence X-ray telescope experiment on the OSO-IV pointed section.

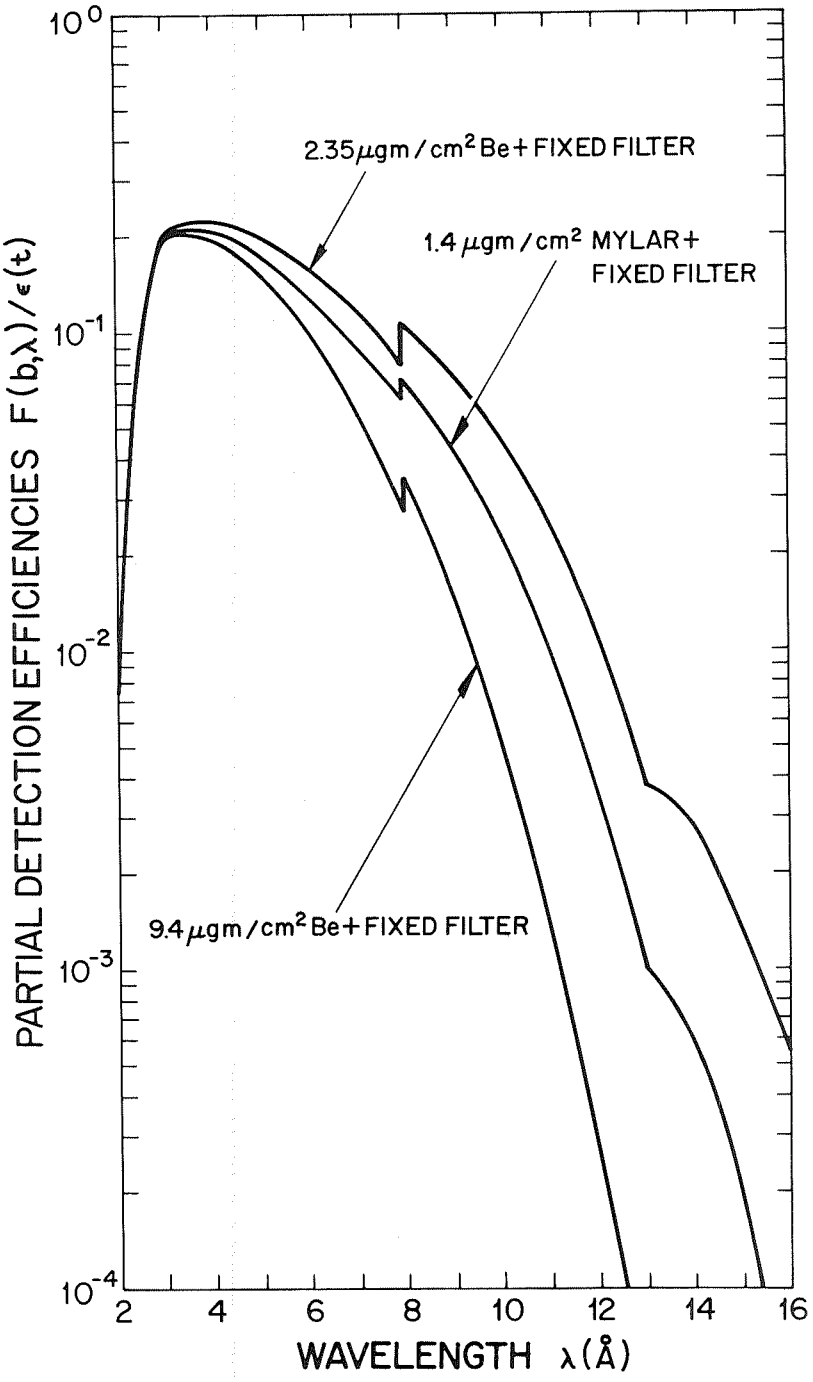

Figure 4. Instrument detection efficiency function for the three filters used in the experiment.

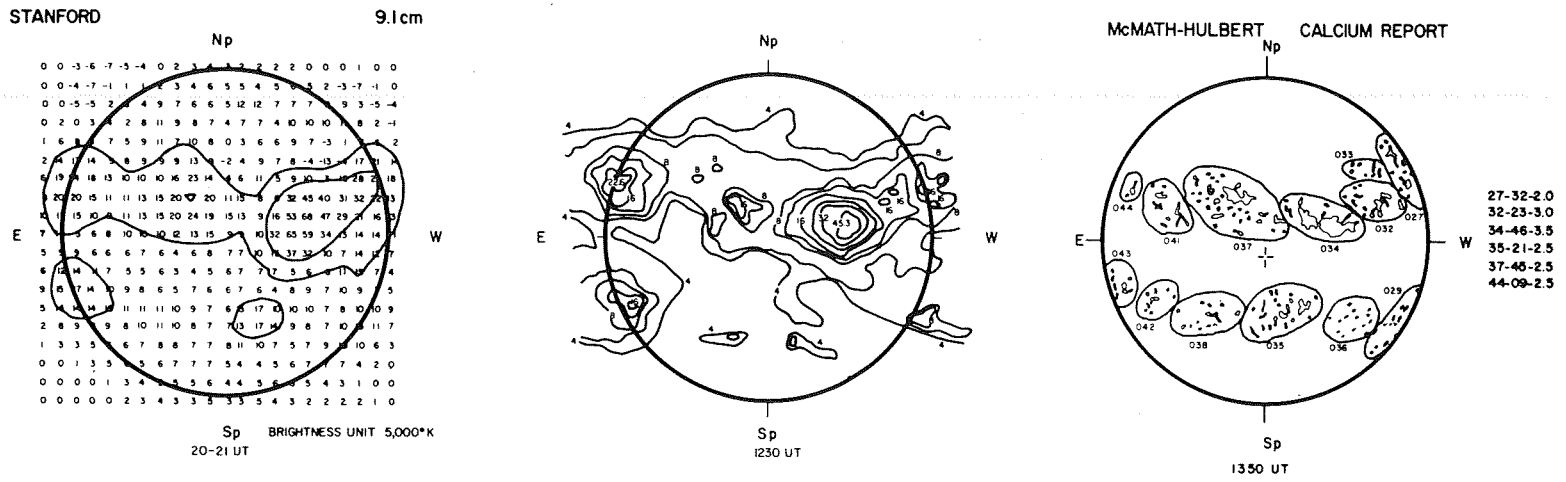

Figure 5. An X-ray contour map of the sun produced on 25 October 1967 by the OSO-IV X-ray telescope experiment. Shown on either side are the 9.1 cm radio and CaK maps for the same date.

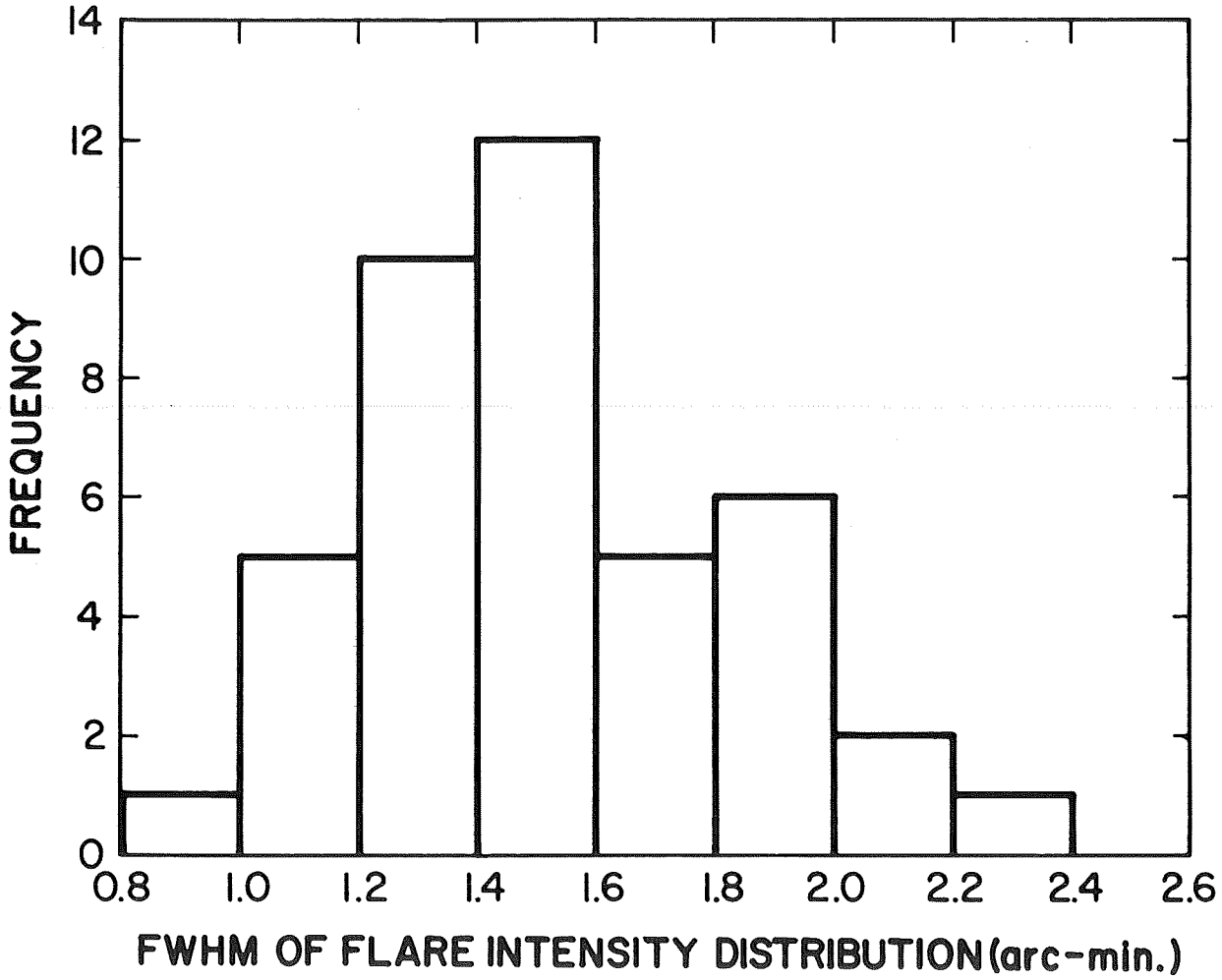

Figure 6. Histogram of the relative frequency of occurrence of the measured full widths at half maximum (FWHM). This is consistent with actual flare sizes of less than one minute of arc.

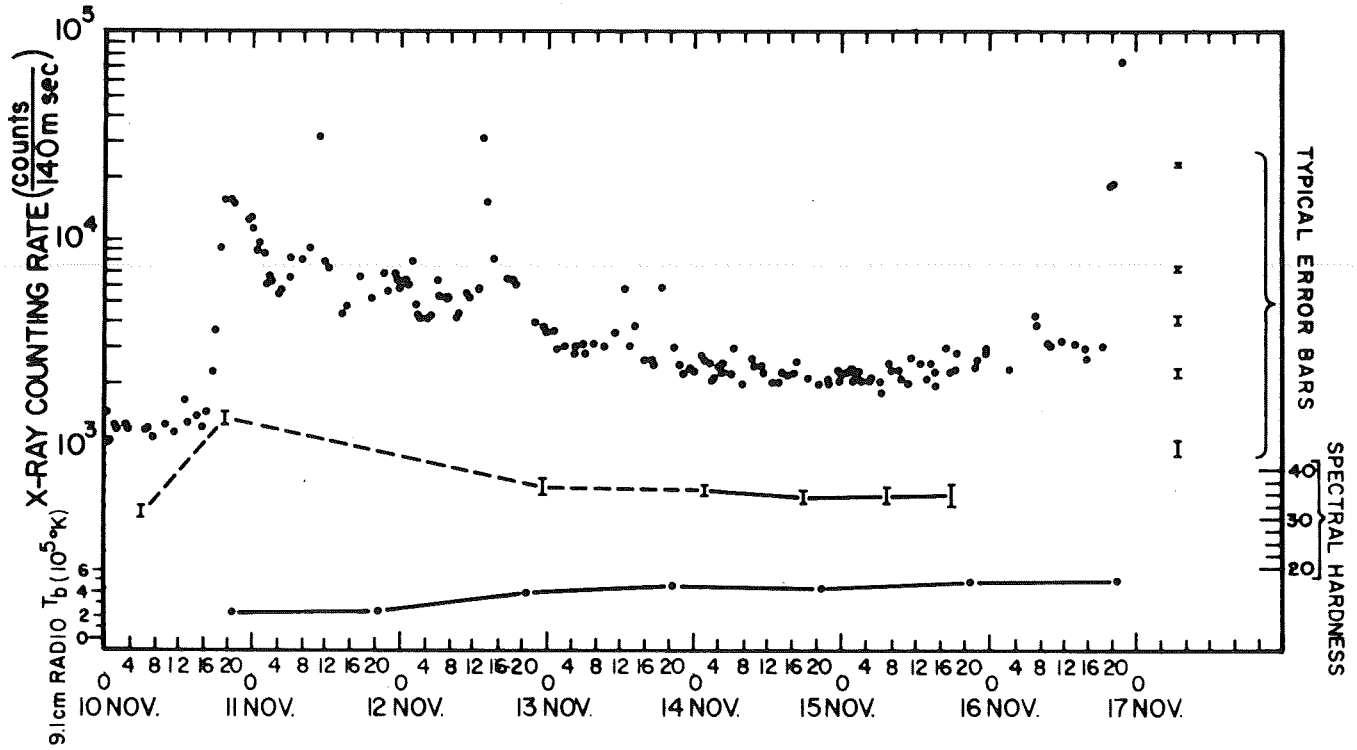

Figure 7. Time history of the 2.5 - 12 Å X-ray emission of McMath plage region 9073 for seven days in November 1967. Also shown are the X-ray spectral hardnesses (see text) and the peak 9.1 cm radio brightness temperatures of the region.

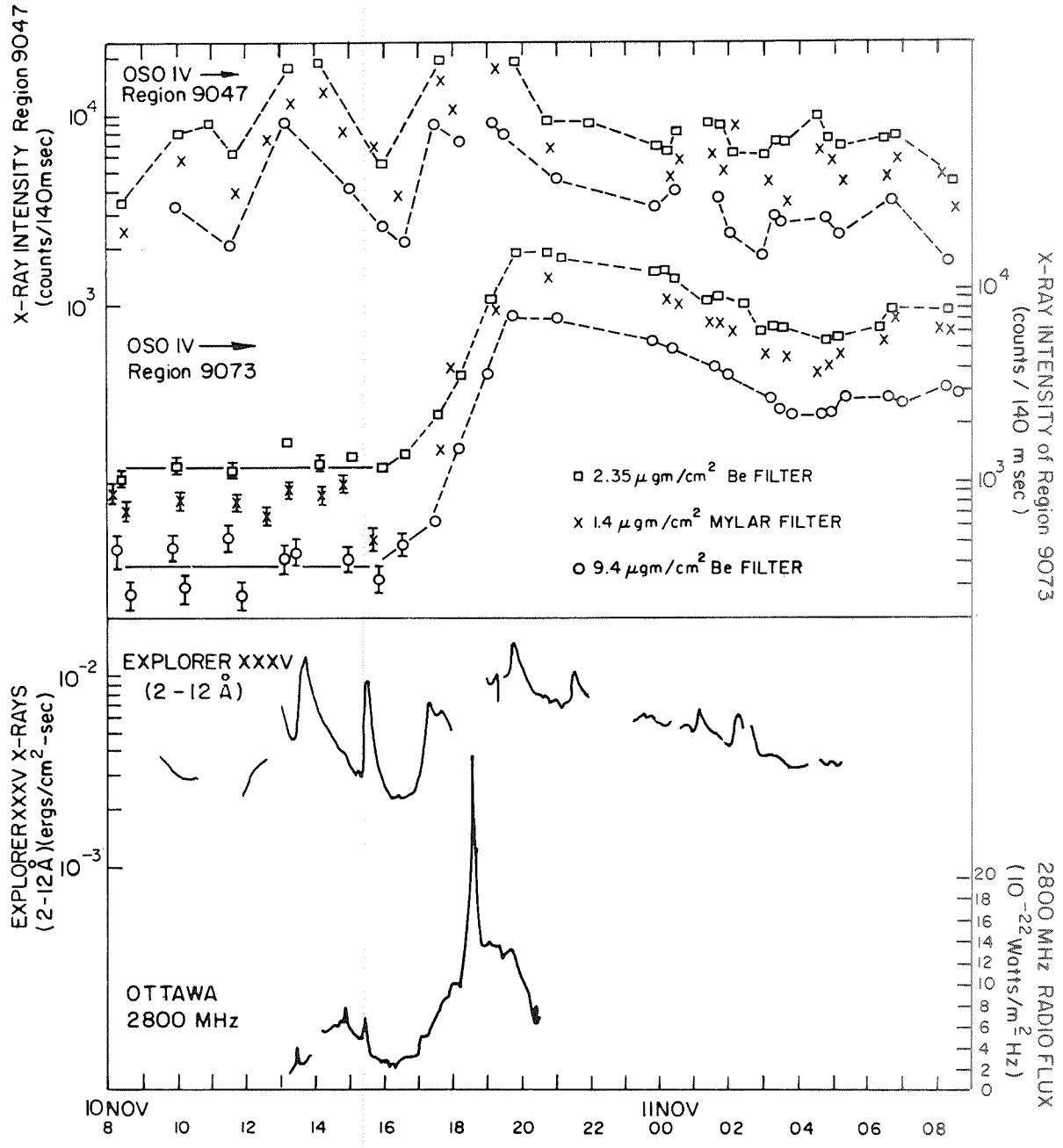

Figure 8. Solar activity from 10 November, 08^h UT, to 11 November 1967, 09^h UT. The top half of the graph shows the X-ray activity from two active regions as observed on OSO-IV. The bottom half shows tracings of data from Explorer XXXV (2-12 Å) and the 2800 MHz radio flux.

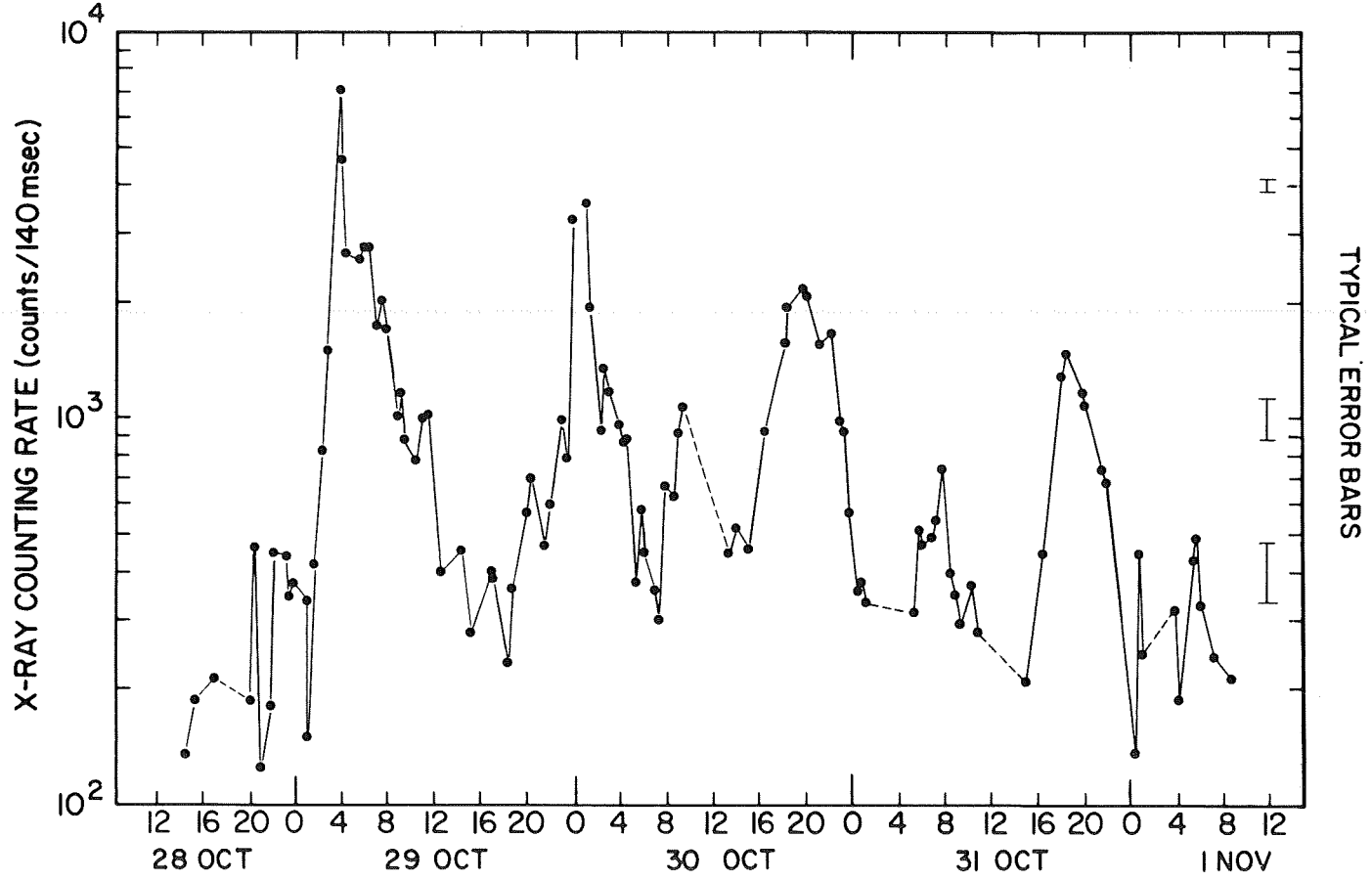

Figure 9. Time history of the 2.5 - 12 Å X-ray emission from McMath plage region 9034 in late October 1967. The aperture mode is one arc-minute. Typical error bars appear on the right side of the plot.

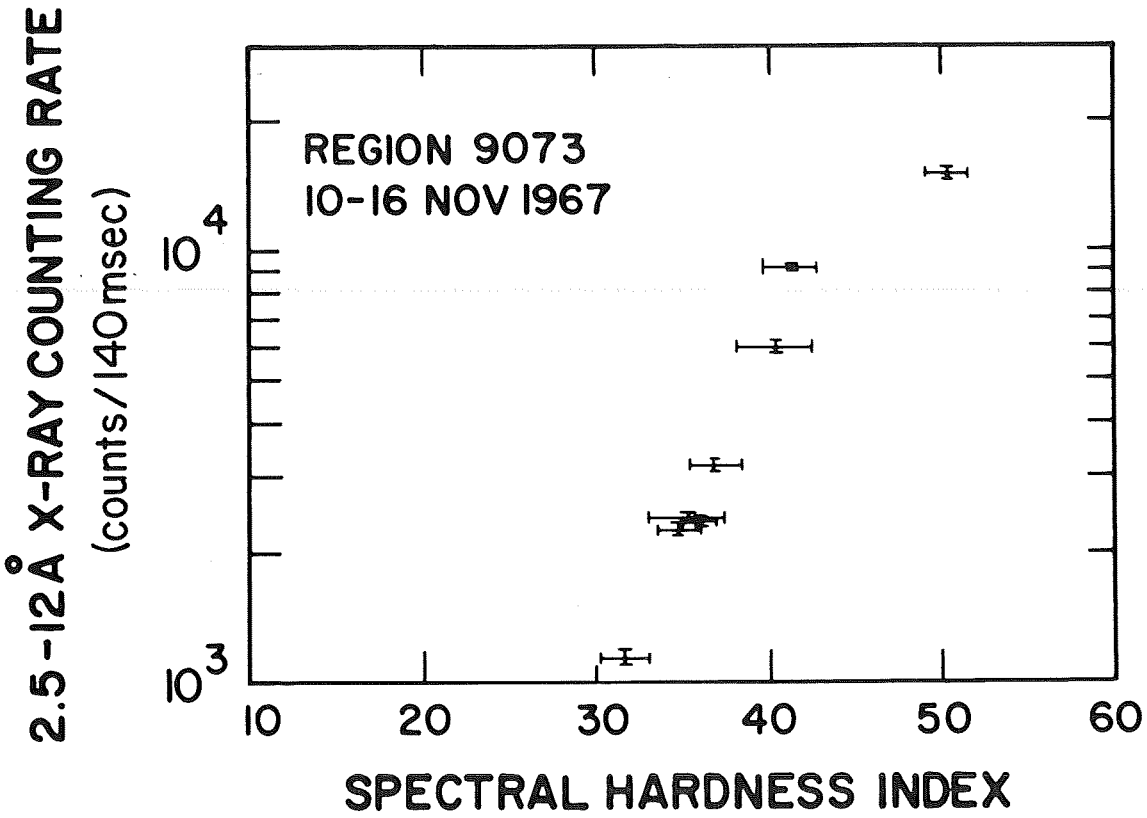

Figure 10. Relationship between the 2.5 - 12 Å X-ray emission and the spectral hardness index for McMath region 9073.

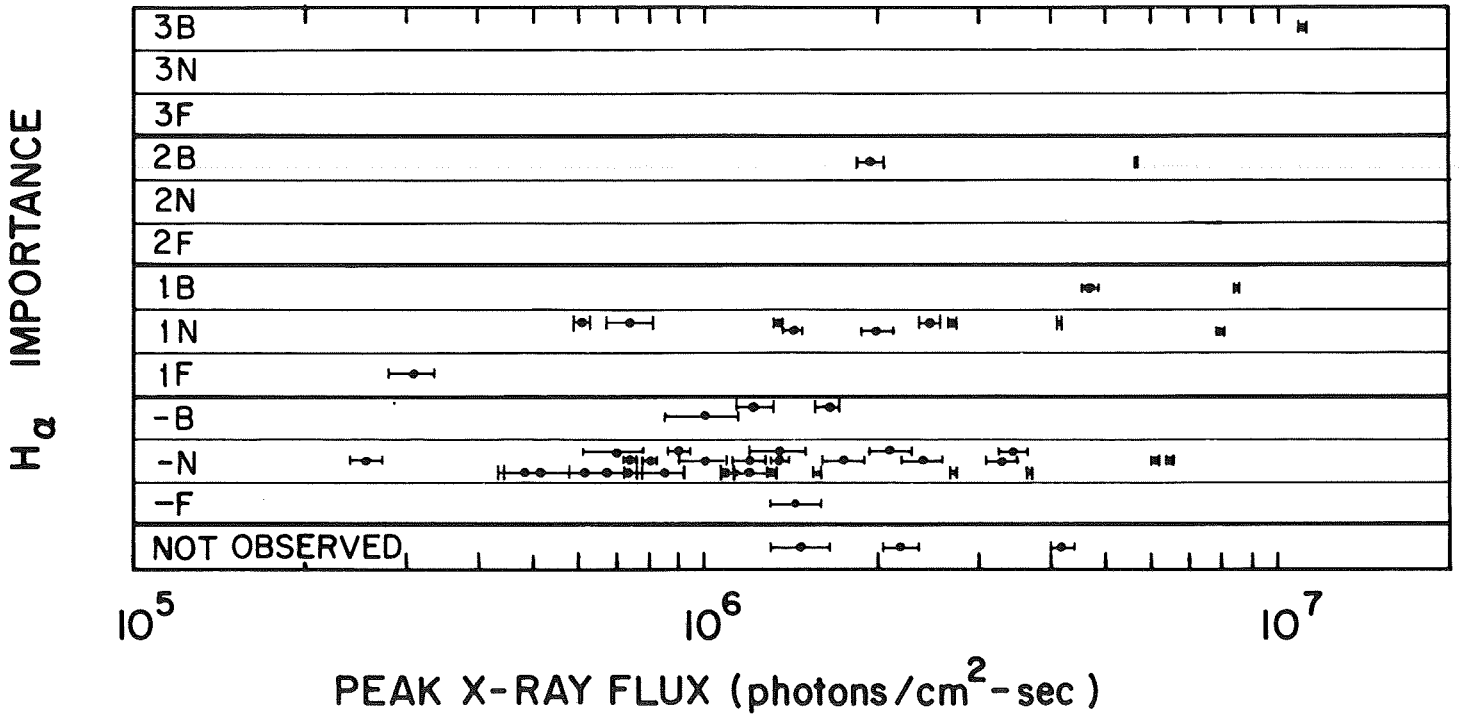

Figure 11. $H\alpha$ importance classification of solar flares as a function of peak X-ray photon flux.

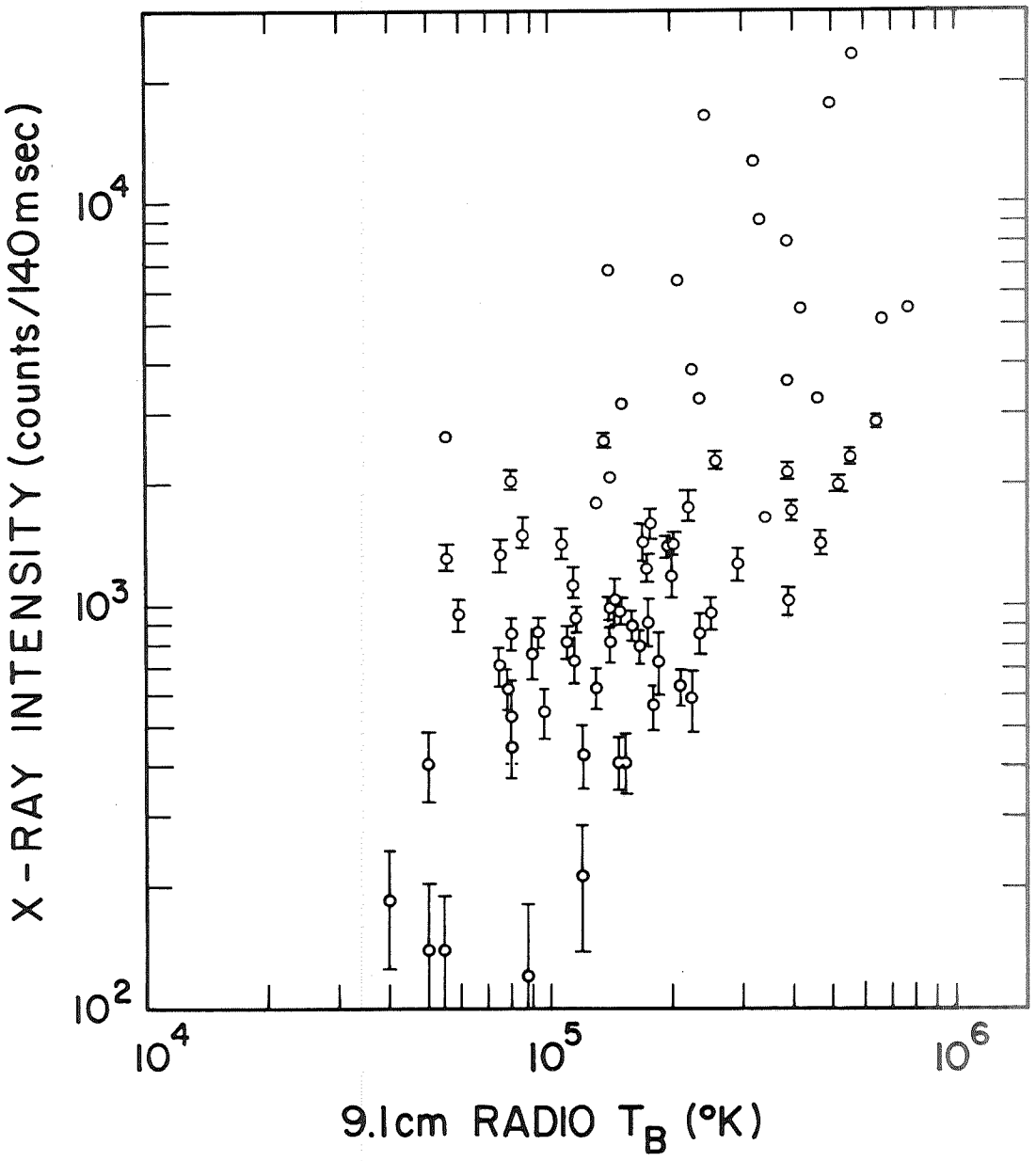

Figure 12. Comparison of X-ray photon flux and 9.1 cm peak brightness temperature for individual active regions.

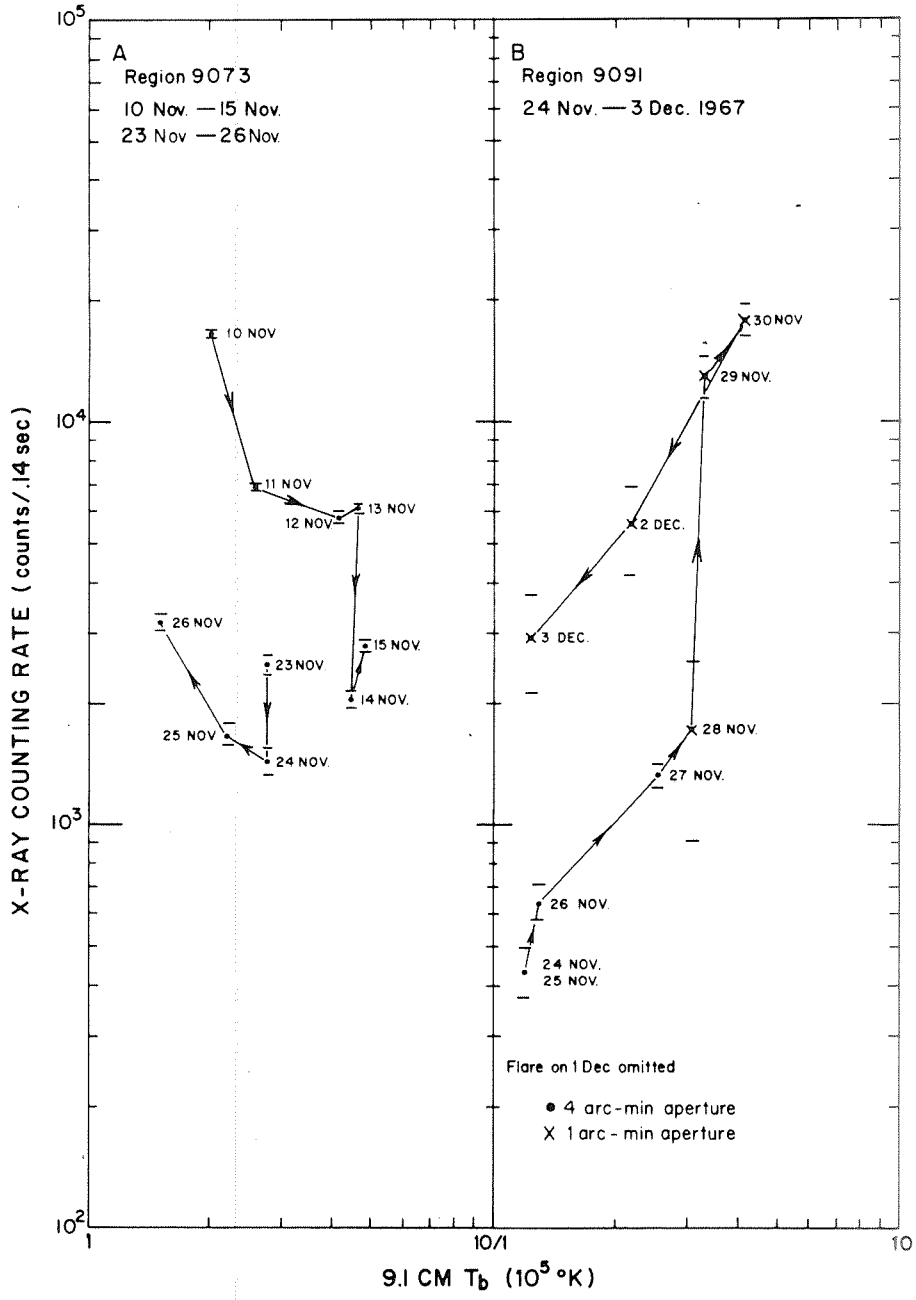

Figure 13. Time behaviour of the X-ray photon flux from two individual active regions as a function of 9.1 cm radio brightness temperature.

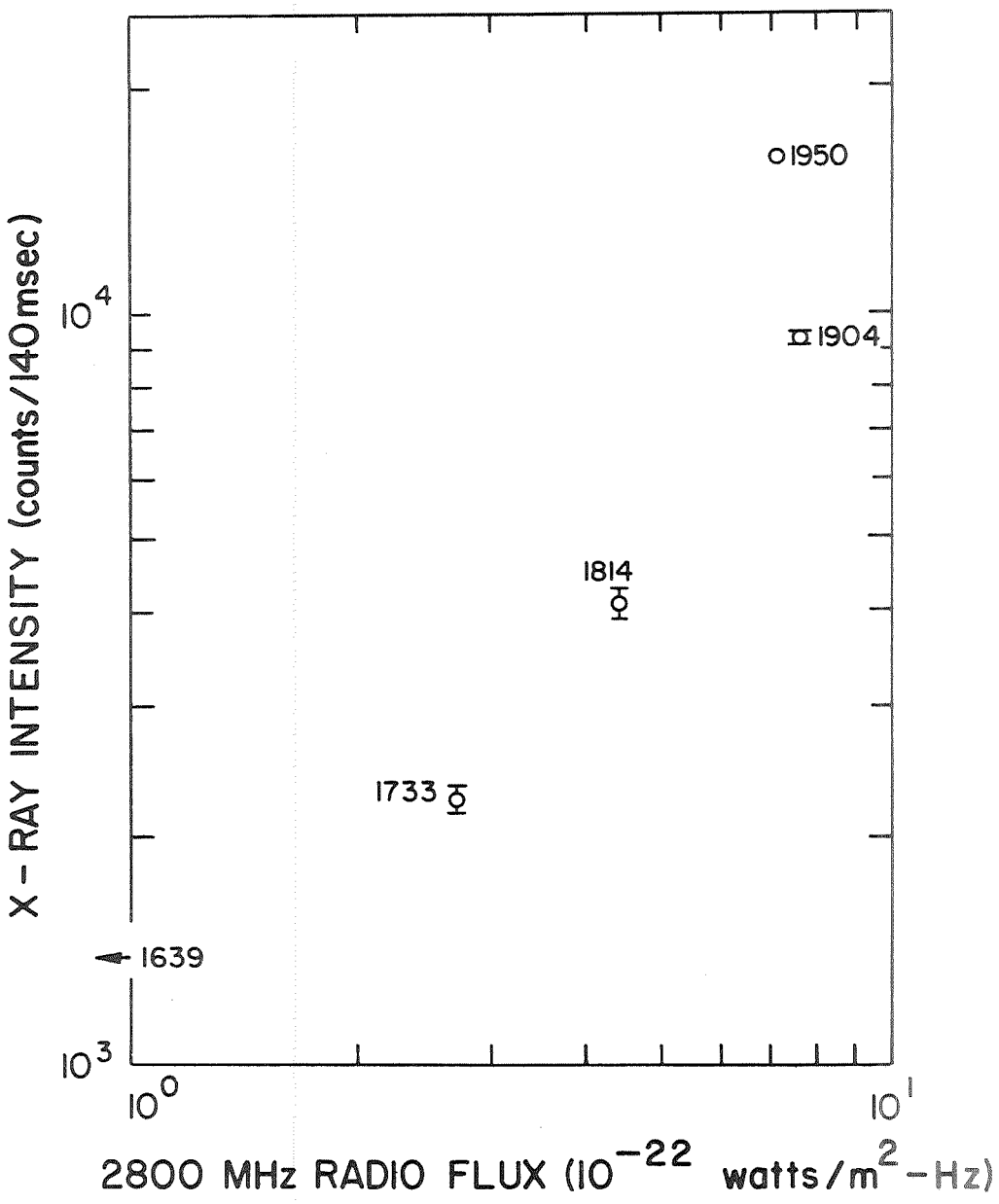

Figure 14. Trajectory of the X-ray photon flux and the 2800 MHz radio flux of an active region (McMath 9073) during the rise phase of a long enduring burst. The time (UT) of each measurement is listed next to the data point. The date was 10 November 1967.

APPENDIX C

ASE-2597-B

RADIATION FROM A HIGH-TEMPERATURE, LOW-DENSITY PLASMA: THE X-RAY SPECTRUM OF THE SOLAR CORONA

Wallace H. Tucker and Marvin Koren*

American Science and Engineering
Cambridge, Massachusetts 02142

Received 1971 February 13

ABSTRACT

The results of calculations of the 0.5 - 70 Å X-ray spectrum of a high-temperature, low-density plasma are presented. The temperature range is $6 \times 10^{5\,o} - 10^{8\,o}$K, and the elemental abundances characteristic of the solar corona have been assumed. We have considered the processes of line emission following electron collisional excitation, radiation resulting from recombination, bremsstrahlung, and two-photon decay following the excitation of the metastable $2\underline{S}$ state in hydrogenic and heliumlike ions.

*Present address: U. S. Army Strategic Communications Command, Fort Huachuaca, Arizona.

INTRODUCTION

We present here the results of calculations of the 0.5 - 70 Å X-ray spectrum of high-temperature, low-density plasma having an electron temperature in the range $6 \times 10^{5\,o} - 10^{8\,o}$K and elemental abundances equal to those generally believed to exist in the solar corona. We have made the usual assumptions of steady-state conditions and negligible absorption and have considered the processes of line emission following electron collisional excitation, radiation resulting from recombination, bremsstrahlung, and the two-photon decay following the excitation of the metastable 2S state in hydrogenic and heliumlike ions.

Apart from differences in the values assumed for some of the cross-sections, these calculations differ from previous ones (Culhane 1969; Landini and Fossi 1970, and references cited therein) primarily in that we have included a large number of lines, some 459 in all, and in the consideration of the two-photon process. It turns out that this latter process is not too important, so our results for the continuous spectrum are not significantly different from those of Culhane (1969) and Landini and Fossi (1970). However, because of the much larger number of lines considered, our results for the total spectrum differ somewhat from those of Landini and Fossi (1970) with regard to both the relative importance of line radiation versus continuum radiation and the detailed shape of the spectrum.

In § II the basic assumptions and equations employed in the calculations are discussed, and in § III the results are presented in the form of tables and graphs.

II. BASIC EQUATIONS AND ASSUMPTIONS

a) The Discrete Spectrum

In a low-density plasma such as the solar corona, line emission results from downward radiative transitions following the population of an excited level either by recombination or by inelastic collisions. The emitted photon may be resonance absorbed and reemitted, but we assume here that it eventually escapes from the hot plasma.

i) Line Emission following Electron Collisional Excitation

The X-ray emission lines in the coronal spectrum are produced primarily as a result of this process. The energy emitted per unit volume per unit time due to excitation of level n followed by a downward transition to a level n' is given by

$$dE_{L,Z,z}(nn')/dtdV = P^{ex}_{L,Z,z}(nn') = N_e N_{Z,z} E_{Z,z}(nn') \langle Q_{Z,z}(n) v \rangle, \qquad (1)$$

where N_e is the electron density, $N_{Z,z}$ is the density of ion species Z, z, $E_{Z,z}(nn')$ is the energy of the line, $Q_{Z,z}(n)$ is the cross-section for excitation of the level n from the ground state, v is the electron velocity, and the angular brackets denote an average over a Maxwellian distribution of electron velocities. Excitation cross-sections are often expressed in terms of the collision strength Ω:

$$Q_{Z,z}(n) = \pi a_o^2 \, \Omega_{Z,z}(n, k_i^2)/k_i^2 , \qquad (2)$$

where k_i^2 is the indicent electron energy in rydbergs and a_o is the Bohr radius. Since Ω is a slowly varying function of energy, the rate of radiative energy loss per unit volume for species Z, z and transition n-n' is given approximately by

$$P^{ex}_{L,Z,z}(nn', T) = 1.86 \times 10^{-19} T_6^{-1/2} N_e N_{Z,z} \langle \Omega(n) \rangle (E(nn')/I_H) B(nn') \times \exp(-E_{Z,z}(n)/kT) \quad \text{ergs cm}^{-3} \text{ sec}^{-1} \qquad (3)$$

where T_6 is the electron temperature in millions of degrees, $\langle\Omega\rangle$ is an appropriate average value of the collision strength which is approximately equal to its value at $k_i^2 = 1.5\,E(n)$; $E_{Z,z}(n)$ is the excitation energy of the level n; I_H is the ionization potential of hydrogen; and $B(nn')$ is a branching ratio giving the fraction of decays of excited state n that lead to the final state n'.

In order to compute the intensity of line radiation as a function of temperature, one needs to know the density, the abundances of the elements, the ionization equilibrium, the collision strengths, the wavelengths of the lines, and the excitation energies.

Abundances of the elements appropriate to the solar corona were taken to be (Pottasch 1967; Jordan 1966a,b): $A(\log N)$ = H(12.00), He(11.30), C(8.70), N(7.80), O(8.50), Ne(7.60), Mg(7.50), Si(7.70), S(7.30), Ca(6.30), Fe(7.70), and Ni(6.70).

As pointed out by Pottasch, the abundances relative to hydrogen are uncertain by about a factor of 3 due to uncertainties in the methods for determining the hydrogen number density. We have adopted a value for $N(Si)/N(H)$ of 5×10^{-4}, which is the value suggested by Jordan and used by Landini and Fossi (1970) and Culhane (1969).

Jordan's (1969, 1970) calculations of the ionization equilibrium were used. She included the processes of collisional ionization from the ground state, collisional excitation followed by autoionization, radiative recombination, and dielectronic recombination reduced by a density-dependent term. This latter term was computed for a particular model for the solar chromosphere and corona according to which $\log N_e T \approx 14.90$ for $\log T \lesssim 6.10$, $\log N_e = 8.30$ for $\log T \geq 6.10$.

A comparison of her results with results of similar calculations in which the full dielectronic recombination rate was used indicates that the population

of a given ionization state may sometimes be changed by as much as a factor of 4, but for ions which make important contributions to the X-ray spectrum of the solar corona the effect is usually less than 10 - 20 %. It should also be noted that for these ions, the difference between the results of Jordan and other similar calculations (Allen and Dupree 1969; Cox and Tucker 1969) is also small, not more than 20 %.

For calcium, we used the ionization-equilibrium calculations of Burgess and Faulkner (private communication). In these calculations the processes of collisional ionization from the ground state, radiative recombination, and dielectronic recombination were included.

In Table 1 the atomic data used to compute the line intensities are listed. The energy levels needed for the calculations were obtained from Kelly (1968), Chapman (1969), Connerade (1970), Moore (1949, 1952), Widing and Sandlin (1968), Walker and Rugge (1970), Rugge and Walker (1970), and Evans and Pounds (1968). Where necessary, energy levels were determined by isoelectronic interpolation and extrapolation. The specific reference for each line is given in Table 1. The lines referenced WS (Widing and Sandlin), RW (Rugge and Walker) and EP (Evans and Pounds) have been observed in the solar corona.

For the sake of convenience, we often lumped several levels together. Thus, for example, the effective excitation energy for transitions to levels with principal quantum number n greater than or equal to 5 was assumed to be the energy of the $n = 5$ level, and the effective wavelength of the lines resulting from transitions from these levels to a lower-lying level was assumed to be equal to the wavelength of the transition from the $n = 5$ level. A similar procedure was also used for many of the transitions in complex ions with levels of the same n often being lumped together. We indicate in Table 1 the wavelength region over which these lines will be distributed.

Also given in Table 1 are "effective collision strengths" or the product of the collision strength Ω and the branching ratio B. The cross-sections for excitation of the 2p level of hydrogenic ions have been computed recently by Beigman, Vainshtein, and Vinogradov (1970). Their results for the excitation of the 2p level are in agreement with the results of Burgess (1961) to within about 20%. Values of the collision strength which approximate the results of Beigman et al. (1970) to within 30% were adopted, i.e., $<\Omega(1s, 2p)> = 1.5/Z^2$. The cross-sections for the excitation of the higher-n levels should scale approximately according to where f(n) is the oscillator strength for the transition to level n from the ground state. Recent calculations by Krinberg (1970) for the hydrogen atom indicates that this is a good approximation. Hence, we have assumed that $<\Omega(1s, 3p)> = 0.24/Z^2$, and $<\Omega(1s, 4p)> = 0.084/Z^2$. All transitions to levels highter than $n = 5$ were lumped together and assigned the energy of the $n = 5$ level, and the collision strengths summed over all bound levels with $n \geq 5.5$ so that $<\Omega(1s, n \geq 5.5)> = 0.11/Z^2$. For the allowed transitions in heliumlike ions, we scaled the collision strengths from the hydrogenic values according to $f(n)/E(n)$. Recently, it has become clear that magnetic-dipole (^3S-^1S) and intercombination (^3P-^1S) transitions are also important in heliumlike ions. Gabriel and Jordan (1969) have computed the expected intensity of these lines relative to the allowed (^1P-^1S) transitions, and we have used their values. The relative strength of the magnetic-dipole and the intercombination lines is a function of density except in the limit of very low densities $N_e << 10^9$. We have used this low-density limit in our calculations.

For lithiumlike ions, we used the results of Bely (1966a, b) for 2s-3ℓ and 2s-4ℓ excitations. For the excitation of levels with $n \geq 5$, the collision strengths were obtained in the same manner as for the highly excited states of hydrogen and heliumlike ions. For berylliumlike ions we assumed that the collision strength was equal to twice that of the corresponding lithiumlike

ion. For boronlike ions we used the collision strengths calculated by Bely and Petrini (1970) for the excitation of $2p$-$n\ell$ transitions in lithiumlike ions. For the other ions containing from two to five $2p$ electrons in the ground state, we scaled the collision strengths from the boronlike values according to $f(n)/E(n)$. We used the results of Bely and Bely (1967) for the neonlike ions of iron and nickel, and those of Bely (1967) for the sodiumlike and magnesium-like ions.

We have not considered the line emission resulting from the excitation of K-shell electrons of ions having one or more electrons in the $n = 2$ shell. For a Maxwellian gas such as we are considering here, the ratio of the power in these lines, $p(K)$, to the power in lines produced by excitation of heliumlike ions of the same species, p(He-like) is given approximately by

$$p(K)/p(\text{He-like}) \sim (N_Z/N_{\text{He-like}})\, K(Z)\,, \qquad (4)$$

where $K(Z)$ is the K-fluorenscence yield. It is a rapidly increasing function of Z; e.g., $K(10) = 0.00963$; $K(16) = 0.06$; $K(26) = 0.30$. From equations (3) and (4) one sees that K-lines may be important in a narrow temperature range where $N(z) > N$(He-like) and $kT \sim E(K)$, the excitation energy for the inner-shell electron. Such a region does not exist except for the high-Z elements such as iron. In case of iron we find that the K-lines are important in the range $10^7 \leq T \leq 3 \times 10^7$ where they are at most about 20% as powerful as the heliumlike ions; outside this range they make a negligible contribution.

ii) Line Emission following Recombination

Line emission is also produced by the recombination of an electron excited state followed by a radiative transition to the ground state. For the steady-state conditions here, the number of recombinations must equal the number of ionizations, which will always be less than the number of excitations to the first excited state. Therefore, recombination radiation will not dominate the strong lines, and will usually be negligible. It can be shown

that the line radiation resulting from radiative recombination is never important; however, in some cases line radiation following dielectronic recombination makes a nonnegligible contribution.

In the dielectronic recombination of an electron to an ion, the ion is stabilized by radiative transitions which eventually take the ion into the ground state. In general, this will involve the emission of at least two line photons, since the recombination process leaves the ion in a doubly excited state $\underline{n}, \underline{n}''$. The rate of radiative energy loss per unit volume due to the de-excitation of the ionic core in the state $\underline{n}$ can be approximated by the expression

$$P^{di}_{L, Z, z}(nn'', n'n'', T) = N_e N_{Z, z+1} E_{Z, z}(nn') \alpha^{di}_{Z, z}(n) \quad , \tag{5}$$

where $\alpha^{di}_{\underline{Z}, \underline{z}}(\underline{n})$ is the rate coefficient for a dielectronic recombination in which the ionic core is excited to the state $\underline{n}$. Note that to the extent that the influence of the electron in the state $\underline{n}''$ can be neglected the photons produced by this process will have an energy equal to the energy of photons resulting from the collisional excitation of the ion $\underline{z}$ to the state $\underline{n}$. Using the general formula given by Burgess (1965) for $\alpha^{di}_{\underline{Z}, \underline{z}}(\underline{n})$, one can relate $P^{di}_{\underline{L}, \underline{Z}, \underline{z}}(\underline{nn}'', \underline{n'n}'', \underline{T})$ to $P^{ex}_{\underline{L}, \underline{Z}, \underline{z}}(\underline{nn'}, \underline{T})$. The recent work of Shore (1969) indicates that for transitions in which the principal quantum number changes, Burgess's results are systematically too large. From the values tabulated by Shore for recombination to hydrogenic ions, one finds that Shore's recombination rates are related to Burgess's (α_B) by $\alpha \approx 3\, \alpha_B \underline{z}^{-1.5}$ for $\underline{z} \gtrsim 6$. If we assume that this correction factor applies to all transitions in which the principal quantum number changes, then one has approximately

$$P^{di}_L / P^{ex}_L = R \approx \begin{cases} 3 \times 10^4 T_6^{-1} (z+1)^3 / [\,1 + 0.1(z+1) + 0.01(z+1)^2\,], & \text{H-, He-like} \\ 4 \times 10^{-5} T_6^{-1} (z+1)^3, & \text{all others.} \end{cases} \tag{6}$$

From Jordan's (1969) ionization tables, one sees that, for hydrogenic and heliumlike ions, an ion z is not present in any appreciable concentration unless $T_6 \geq (z+1)^2/100$, so that $R \leq 10^{-2}\ (z+1)$ for $z \leq 15$, $R \leq 0.3/(z+1)$ for $z \geq 15$. In an analogous manner we find for the other ions that $R \leq 10^{-2}$ $(z+1)$ for all $z \leq 25$.

The de-excitation of the electron in the highly excited state n'' is more complicated, since in this case one has to take into accound the rate of population of the various ℓ''-levels of the state n'', and the cascade probabilities to the lower states $n'''\ell'''$. In order to obtain a rough estimate of the relative importance of this porcess, we assume that the branching ratio for the rate of population of a state $n'''\ell'''$ due to dielectronic recombination followed by cascade is equal to the branching-ratio rate for collisional excitation from the ground state. Then the ratio of the power produced in a given line by these processes can be approximated by

$$R^1(z) \approx R(z) \exp\left[(E_{Z,z}(n''') - E_{Z,z+1}(n'')/kT) \right] .$$

Since in general $E_{Z,z}(n''') < E_{Z,z+1}(n'')$, we have $R^1(z) < R(z)$.

b) The Continuous Spectrum

The continuous X-ray spectrum of a hot, dilute, optically thin plasma is due to three processes: bremsstrahlung, radiative recombination, and two-photon decay of metastable states of hydrogen and helium.

i) Bremsstrahlung

In a hydrogenic approximation the energy emitted per unit time, volume, and wavelength interval due to encounters of Maxwellian electrons at a temperature T with ions of atomic number Z and charge z is given by

$$\frac{dE_{B,Z,z}}{dtdVd\lambda} = \frac{dP_{B,Z,z}}{d\lambda}(T) = \frac{2.04 \times 10^{-22}}{\lambda^2 T_6^{1/2}} z^2 N_e N_H \left(\frac{N_{Z,z}}{N_Z}\right)\left(\frac{N_Z}{N_H}\right)$$

$$\times \quad g_B(\lambda, z, T) \exp(-144/\lambda T_6) \quad \text{ergs (cm}^3 \text{ sec Å)}^{-1} \tag{7}$$

where λ is in Å, and $g_B(\lambda, z, T)$ is an averaged bremsstrahlung Gaunt factor of order unity which has been computed by Karzas and Latter (1961). The bremsstrahlung spectrum of a plasma which is a mixture of a number of different ions is obtained by summing equation (7) over all Z, z. In the case of the solar corona it is possible to simplify this summation considerably since the principal contributors to the sum are hydrogen and helium, both of which are fully ionized in the solar corona. The contribution of the other elements to the sum is small, amounting to about 6 %, and can, to a good approximation, be treated as a constant, independent of wavelength and temperature. One can then compute the bremsstrahlung spectrum from equation (7), using the values of the hydrogen and helium Gaunt factors obtained from the graphs given by Karzas and Latter (1961).

ii) Radiative Recombination

If we use a hydrogenic approximation to the cross-section for radiative recombination, then for a Maxwellian electron gas with temperature T, the emission spectrum due to captures into the state n of an ion Z, z is given by (Elwert 1954; Tucker and Gould 1966; Culhane 1969)

$$\frac{dE_{RR,Z,z}}{dtdVd\lambda}(T) = \frac{dP_{RR,Z,z}}{d\lambda}(T) = \frac{6.52 \times 10^{-23}}{\lambda^2 T_6^{3/2}} N_e N_H X_{Z,z,n}(T) \exp(-144/\lambda T_6)$$

$$\text{ergs (cm}^3 \text{ sec Å)}^{-1}$$

$$(\lambda < 12400/I_{Z,z,n}) \ , \tag{8}$$

$$= 0 \quad (\lambda > 12400/I_{Z,z,n}) \ ,$$

where λ is in angstroms, $I_{Z, z, n}$ is the ionization potential of the state n in electron volts, and

$$X_{Z, z, n}(T) = (N_{Z, z+1}/N_Z)(N_Z?N_H)(\bar{s}/2n^2)n(I_{Z, z, n}/I_H)^2 \exp(0.0116\, I_{Z, z, n}/T_6). \quad (9)$$

Here $(\bar{s}/2n^2)$ is the incompleted fraction of shell n, and we have set the recombination Gaunt factor equal to unity. To obtain the spectrum of a plasma consisting of a mixture of ions Z, z, equation (8) must be summed over all ions and all levels n for which $I_{Z, z, n} > 12400/\lambda$. In performing this sum, we included sixty-four terms $X_{Z, z, n}$ which consisted of the five or six lowest levels for the more abundant species and the one or two lowest levels for the less abundant species. At any given temperature and wavelength only a few terms (< 10) in the sum contributed appreciably to the spectrum.

iii) Two-Photon Decay of the 2S States of Hydrogenic and Heliumlike Ions

Since the excitation rates of the metastable $2S$ states of hydrogenic and heliumlike ions are about one-third the rates for excitation of the $2P$ states (Beigman et al. 1970), the energy emitted in the two-photon process will be about a third of the energy emitted in the $2P$-$1S$ resonance transitions of these ions, unless collisional or single-photon processes are more efficient in depopulating the $2S$ state.

For hydrogenic ions, the two-photon transition probability is $A(2S-1S) \approx 8\ \text{sec}^{-1}$ (Spitzer and Greenstein 1951; Shapiro and Breit 1959). By comparison, single-photon processes are negligible. The most important collisional depopulation process is proton excitation to the $2P$ state, which occurs at a rate $\sim 3 \times 10^{-5}\, n_H T_6^{-1/2}\ \text{sec}^{-1}$ (Seaton 1955). Thus for coronal conditions ($n_H \sim 10^8\ \text{cm}^{-3}$; $T_6 \sim 1$) collisional depopulation is completely negligible for $Z \geq 6$. The shape of the two-photon continuum has been computed for hydrogen by Spitzer and Greenstein (1951). It extends from the frequency $\nu = 0$ to $\nu = \nu_T = E(2S)/h$, is symmetric about the central symmetric about the central frequency $\frac{1}{2}\nu_T$, and has a maximum at $\frac{1}{2}\nu_T$. To

a good approximation the spectral shape may be approximated by the function $\underline{H}(\nu/\nu_{\underline{T}}) = \nu/\nu_{\underline{T}})(1 - \nu/\nu_{\underline{T}})$. If we assume that this spectral shape applies to all hydrogenic ions, then the energy emitted per cm^3 per second per angstrom as a result of the two-photon decay of the $2\underline{S}$ state of the ion $\underline{Z}$, $\underline{Z}-1$ is given by

$$\frac{dP_{2\gamma,Z,Z-1}}{d\lambda}(T) = \frac{4P_{L,Z,Z-1}(2P-1S)}{\lambda}\left(\frac{\lambda_T}{\lambda}\right)\left(1-\frac{\lambda_T}{\lambda}\right), \qquad (10)$$

where $\lambda_{\underline{T}} = \underline{c}/\nu_{\underline{T}}$ and $P_{\underline{L},\underline{Z},\underline{Z}-1}$ is the power per cm^3 in the L-α line of the ion $\underline{Z}, \underline{Z}-1$.

In the case of heliumlike ions the metastable states $2^1\underline{S}$ and $2^3\underline{S}$ must be considered separately. Two-photon decay of $2^3\underline{S}$ is unimportant, since the $2^3\underline{S}$ state can decay through a single-photon magnetic-dipole transition which has a much larger probability than the two-photon process (Griem 1970; Gabriel and Jordan 1970).

The results for the $2^1\underline{S}$ state are very similar to those for hydrogenic ions. The spectrum is roughly the same, and the transition probability is asymptotically equal to $16(\underline{Z}-1)^6$, or twice the two-photon decay rate of the hydrogenic $2\underline{S}$ state with nuclear change $\underline{Z}-1$ (Drake, Victor, and Dalgarno 1969). Thus, collisional depopulation is unimportant for coronal conditions, and the intensity due to the two-photon continuum is proportional to the rate of excitation of the $2^1\underline{S}$ from the ground state. The probability of exciting the $2^1\underline{S}$ state is about one-third the probability of exciting the $2^3\underline{P}$, $2^1\underline{P}$, and $2^3\underline{S}$ states, so that the intensity of the $2^1\underline{S}$ two-photon continuum can be computed to a good approximation by using equation (10) with $P_{\underline{L},\underline{Z},\underline{Z}-1}(2\underline{P}\text{-}1\underline{S},\underline{T})$ replaced by $P_{\underline{L},\underline{Z},\underline{Z}-2}(2^3\underline{P}\text{-}1^1\underline{S},\underline{T}) + P_{\underline{L},\underline{Z},\underline{Z}-2}(2^1\underline{P}\text{-}1^1\underline{S},\underline{T}) + P_{\underline{L},\underline{Z},\underline{Z}-2}(2^3\underline{S}\text{-}1^1\underline{S},\underline{T})$.

III. RESULTS

The results of the calculation are presented in Tables 2 and 3, and in Figures 1 - 3. In Table 2 we list $-\log_{10} P^{ex}_{L, Z, z}(nn', T)/N_e^2$, the negative logarithm of the power in the lines, as a function of temperature. The lines are listed according to ionic species and wavelengths. The corresponding transition can be found in Table 1. In Table 2 the ions were specified by arabic rather than roman numerals to save space. The cutoffs in the table were determined by the availability of ionization-equilibrium calculations. This explains why the numbers for calcium ions cutoff at 10^{7} °K in every case. In the future, we hope to extend the ionization-equilibrium calculations in order to eliminate such artificial cutoffs. The numbers in Table 1 refer only to line emission resulting from electron collisional excitation. Equations (4) and (6) can be used to obtain an estimate of the line emission produced as a result of K-shell excitation and dielectronic recombination.

To facilitate computation of radiative-recombination spectra, we have tabulated in Table 3 the recombination sum $X = \Sigma X_{Z, z, n}(\lambda, T)/T_6$ (see eq. 9) as a function of wavelength and temperature. Only the values at the edges are given, since between the edges the sum is constant. Note that the ratio of S to the bremsstrahlung gaunt factor g_B is equal to the ratio of recombination radiation to bremsstrahlung radiation. Since $g_B \approx 1 - 1.3$ for most wavelengths and temperatures of interest, S gives the ratio of recombination to bremsstrahlung emission within a factor of 2. From the numbers given in Table 3, we see that for a given temperature T_6, recombination dominates bremsstrahlung at wavelengths below about $600/T_6$ Å. For wavelengths larger than this value, bremsstrahlung dominates.

In Figure 1 we have plotted the spectrum of a coronal plasma for several different temperatures. A resolution of 0.5 Å was assumed, and some prominent lines are labeled according to the ion and wavelength. The smooth curves show the contribution of the various continuum processes.

The processes of bremsstrahlung (B), radiative recombination (RR), and two-photon emission (2γ) are shown. The dashed line represents the total continuum emission (C). The spectrum is expressed in units of ergs $cm^3/sec^{-1}\mathring{A}^{-1}$, so that multiplication by the emission integral $\int \underline{N}_{\underline{e}}^2 \underline{dV}$ gives the power emitted per angstrom.

These figures show the gradual shift from a line to a continuous spectrum and the concentration of the lines toward shorter wavelengths as the temperature increases.

In Figure 2 the power radiated in various wavelength bands is plotted as a function of temperature.

Finally, in Figure 3 the intensities of several of the strongest lines are plotted as a function of temperature.

We thank A. Krieger, L. VanSpeybroeck, G. Vaiana, and D. Webb for helpful discussions, H. Chasan for programming assistance, and E. O'Neill for typing a difficult manuscript. This research was supported by NASA contract NASW-2070 and by the Air Force Office of Scientific Research contract F44620-71-C-0019.

FIGURE CAPTIONS

Figure 1. The spectrum of a coronal plasma, if a resolution of 0.5 Å is assumed. Some prominent lines are labeled according to ion and wavelength. The continuum processes of bremsstrahlung (B), radiative recombination (RR), and two-photon emission (2γ) are shown. Dashed line represents the total continuum emission (C). (a) $T = 1.6 \times 10^6$ °K; (b) $T = 5 \times 10^6$ °K; (c) $T = 1.6 \times 10^7$ °K; (d) $T = 5 \times 10^7$ °K.

Figure 2. Power radiated in various wavelength bands as a function of temperature.

Figure 3. The intensity as a function of temperature of some of the strong emission lines. (a) Carbon; (b) oxygen; (c) silicon; (d) iron.

REFERENCES

Allen, J., and Dupree, A. 1969, Ap. J. 155, 27.

Beigman, I. L., Vainshtein, L. A. and Vinogradov, A. 1970, Soviet Astr. -AJ 13, 775.

Bely, O. 1966a, Proc. Phys. Soc., 88, 587.

_____ 1966b, Ann. d'ap., 29, 131.

_____ 1967, ibid, 30, 953.

Bely, O., and Bely, F. 1967, Solar Phys. 2, 285.

Bely, O., and Petrini, D. 1970, Astr. and Ap., 6, 318.

Burgess, A. 1961, Mem. Soc. R. Sci. Liege, 4, 299.

_____ 1965, Ap. J. 141, 1588.

Chapman, R. 1969, Ap. J., 156, 87.

Connerade, J. 1970, Ap. J. (Letters), 162, L139.

Cox, D., and Tucker, W. 1969, Ap. J., 157, 1157.

Culhane, J. 1969, M. N. R. A. S., 144, 375.

Drake, G., Victor, G., and Dalgarno, A. 1969, Phys. Rev., 180, 25.

Elwert, G. Z. 1954, Zs. F. Naturforschung, 53, 637.

Evans, K., and Pounds, K. 1968, Ap. J., 152, 319.

Gabriel, A., and Jordan, C. 1969, Nature, 221, 947.

Griem, H. 1970, Ap. J. (Letters), 161, L155.

Jordan, C. 1966a, M. N. R. A. S., 132, 463.

_____ 1966b, ibid., p. 515.

_____ 1969, ibid., 142, 499.

_____ 1970, ibid., 149, 1.

Karzas, W., and Latter, R. 1961, Ap. J. Suppl., 6, 167.

Kelly, R. 1968, Atomic Emission Lines Below 2000 Angstroms: Hydrogen through Argon (NRL Report 6648; Washington: U. S. Govt. Printing Office).

Krinberg, I. 1970, Soviet Astr. -AJ, 13, 780.

Landini, M., and Fossi, B. 1970, Astr. and Ap., 6, 468.

Moore, C. E. 1949, N. B. S. Circ., No. 467, Vol. 1.

_____ 1952, ibid., Vol. 2.

Pottasch, S. 1967, Bull. Astr. Inst. Netherlands, 19, 113.

Rugge, H., and Walker, A. B. C., Jr. 1970, Space Res., 8, 439.

Seaton, M. 1955, Proc. Roy. Soc. London, A, 68, 457.

Shapiro, J., and Breit, G. 1959, Phys. Rev., 113, 179.

Shore, B. 1969, Ap. J., 158, 1205.

Spitzer, L., and Greenstein, J. 1951, Ap. J., 114, 407.

Tucker, W. H., and Gould, R. J. 1966, Ap. J., 144, 244.

Walker, A., and Rugge, H. 1970 (preprint).

Widing, K., and Sandlin, G. 1968, Ap. J., 152, 545.

TABLE 1

Atomic Data Used to Compute the Line Intensities

Ion	Transition	Wavelength (Å)	Excitation Energy (eV)	Effective Collision Strength	Reference
CVI	1s-np	26.4	470	0.003	(K)
	1s-4p	27.0	459	.002	
	1s-3p	28.5	435	.006	WS
	1s-2p	33.7	368	.042	(K)
CV	$1s^2$-1snp	32.8	378	.008	(K)
	$1s^2$-1s4p	33.4	371	.006	(K)
	$1s^2$-1s3p	35.0-35.1	353	.014	WR
	$1s^2$-1s2p(^{1}P)	40.3	308	.084	WS
	$1s^2$-1s2p(^{3}P)	40.7	306	.008	(M)
	$1s^2$-1s2p(^{3}S)	41.5	300	0.089	(M)

Ion	Transition	Wavelength (Å)	Excitation Energy (eV)	Effective Collision Strength	Reference
NVII	1s-np	19.4	639	0.002	
	1s-4p	19.8	626	.002	
	1s-3p	20.9	593	.005	RW
	1s-2p	24.8	500	.031	RW
NVI	$1s^2$-1snp	23.3	532	.005	(K)
	$1s^2$-1s4p	23.8	521	.004	
	$1s^2$-1s3p	24.9-25.0	496	.010	(K)
	$1s^2$-1s2p(^{1}P)	28.8	430	.056	(M)
	$1s^2$-1s2p(^{3}P)	29.1	425	.010	(M)
	$1s^2$-1s2p(^{3}S)	29.5	420	0.063	(M)

Ion	Transition	Wavelength (Å)	Excitation Energy (eV)	Effective Collision Strength	Reference
OVIII	1s-np	14.8	837	0.002	RW
	1s-4p	15.2	816	.002	RW
	1s-3p	16.0	775	.005	RW, EP(CO)
	1s-2p	19.0	653	.023	RW, EP(CO)
OVII	$1s^2$-1snp	17.4	713	.004	RW
	$1s^2$-1s4p	17.8	697	.004	RW
	$1s^2$-1s3p	18.7	663	.009	RW, EP(CO)
	$1s^2$-1s2p(^{1}P)	21.6	575	.056	WR, EP(CO)
	$1s^2$-1s2p(^{3}P)	21.8	570	.010	WR, EP(CO)
	$1s^2$-1s2p(^{3}S)	22.1	560	0.063	WR, EP(CO)

Ion	Transition	Wavelength (Å)	Excitation Energy (eV)	Effective Collision Strength	Reference
NeX	1s-np	9.5	1305	0.0010	RW
	1s-4p	9.7	1280	.00084	RW
	1s-3p	10.2	1215	.0024	RW
	1s-2p	12.2	1020	.015	RW, EP(CO)
NeIX	$1s^2$-1snp	10.8	1148	.003	(K)
	$1s^2$-1s4p	11.0	1130	.002	(K)
	$1s^2$-1s3p	11.6	1070	.005	RW, EP(CO)
	$1s^2$-1s2p(^{1}P)	13.4	925	.030	RW, EP(CO)
	$1s^2$-1s2p(^{3}P)	13.6	912	.008	RW, EP(CO)
	$1s^2$-1s2p(^{3}S)	13.7	905	.025	W, R
NeVIII	2s-nℓ	52-65.9	188	.050	(K)
	2s-4ℓ	67.4-74.6	165	0.050	(K)

Ion	Transition	Wavelength (Å)	Excitation Energy (eV)	Effective Collision Strength	Reference
MgXII	1s-np	6.6	1879	0.00076	(K)
	1s-4p	6.7	1850	.00058	
	1s-3p	7.11	1740	.0017	WR
	1s-2p	8.42	1470	.010	WR, EP(CO)
MgXI	$1s^2$-1snp	7.30	1698	.002	(K)
	$1s^2$-1s4p	7.47	1660	.0016	(K)
	$1s^2$-1s3p	7.85-7.86	1570	.0035	WR
	$1s^2$-1s2p(^{1}P)	9.17	1350	.022	RW, EP(CO)
	$1s^2$-1s2p(^{3}P)	9.23	1340	.007	RW, EP(CO)
	$1s^2$-1s2p(^{3}S)	9.31	1330	.017	RW, EP(CO)
MgX	2ℓ-nℓ	33.8-43.0	290	.04	(K)
	2ℓ-4ℓ	44.0-47.3	260	.04	(K)
	2s-3p	57.9	214	.037	WS
	2p-3d	63.2-63.3	215	.09	WS
	2p-3s	65.7-65.9	208	.045	WS
MgIX	2s2ℓ-2snℓ'	38-47	262	.090	(K)
	2s2ℓ-2s4ℓ'	48-52	237	.090	(K)
	$2s^2$-2s3p	62.8	196	.092	WS
	2s2p-2s3d(^{3}D)	67.2	214	.12	WS
	2s2p-2s3d(^{1}D)	72.3	201	.12	WS
	2s2p-2s3s	77.7	189	.11	WS
MgVIII	2s2ℓ2ℓ'-2s2ℓnℓ"	46.5-53.5	232	.26	(K)
	2s2ℓ2ℓ'-2s2ℓ4ℓ"	52.4-64.3	193	.26	(K)
	$2s^2$2p-2s2p3p	64.2-71.7	182	.09	(K)
	2s$2p^2$-2s2p3d	72.6-77.4	193	.27	(K)
	2p-3d	75.0	165	.32	WS
MgVII	2s$2p^2$-2s2p2ℓnℓ"	55-66.8	186	.33	(K)
	$2s^2$$2p^2$-2s2$p^2$4p	63.4	196	.04	(K)
	$2s^2$$2p^2$-$2s^2$2p4d	68.0-71.8	173	.16	(K)
	2s$2p^3$-2s$2p^2$4d, 4s	67.5-72.9	201	.09	(K)
	$2s^2$$2p^2$-2s$2p^2$3p	77.0-81.0	186	0.11	(K)

Ion	Transition	Wavelength (Å)	Excitation Energy (eV)	Effective Collision Strength	Reference
SiXIV	1s-np	4.83	2567	0.00056	(K)
	1s-4p	4.95	2500	.00043	(K)
	1s-3p	5.22	2460	.0012	WR
	1s-2p	6.18	2000	.0077	WR
SiXIII	$1s^2$-1snp	5.29	2344	.002	(K)
	$1s^2$-1s4p	5.40	2290	.001	(K)
	$1s^2$-1s3p	5.68	2180	.0025	WR
	$1s^2$-1s2p(^{1}P)	6.65	1860	.016	WR, EP(CO)
	$1s^2$-1s2p(^{3}P)	6.69	1850	.006	WR, EP(CO)
	$1s^2$-1s2p(^{3}S)	6.74	1840	.011	WR, EP(CO)
SiXII	2ℓ-nℓ'	23.7-29.8	415	.026	
	2ℓ-4ℓ'	30.6-32.8	378	.026	
	2s-3p	40.9	303	.029	WS
	2p-3d	44.2	304	.065	WS
	2p-3s	45.6	296	.033	WS
SiXI	2s2ℓ-2snℓ'	26.0-32.7	379	.061	
	2s2ℓ-2s4ℓ'	33.3-36.2	357	.061	
	$2s^2$-2s3p	43.8	283	.066	WS
	2s2p-2s3d(^{3}D)	46.3	309	.079	WS
	2s2p-2s3d(^{1}D)	49.2	293	.079	WS
	2s2p-2s3s	52.3	288	.076	WS
SiX	2s2p2ℓ-2s2pnℓ'	30.0-34.2	362	.12	
	2s2p2ℓ-2s2p4ℓ'	33.5-41.0	336	.12	
	$2s^2$2p-2s2p3p	48.0	258	.074	(K)
	2s$2p^2$-2s2p3d	49.7-56.8	269	.18	(K)
	2p-3d	50.6	244	.21	WS
	2s$2p^2$-2s2p3s	53.5-60.5	271	.090	
	$2s^2$2p-$2s^2$3s	54.0	230	0.059	

Ion	Transition	Wavelength (Å)	Excitation Energy (eV)	Effective Collision Strength	Reference
SiIX	$2s2p^2 2\ell - 2s2p2\ell n\ell'$	35-40	310	0.10	
	$2s^2 2p^2 - 2s2p^2 4p$	38	326	.02	
	$2s^2 2p^2 - 2s^2 2p4d$	44.2	280	.10	(K)
	$2s2p^3 - 2s2p^2 4d, s$	41-43	331	.06	
	$2s^2 2p^2 - 2s2p^2 3p$	51-54	236	.08	(K)
	$2s2p^3 - 2s2p^2 3d$	52.7-55.7	265	.22	(K)
	$2p^2 - 2p3d$	55.3	222	.52	WS
	$2s2p^3 - 2s2p^2 3s$	61.2	244	.11	(K)
	$2p^2 - 2p3s$	61.7	201	.14	WS
SiVIII	$2s^2 2p^3 - 2s^2 2p^2 nd$	47.6	260	.03	
	$2s2p^4 - 2s2p^3 nd$	47.7	296	.02	
	$2s^2 2p^3 - 2s^2 2p^2 4d$	50.0-52.4	242	.04	(K)
	$2s2p^4 - 2s2p^3 4d$	52.5	275	.03	
	$2s^2 2p^3 - 2s^2 2p^2 4s$	53.8	230	.02	(K)
	$2s2p^4 - 2s2p^3 4s$	54.5	266	.01	
	$2s^2 2p^3 - 2s2p^3 3p$	58.9	210	.09	(K)
	$2p^3 - 2p^2 3d(^4P, ^4D)$	61.0	203	.36	WS
	$2p^3 - 2p^2 3d(^2S, ^2P, ^2D, ^2F)$	61.4-65.8	195	.36	(K)
	$2s2p^4 - 2s2p^3 3d$	67.3	223	.26	(K)
	$2p^3 - 2p^2 3s(^4P)$	69.8	177	.10	(K)
	$2p^3 - 2p^2 3s(^2P, ^2D)$	70.5-74.2	172	.10	(K)
	$2s2p^4 - 2s2p^3 3s$	76.0	202	.13	(K)
SiVII	$2s2p^4 2\ell - 2s2p^3 2\ell n\ell'$	50.5-56.5	219	.11	(K)
	$2s2p^4 2\ell - 2s2p^3 2\ell 4\ell'$	57.3-65.6	202	.11	(K)
	$2s^2 2p^4 - 2s2p^5 3p$	64	193	.11	
	$2p^4 - 2p^3 3d$	68.0-73.4	176	.23	(K)
	$2s2p^5 - 2s2p^4 3d$	65-72.5	227	.34	
	$2p^4 - 2p^3 3s(^3P)$	79.5	156	0.08	(K)

Ion	Transition	Wavelength (Å)	Excitation Energy (eV)	Effective Collision Strength	Reference
SXVI	1s-np	3.70	3340	0.00043	(K)
	1s-4p	3.78	3270	.00033	(K)
	1s-3p	3.99	3100	.00094	(K)
	1s-2p	4.73	2620	.0059	WR
SXV	$1s^2$-1snp	4.01	3080	.001	
	$1s^2$-1s4p	4.10	3010	.001	
	$1s^2$-1s3p	4.30	2870	.0019	
	$1s^2$-1s2p(^{1}P)	5.04	2460	.012	WR
	$1s^2$-1s2p(^{3}P)	5.07	2450	.005	WR
	$1s^2$-1s2p(^{3}S)	5.10	2430	.008	WR
SXIV	2ℓ-nℓ'	17.6-22	557	.02	
	2ℓ-4ℓ'	22.6-24.2	509	.02	
	2s-3p	30.2	406	.02	
	2p-3d	32.6	409	.05	
	2p-3s	33.8	398	.02	
SXIII	2s2ℓ-2snℓ'	19-21	519	.043	
	2s2ℓ-2s4ℓ'	24-26	489	.043	
	$2s^2$-2s3p	31	387	.047	
	2s2p-2s3d	33-35	412	.11	
	2s2p-2s3s	37	394	.054	
SXII	2s2p2ℓ-2s2pnℓ'	22-23.9	494	.084	
	2s2p2ℓ-2s2p4ℓ'	23.4-28.7	456	.084	
	$2s^2$2p-2s2p3p	33.3	350	.052	
	$2s2p^2$-2s2p3d	34.7-39.8	366	.13	
	2p-3d	35.4	352	.15	
	$2s2p^2$-2s2p3s	37.4-42.4	359	.063	
	2p-2s	37.8	328	0.041	

Ion	Transition	Wavelength (Å)	Excitation Energy (eV)	Effective Collision Strength	Reference
SXI	$2s2p^2 2\ell - 2s2p2\ell n\ell'$	24.6-26.8	441	0.067	
	$2s2p^2 2\ell - 2s2p2\ell 4\ell'$	25.4-28.8	450	.067	
	$2s^2 2p^2 - 2s2p^2 3p$	34.2-36.2	336	.054	
	$2s2p^3 - 2s2p^2 3d$	35.2-37.3	378	.15	
	$2p^2 - 2p3d$	37.0	326	.35	
	$2s2p^2 2\ell - 2s2p^2 2\ell 3s$	41.0	316	.17	
SX	$2s2p^3 2\ell - 2s2p2\ell n\ell'$	28.0-31.4	396	.11	
	$2s2p^3 2\ell - 2s2p2\ell 4\ell'$	34.0-37.2	360	.11	
	$2s^2 2p^3 - 2s2p^3 3p$	40.2	308	.058	
	$2p^3 - 2p^2 3d(^4P, ^4D)$	42.5	292	.24	(K)
	$2p^3 - 2p^2 3d(^2S, ^2P, ^2D, ^2F)$	42.9-45.8	280	.24	(K)
	$2s2p^4 - 2s2p^3 3d$	47	326	.17	
	$2p^3 - 2p^2 3s(^4P)$	47.7	259	.06	(K)
	$2p^3 - 2p^2 3s(^2P, ^2D)$	48.2-50.6	252	.06	
	$2s2p^4 - 2s2p^3 3s$	52.0	296	.08	
SIX	$2s2p^4 2\ell - 2s2p^3 2\ell n\ell'$	32.8-36.8	300	.09	
	$2s2p^4 2\ell - 2s2p^3 2\ell 4\ell'$	37.2-42.6	276	.09	
	$2s2p^5 - 2s2p^4 3d$	41.2-47	312	.27	
	$2s^2 2p^4 - 2s2p^5 3p$	41.5	295	.09	
	$2p^4 - 2p^3 3d$	46.4-49.3	259	.18	(K)
	$2p^4 - 2p^3 3s$	54.2-56.3	224	.06	(K)
	$2s2p^5 - 2s2p^4 3s$	57.0	284	.11	
SVIII	$2s2p^5 2\ell - 2s2p^4 2\ell n\ell'$	37.6-41.6	298	.07	(K)
	$2s2p^5 2\ell - 2s2p^4 2\ell 4\ell'$	44.4-47.8	270	0.07	(K)

Ion	Transition	Wavelength (Å)	Excitation Energy (eV)	Effective Collision Strength	Reference
SVIII	$2s^2 2p^5 - 2s2p^5 3p$	46	270	0.07	
	$2p^5 - 2p^4 3d$	51.2-54.6	234	.44	(K)
	$2s2p^6 - 2s2p^5 3d$	58.5	212	.21	
	$2p^5 - 2p^4 3s$	59.2-64.3	201	.62	(K)
	$2s2p^6 - 2s2p^5 3s$	65.0	191	.09	(K)
SVII	$2s^2 2p^6 - {}_5 2s2p^5 2\ell n\ell'$	44-50	247	.30	(K)
	$2s^2 2p^6 - {}_5 2s2p^5 2\ell 4\ell'$	51.8-54.9	233	.30	(K)
	$2s^2 2p^6 - 2s2p^6 3p$	55	225	.40	
	$2p^6 - 2p^5 3d$	60.8	204	.30	(K)
	$2p^6 - 2p^5 3s$	72.4	171	0.79	(K)

Ion	Transition	Wavelength (Å)	Excitation Energy (eV)	Effective Collision Strength	Reference
CaXX	1s-np	2.3	5250	0.00028	
	1s-4p	2.4	5150	.00021	
	1s-3p	2.54	4860	.00060	
	1s-2p	3.02	4100	.0037	
CaXIX	$1s^2$-1snp	2.5	4850	.0007	
	$1s^2$-1s4p	2.6	4750	.0006	
	$1s^2$-1s3p	2.70	4570	.0012	
	$1s^2$-1s2p(^{1}P)	3.18	3900	.008	
	$1s^2$-1s2p(^{3}P)	3.20	3880	.004	
	$1s^2$-1s2p(^{3}S)	3.22	3850	.005	
CaXVIII	2ℓ-nℓ'	11-12	890	.01	
	2ℓ-4ℓ'	14-15	811	.01	
	2s-3p	18	650	.01	
	2p-3d	19-20	654	.03	
	2p-3s	21	635	.01	
CaXVII	2s2ℓ-2snℓ'	11-13	896	.03	
	2s2ℓ-2s4ℓ'	14-16	845	.03	
	2s2ℓ-2s3ℓ'	19-22	701	.13	
CaXVI	2s2p2ℓ-2s2pnℓ'	12.3-13	884	.04	
	2s2p2ℓ-2s2p4ℓ'	12.7-15	816	.04	
	2s2p2ℓ-2s2p3ℓ'	17.2-19.5	608	.23	
CaXV	$2s2p^2$2ℓ-2s2p2ℓnℓ'	13.9-15.1	780	.038	
	$2s2p^2$2ℓ-2s2p2ℓ4ℓ'	14.3-16.3	795	.038	
	$2s^2 2p^2$-$2s2p^2$3p	19.3-20.4	594	.030	
	$2s2p^3$-$2s2p^2$3d	19.9-21.1	667	.085	
	$2p^2$-2p3d	20.9	560	.20	
	$2s2p^2$2ℓ-2s2p3s2ℓ	23.2	560	0.096	

Ion	Transition	Wavelength (Å)	Excitation Energy (eV)	Effective Collision Strength	Reference
CaXIV	$2s2p^3 2\ell - 2s2p2\ell n\ell'$	15.3-17.2	725	0.060	
	$2s2p^3 2\ell - 2s2p2\ell 4\ell'$	18.7-20.4	658	.060	
	$2s^2 2p^3 - 2s2p^3 3p$	22.0	564	.032	
	$2p^3 - 2p^2 3d$	23.2-25	524	.26	
	$2s2p^4 - 2s2p^3 3d$	25.8	595	.093	
	$2p^3 - 2p^2 3s$	26.2-27.8	467	.066	
	$2s2p^4 - 2s2p^3 3s$	28.5	540	.044	
CaXIII	$2s2p^4 2\ell - 2s2p^3 2\ell n\ell'$	17.2-19.2	572	.047	
	$2s2p^4 2\ell - 2s2p^3 2\ell 4\ell'$	19.4-22.2	525	.047	
	$2s^2 2p^4 - 2s2p^5 3p$	21.6	503	.047	
	$2p^4 - 2p^3 3d$	24.2-25.8	494	.094	
	$2s2p^5 - 2s2p^4 3d$	21.9-24.5	595	.14	
	$2p^4 - 2p^3 3s$	28.3-29.4	426	.031	
	$2s2p^5 - 2s2p^4 3s$	29.8	540	.057	
CaXII	$2s2p^5 2\ell - 2s2p^4 2\ell n\ell'$	18.8-20.8	596	.035	
	$2s2p^5 2\ell - 2s2p^4 2\ell 4\ell'$	22.2-23.9	540	.035	
	$2s^2 2p^5 - 2s2p^5 3p$	23	540	.035	
	$2p^5 - 2p^4 3d$	26.7-27.3	459	.22	
	$2s2p^6 - 2s2p^5 3d$	29.2	424	.11	
	$2p^5 - 2p^4 3s$	31.6-32.7	384	.31	
	$2s2p^6 - 2s2p^5 3s$	32.5	382	.045	
CaXI	$2s^2 2p^6 - 2s2p^5 2\ell n\ell'$	21-24	520	.14	
	$2s^2 2p^6 - 2s2p^5 2\ell 4\ell'$	23.6-26.7	477	.14	
	$2s^2 2p^6 - 2s2p^6 3p$	27.0	459	.19	
	$2p^6 - 2p^5 3d$	30.4-31.2	401	.14	
	$2p^6 - 2p^5 3s$	35.2	350	0.38	

Ion	Transition	Wavelength (Å)	Excitation Energy (eV)	Effective Collision Strength	Reference
FeXXVI	1s-np	1.40	8840	0.00016	(H)
	1s-4p	1.43	8650	.00012	
	1s-3p	1.51	8190	.00036	(H)
	1s-2p	1.79	6900	.0022	(H)
FeXXV	$1s^2$-1snp	1.50	8400	.0004	(C)
	$1s^2$-1s4p	1.51	8200	.0003	
	$1s^2$-1s3p	1.59	7760	.0008	(C)
	$1s^2$-1s2p(^{1}P)	1.87	6630	.0045	N
	$1s^2$-1s2p(^{3}P)	1.88	6600	.0026	
	$1s^2$-1s2p(^{3}S)	1.89	6561	.0022	
FeXXIV	2ℓ-nℓ'	6.06-7.21	1720	.0071	
	2ℓ-4ℓ'	8.35	1480	.0071	(C)
	2s-3p	10.8	1150	.0095	CO
	2p-3d	11.2	1150	.018	(C)
	2p-3s	11.4	1130	.0086	(C)
FeXXIII	2s2ℓ-2snℓ'	6.3-8.00	1550	.0076	
	2s2ℓ-2s4ℓ'	8.45-8.86	1430	.0076	(C)
	$2s^2$-2s3p	11.2	1110	.010	(C)
	2s2p-2s3d(^{3}D)	11.5	1150	.0095	(C)
	2s2p-2s3d(^{1}D)	11.8	1130	.0095	(C)
	2s2p-2s3s	12.0	1110	.0095	(C)
FeXXII	2s2p2ℓ-2s2pnℓ'	6.91-7.89	1560	.03	
	2s2p2ℓ-2s2ℓ4ℓ'	7.72-9.45	1440	.03	
	$2s^2$2p-2s2p3p	11.5	1110	.024	CO
	2s$2p^2$-2s2p3d	11.5-13.1	1150	.042	
	2p-3d	11.9	1040	.047	(C)
	2s$2p^2$-2s2p3s	12.3-13.9	1130	.026	
	$2s^2$2p-$2s^2$3s	12.4	1000	0.012	(C)

Ion	Transition	Wavelength (Å)	Excitation Energy (eV)	Effective Collision Strength	Reference
FeXXI	$2s^2 2p^2 - 2s2p^2 np$	7.4	1470	0.007	
	$2s^2 2p^2 - 2s2p^2 4p$	7.9	1550	.0072	
	$2s2p^3 - 2s2p^2 nd, s$	8.0	1470	.012	
	$2s^2 2p^2 - 2s^2 2pnd$	8.3	1470	.019	
	$2s2p^3 - 2s2p^2 4d, s$	8.55-8.95	1330	.012	
	$2s^2 2p^2 - 2s^2 2p4d$	9.81	1570	.019	CO
	$2s^2 2p^2 - 2s2p^2 3p$	11.6-12.0	1120	.026	CO
	$2s2p^3 - 2s2p^2 3d$	11.7-12.3	1260	.046	CO
	$2p^2 - 2p3d$	12.4-12.7	1050	.11	CO
	$2s2p^3 - 2s2p^2 3s$	12.9	1160	.028	
	$2p^2 - 2p3s$	13.0-13.5	955	.026	CO
FeXX	$2p^3 - 2p^2 nd(4)$	9.2	1330	.008	
	$2p^3 - 2p^2 nd(2)$	9.6	1330	.008	
	$2p^3 - 2p^2 4d(4)$	9.7	1270	.008	
	$2p^3 - 2p^2 4d(2)$	10.2-10.5	1270	.008	CO
	$2s2p^4 - 2s2p^3 nd$	10.2	1330	.007	
	$2s2p^4 - 2s2p^3 4d$	10.7	1270	.007	
	$2s^2 2p^3 - 2s2p^3 3p$	12.0-12.7	1100	.027	CO
	$2p^3 - 2p^2 3d(^4P, ^4D)$	13.4	1040	.056	CO
	$2p^3 - 2p^2 3d$ $(^2S, ^2P, ^2D, ^2F)$	13.4-14.4	1000	.056	CO
	$2s2p^4 - 2s2p^3 3d$	14.7	1160	.050	
	$2p^3 - 2p^2 3s(^4P)$	15.2	925	.014	
	$2p^3 - 2p^2 3s(^2P, ^2D)$	15.4-16.3	910	.014	
	$2s2p^4 - 2s2p^3 3s$	16.6	1060	.025	
FeXIX	$2s^2 2p^4 - 2s2p^4 np$	8.6	1440	.006	
	$2p^4 - 2p^3 nd$	9.5	1310	.006	
	$2s2p^5 - 2s2p^4 nd$	9.7	1310	.012	
	$2s^2 2p^4 - 2s2p^4 4p$	9.7	1240	0.006	

Ion	Transition	Wavelength (Å)	Excitation Energy (eV)	Effective Collision Strength	Reference
FeXIX	$2s2p^5-2s2p^4ns$	10.0	1240	0.006	
	$2p^4-2p^34d$	10.8	1240	.006	CO
	$2s2p^5-2s2p^44d$	10.4	1240	.012	
	$2s^22p^4-2s2p^53p$	10.8	1020	.029	
	$2s2p^5-2s2p^44s$	11.1	1240	.006	
	$2p^4-2p^33d$	13.5-14.2	1000	.030	CO
	$2s2p^5-2s2p^43d$	12.6-14.0	1210	.055	CO
	$2p^4-2p^33s$	14.5-15.0	870	.0083	CO
	$2s2p^5-2s2p^43s$	15.2	1100	.027	
FeXVIII	$2s^22p^5-2s2p^5np$	9.15	1340	.007	
	$2p^5-2p^4nd$	10.2	1210	.012	
	$2p^5-2p^4ns$	10.4	1210	.016	
	$2s2p^6-2s2p^5ns$	10.7	1340	.007	
	$2s^22p^5-2s2p^5nd$	10.9	1340	.008	
	$2s^22p^5-2s2p^54p$	10.9	1140	.007	
	$2p^5-2p^44d$	12.2	1020	.012	
	$2p^5-2p^44s$	12.4	1020	.016	
	$2s^22p^5-2s2p^53p$	13.4	1110	.025	CO
	$2s2p^5-2s2p^44d$	13.0	1140	.008	
	$2s2p^5-2s2p^44s$	13.7	1140	.007	
	$2p^5-2p^43d$	14.3-14.4	862	.088	RW, EP(CO)
	$2s2p^6-2s2p^53d$	15.4	872	.058	
	$2p^5-2p^43s$	15.6-16.0	796	.128	RW
	$2s2p^6-2s2p^53s$	16.2	785	.050	
FeXVII	$2s^22p^6-2s2p^6np$	9.9	1250	.02	
	$2p^6-2p^5nd$	10.1	1230	.01	
	$2s^22p^6-2s2p^64p$	11.0	1130	.02	
	$2p^6-2p^5ns$	11.1	1120	.02	
	$2s^22p^6-2s^22p^54d$	12.3	1010	0.03	RW, EP(CO)

Ion	Transition	Wavelength (Å)	Excitation Energy (eV)	Effective Collision Strength	Reference
FeXVII	$2p^6-2p^5 4s$	12.7	930	0.02	CO
	$2s^2 2p^6-2s2p^6 3p$	13.8	895	.130	RW, EP(CO)
	$2s^2 2p^6-2s^2 2p^5 3s(^1P)$	15.0	824	.06	RW, EP(CO)
	$2s^2 2p^6-2s^2 2p^5 3d$ (^3D)	15.3	806	.047	RW, EP(CO)
	$2s^2 2p^6-2s^2 2p^5 3s$ (^3P)	15.5	796	.07	RW, EP(CO)
	$2s^2 2p^6-2s^2 2p^5 3s$ (^1P)	16.8	735	.062	RW, EP(CO)
	$2s^2 2p^6-2s^2 2p^5 3s$ (^3P)	17.1	722	.07	RW, EP(CO)
FeXVI	$2s^2 2p^6 3s-$ $2s2p^6 3s3p$	15.4	895	.120	
	$2s^2 2p^6 3s-2p^5 3s3d$	17.1	806	.050	
	$2p^6 3s-2s^2 2p^5 3s^2$	17.5	730	.130	CO
	3s-5p	37.1	334	.007	
	3p-5d	40.0	344	.02	(M)
	3p-5s	42.5	326	.009	
	3d-5f	47.4	350	.02	(M)
	3s-4p	50.3-54.2	244	.04	WS
	3p-4d	54.7	264	.09	WS
	3p-4s	63.7	232	.05	WS
	3d-4f	66.4	271	.13	WS
FeXV	$2s^2 2p^6 3s^2-$ $2s2p^6 3s^2 4\ell$	13-18	820	.13	
	$2p^6 3s^2-2p^5 3s^2 4\ell$	14-17	807	.23	
	$3s3\ell-3sn\ell'$	27.2-41	332	.28	
	$3s^2-3s4p$	52.9	234	.26	WS
	3s3p-3s4d	53.9	252	.10	M
	3s3d-3s4f	70.0	177	.08	WS
	3s3p-3s4s	74.5	196	0.18	

Ion	Transition	Wavelength (Å)	Excitation Energy (eV)	Effective Collision Strength	Reference
FeXIV	$3s3\ell 3\ell'$-$3s3\ell n\ell''$	31.7-56	221	0.20	
	$3s^2 3p$-$3s3p4p$	56.2	220	.086	
	$3s3p^2$-$3s3p4d$	58	282	.20	
	$3s^2 3p$-$3s^2 4d$	60.0	206	.29	WS
	$3s3p^2$-$3s3p4s$	70	245	.12	
	$3s^2 3p$-$3s^2 4s$	71	175	.078	WS
FeXIII	$3s3p3\ell 3\ell'$-$3s3p3\ell n\ell''$	34.2-59	210	.15	
	$3s3p^3$-$3s3p^2 4d$	60	271	.24	
	$3s^2 3p^2$-$3s^2 3p4d$	65	191	.61	
	$3s3p^3$-$3s3p^2 4s$	70	241	.13	
	$3s^2 3p^2$-$3s^2 3p4s$	76.0	163	0.17	WS

Ion	Transition	Wavelength (Å)	Excitation Energy (eV)	Effective Collision Strength	Reference
NiXXVIII	1s-np	1.21	10,300	0.00016	(H)
	1s-4p	1.24	10,000	.00012	(H)
	1s-3p	1.31	9,450	.00031	
	1s-2p	1.55	8,000	.0019	
NiXXVII	$1s^2$-1snp	1.29	9600	.0004	
	$1s^2$-1s4p	1.30	9550	.0003	
	$1s^2$-1s3p	1.37	9050	.0007	
	$1s^2$-1s2p(^{1}P)	1.60	7750	.0038	
	$1s^2$-1s2p(^{3}P)	1.61	7700	.0023	
	$1s^2$-1s2p(^{3}S)	1.62	7650	.0018	
NiXXVI	2ℓ-nℓ'	5.15-6.14	2010	.0061	
	2ℓ-4ℓ'	7.10	1730	.0061	
	2s-3p	9.20	1350	.0081	
	2p-3d	9.52	1350	.010	
	2p-3s	9.70	1320	.0073	
NiXXV	2s2ℓ-2snℓ'	5.40-6.76	1810	.0064	
	2s2ℓ-2s4ℓ'	7.15-7.50	1670	.0064	
	$2s^2$-2s3p	9.50	1300	.0085	
	2s2p-2s3d(^{3}D)	9.75	1350	.0081	
	2s2p-2s3d(^{1}D)	10.0	1320	.0081	
	2s2p-2s3s	10.2	1300	.0081	
NiXXIV	2s2p2ℓ-2s2pnℓ'	5.81-6.62	1860	.025	
	2s2p2ℓ-2s2ℓ4ℓ'	6.50-7.94	1710	.025	
	$2s^2$2p-2s2p3p	9.32	1320	.020	
	2s$2p^2$-2s2p3d	9.65-11.0	1370	.035	
	2p-3d	10.0	1240	.040	
	2s$2p^2$-2s2p3s	10.4-11.7	1340	.022	
	$2s^2$2p-$2s^2$3s	10.4	1190	0.010	

Ion	Transition	Wavelength (Å)	Excitation Energy (eV)	Effective Collision Strength	Reference
NiXXIII	$2s2p^2 2\ell - 2s2p2\ell n\ell'$	6.15-6.94	1760	0.031	
	$2s2p^2 2\ell - 2s2p^2 4\ell$	6.60-7.70	1780	.032	
	$2s^2 2p^2 - 2s2p^2 3p$	8.85-9.35	1340	.022	
	$2s2p^3 - 2s2p^2 3d$	9.20-9.70	1510	.038	
	$2p^2 - 2p3d$	9.60	1260	.092	
	$2s2p^3 - 2s2p^2 3s$	10.6	1390	.023	
	$2p^2 - 2p3s$	10.7	1150	.022	
NiXXII	$2s2p^3 2\ell - 2s2p^2 2\ell n\ell'$	6.45-7.26	1710	.027	
	$2s^2 2p^3 2\ell - 2s2p^2 2\ell 4\ell'$	7.90-8.60	1550	.027	
	$2s^2 2p^3 - 2s2p^3 3p$	9.25	1330	.022	
	$2p^3 - 2p^2 3d(^4P, ^4D)$	9.65	1260	.046	
	$2p^3 - 2p^2 3d$ $(^2S, ^2P, ^2D, ^2F)$	9.65-10.04	1210	.046	
	$2s2p^4 - 2s2p^3 3d$	10.7	1400	.041	
	$2p^3 - 2p^2 3s$	11.0-11.7	1120	.024	
	$2s2p^4 - 2s2p^3 3s$	12.0	1280	.021	
NiXXI	$2s2p^4 2\ell - 2s2p^3 2\ell n\ell'$	6.72-7.60	1460	.023	
	$2s2p^4 2\ell - 2s2p^3 2\ell 4\ell'$	7.70-8.83	1350	.023	
	$2s^2 2p^4 - 2s2p^5 3p$	8.60	1290	.023	
	$2s2p^5 - 2s2p^4 3d$	8.75-9.70	1460	.044	
	$2p^4 - 2p^3 3d$	9.15-9.86	1260	.024	
	$2p^4 - 2p^3 3s$	10.6-11.6	1100	.0066	
	$2s2p^5 - 2s2p^4 3s$	11.8	1390	0.021	

Ion	Transition	Wavelength (Å)	Excitation Energy (eV)	Effective Collision Strength	Reference
NiXX	$2s2p^5 2\ell - 2s2p^4 2\ell n\ell'$	7.40-8.25	1510	0.040	
	$2s2p^5 2\ell - 2s2p^4 2\ell 4\ell'$	10.1-10.8	1380	.040	
	$2s^2 2p^5 - 2s2p^5 3p$	10.4	1380	.020	
	$2p^5 - 2p^4 3d$	11.6	1070	.071	
	$2s2p^6 - 2s2p^5 3d$	12.5-12.6	1080	.047	
	$2p^5 - 2p^4 3s$	12.6-12.9	987	.10	
	$2s2p^6 - 2s2p^5 3s$	13.1	973	.040	
NiXIX	$2s^2 2p^6 - 2s2p^6 np$	8.1	1530	.02	
	$2p^6 - 2p^5 nd$	8.3	1490	.008	
	$2s^2 2p^6 - 2s2p^5 4p$	9.0	1370	.02	
	$2p^6 - 2p^5 ns$	9.1	1360	.02	
	$2p^6 - 2p^5 4d$	10.0	1240	.008	
	$2s^2 2p^6 - 2s^2 2p^6 4d$	10.0	1240	.024	RW,EP(CO)
	$2s^2 2p^6 - 2s2p^6 3p$	10.3	1090	.09	
	$2p^6 - 2p^5 4s$	11.0	1130	.02	
	$2s^2 2p^6 - 2s^2 2p^5 3d(^1P)$	12.4	1010	.00094	RW,EP(CO)
	$2s^2 2p^6 - 2s^2 2p^5 3d(^3D)$	12.6	983	.039	RW,EP(CO)
	$2s^2 2p^6 - 2s^2 2p^5 3d(^3P)$	12.8	971	.0010	RW,EP(CO)
	$2s^2 2p^6 - 2s^2 2p^5 3s(^1P)$	13.8	897	.05	RW,EP(CO)
	$2s^2 2p^6 - 2s^2 2p^5 3s(^3P)$	14.3	881	.06	RW,EP(CO)
NiXVIII	$2s^2 2p^6 3s - 2s2p^6 3sn\ell$	10.5-14.5	1030	.10	RW
	$2p^6 3s - 2p^5 3sn\ell$	11.3-13.7	1010	.19	
	$3\ell - n\ell'$	20-37	335	.11	
	3s-4p	40.6-43.7	305	.03	
	3p-4d	44.2	330	.07	
	3p-4s	51.7	290	.04	
	3d-4f	53.5	339	0.11	

Ion	Transition	Wavelength (Å)	Excitation Energy (eV)	Effective Collision Strength	Reference
NiXVII	$2s^2 2p^6 3s^2$ - $2s2p^6 3s^2 4\ell$	10.4-14.4	943	0.10	
	$2p^6 3s^2$ - $2p^5 3s^2 4\ell$	11.2-13.6	928	.18	
	$3s3\ell$ - $3sn\ell'$	23.7-32.8	382	.22	
	$3s^2$ - 3s 4p	42.2	269	.21	
	3s3p-3s4d	45.6	290	.08	
	3s3d-3s4f	56.0	204	.064	
	3s3p-3s4s	59.5	225	.14	
NiXVI	$3s3\ell 3\ell'$ - $3s3\ell n\ell''$	24.9-43	281	.16	
	$3s^2 3p$ - 3s3p4p	44	279	.068	
	$3s3p^2$ - 3s3p4d	45.5	358	.16	
	$3s^2 3p$ - $3s^2 4d$	47.0	262	.23	
	$3s3p^2$ - 3s3p4s	55	311	.094	
	$3s^2 3p$ - $3s^2 4s$	55.7	222	.061	
NiXV	$3s3p3\ell 3\ell'$ - $3s3p3\ell n\ell''$	26.6-45	271	.12	
	$3s3p^3$ - $3s3p^2 4d$	46.6	350	.19	
	$3s^2 3p^2$ - $3s^2 3p4d$	50	246	.47	
	$3s3p^3$ - $3s3p^2 4s$	54	311	.10	
	$3s^2 3p^2$ - $3s^2 3p4s$	59.0	210	0.13	

REFERENCES QUOTED IN TABLE 1

Lines observed in solar corona:

WS: Widing and Sandlin

WR: Walker and Rugge

EP: Evans and Pounds

Lines observed in laboratory or computed theoretically:

(K): Kelley

(CO): Connerade

(M): Moore

(H): Hydrogenic

Lines not referenced were obtained by extrapolation or interpolation.

Table 2. Log Power In Lines (erg cm^{-3} sec^{-1}) as a Function of Temperature (^{o}K)

ELT ION	LAMBDA	-LOG POWER IN LINES														
LOG T=		5.9	6.0	6.1	6.2	6.3	6.4	6.5	6.6	6.7	6.8	6.9	7.0	7.3	7.5	7.6	8.0
NI 28	1.21	**********	**********	**********	**********	**********	**********	**********	**********	**********	**********	**********	**********	31.52	29.15	28.42	27.01
NI 28	1.24	**********	**********	**********	**********	**********	**********	**********	**********	**********	**********	**********	**********	31.32	28.98	28.25	26.87
NI 27	1.29	**********	**********	**********	**********	**********	**********	**********	**********	**********	**********	**********	34.28	28.15	27.11	26.83	26.81
NI 27	1.30	**********	**********	**********	**********	**********	**********	**********	**********	**********	**********	**********	34.37	28.25	27.21	26.93	26.92
NI 28	1.31	**********	**********	**********	**********	**********	**********	**********	**********	**********	**********	**********	**********	30.88	28.59	27.88	26.54
NI 27	1.37	**********	**********	**********	**********	**********	**********	**********	**********	**********	**********	**********	33.76	27.76	26.77	26.51	26.53
FE 26	1.40	**********	**********	**********	**********	**********	**********	**********	**********	**********	**********	**********	**********	29.76	27.85	27.20	26.06
FE 26	1.43	**********	**********	**********	**********	**********	**********	**********	**********	**********	**********	**********	**********	29.58	27.70	27.05	25.97
FE 25	1.50	**********	**********	**********	**********	**********	**********	**********	**********	**********	**********	**********	30.86	26.69	25.89	25.67	25.79
FE 25	1.51	**********	**********	**********	**********	**********	**********	**********	**********	**********	**********	**********	30.87	26.75	25.97	25.75	25.89
FE 26	1.51	**********	**********	**********	**********	**********	**********	**********	**********	**********	**********	**********	**********	29.17	27.32	26.69	25.60
NI 28	1.55	**********	**********	**********	**********	**********	**********	**********	**********	**********	**********	**********	**********	29.80	27.64	26.98	25.75
FE 25	1.59	**********	**********	**********	**********	**********	**********	**********	**********	**********	**********	**********	30.29	26.28	25.54	25.34	25.51
NI 27	1.60	**********	**********	**********	**********	**********	**********	**********	**********	**********	**********	**********	32.43	26.76	25.89	25.68	25.80
NI 27	1.61	**********	**********	**********	**********	**********	**********	**********	**********	**********	**********	**********	32.63	26.97	26.10	25.89	26.01
NI 27	1.62	**********	**********	**********	**********	**********	**********	**********	**********	**********	**********	**********	32.71	27.07	26.21	25.99	26.12
FE 26	1.79	**********	**********	**********	**********	**********	**********	**********	**********	**********	**********	**********	**********	28.12	26.40	25.81	24.81
FE 25	1.87	**********	**********	**********	**********	**********	**********	**********	**********	**********	**********	**********	29.05	25.32	24.69	24.52	24.78
FE 25	1.88	**********	**********	**********	**********	**********	**********	**********	**********	**********	**********	**********	29.27	25.55	24.93	24.76	25.02
FE 25	1.89	**********	**********	**********	**********	**********	**********	**********	**********	**********	**********	**********	29.32	25.61	24.99	24.82	25.08

S 16	3.70	**********	**********	**********	**********	**********	35.34	32.99	31.18	29.82	28.73	27.92	26.60	26.64	26.78	27.54
S 16	3.78	**********	**********	**********	**********	**********	35.11	32.78	30.98	29.64	28.56	27.76	26.46	26.51	26.65	27.41
S 16	3.99	**********	**********	**********	**********	**********	34.54	32.26	30.51	29.20	28.15	27.38	26.12	26.18	26.33	27.10
S 15	4.01	**********	**********	37.64	33.81	31.12	29.47	28.37	27.59	26.99	26.55	26.22	25.98	26.36	26.86	28.50
S 15	4.10	**********	**********	37.52	33.75	31.09	29.47	28.39	27.63	27.05	26.61	26.29	26.07	26.46	26.96	28.60
S 15	4.30	**********	**********	36.77	33.08	30.50	28.94	27.91	27.18	26.63	26.22	25.91	25.73	26.13	26.64	28.29
S 16	4.73	**********	**********	**********	**********	**********	33.07	30.75	29.33	28.12	27.15	26.44	25.30	25.40	25.57	26.38
SI 14	4.83	**********	**********	**********	**********	33.90	31.68	30.26	28.58	27.54	26.77	26.25	26.10	26.44	26.62*******	
SI 14	4.95	**********	**********	**********	**********	34.02	31.81	31.08	28.71	27.66	26.89	26.38	26.23	26.56	26.74*******	
S 15	5.04	**********	**********	34.75	31.33	28.96	27.56	26.67	26.05	25.58	25.23	24.98	24.90	25.34	25.86	27.55
S 15	5.07	**********	**********	35.11	31.70	29.34	27.95	27.05	26.43	25.97	25.63	25.38	25.30	25.74	26.26	27.94
S 15	5.10	**********	**********	34.93	31.43	29.07	27.69	26.81	26.19	25.73	25.39	25.14	25.07	25.52	26.04	27.72
SI 14	5.22	**********	**********	**********	**********	33.51	31.32	30.60	28.24	27.20	26.44	25.93	25.79	26.13	26.31*******	
SI 13	5.29	*******	39.67	35.22	32.03	29.94	28.61	27.65	26.93	26.40	25.99	25.76	25.71	26.56	27.42**********	
SI 13	5.40	*******	39.78	35.33	32.14	30.05	28.72	27.75	27.04	26.51	26.10	25.87	25.82	26.67	27.53**********	
SI 13	5.68	*******	38.94	34.61	31.50	29.49	28.21	27.29	26.62	26.11	25.73	25.51	25.48	26.36	27.23**********	
NI 26	6.14	**********	**********	**********	**********	**********	**********	**********	**********	**********	**********	**********	**********	31.37	29.13	25.92	26.03	26.19	27.43
SI 14	6.18	**********	**********	**********	**********	31.87	29.87	29.30	27.06	26.12	25.43	24.98	24.95	25.34	25.53*******	
MG 12	6.60	**********	**********	**********	32.85	30.86	29.27	28.05	27.14	26.55	26.28	26.25	26.69	27.10**********		
NI 24	6.62	**********	**********	**********	**********	**********	**********	**********	**********	**********	**********	30.43	28.38	26.95	25.68	26.83	27.47	30.46	
SI 13	6.65	*******	36.58	32.58	29.74	27.93	26.83	26.04	25.47	25.05	24.73	24.56	24.57	25.53	26.43**********		
SI 13	6.69	*******	36.97	32.98	30.15	28.35	27.25	26.47	25.90	25.48	25.17	25.00	25.01	25.98	26.87**********		
MG 12	6.70	**********	**********	**********	32.97	30.98	29.40	28.17	27.27	26.68	26.40	26.37	26.82	27.22**********			
SI 13	6.74	*******	36.63	32.65	29.93	28.03	26.94	26.16	25.60	25.18	24.87	24.70	24.71	25.68	26.58**********		
NI 25	6.76	**********	**********	**********	**********	**********	**********	**********	**********	**********	**********	**********	30.32	28.48	26.30	26.95	27.35	29.46	
NI 23	6.94	**********	**********	**********	**********	**********	**********	**********	**********	30.90	28.70	27.40	26.31	25.95	27.63	28.51*******			
NI 26	7.10	**********	**********	**********	**********	**********	**********	**********	**********	**********	**********	**********	31.26	29.05	25.92	26.05	26.22	27.48	
MG 12	7.11	**********	**********	32.27	30.33	28.80	27.61	26.73	26.16	25.91	25.89	26.36	26.78**********						
FF 24	7.21	**********	**********	**********	**********	**********	**********	**********	**********	**********	**********	**********	30.43	28.40	26.58	24.95	25.13	25.29	26.58
NI 22	7.26	**********	**********	**********	**********	**********	**********	**********	31.20	29.47	27.89	26.75	25.88	26.46	28.62	29.75*******			
MG 11	7.30	36.16	32.84	30.74	29.29	28.23	27.42	26.79	26.33	26.04	25.95	26.09	26.42**********						
FF 21	7.40	**********	**********	**********	**********	**********	**********	**********	**********	28.73	26.84	25.82	25.14	26.22	27.93**********				
MG 11	7.47	36.39	33.04	30.92	29.47	28.39	27.57	26.93	26.46	26.17	26.07	26.21	26.54**********						

```
NI 25  7.50 ************************************************************************ 30.27 28.45 26.30 26.96 27.37 29.49
NI 21  7.60 ************************************** 30.86 29.08 27.90 26.78 26.05 25.58 27.08 29.73**************
NI 23  7.70 ******************************************************* 30.90 28.70 27.39 26.30 25.94 27.61 28.50********
MG 11  7.86   35.49 32.26 30.23 28.85 27.83 27.06 26.46 26.02 25.75 25.67 25.82 26.16******************************
FE 22  7.89 ************************************************************** 27.23 25.73 24.72 24.93 26.11 26.72********
FE 21  7.90 ******************************************************** 28.78 26.87 25.83 25.15 26.21 27.90**************
NI 24  7.94 ***************************************************************** 30.35 28.32 26.91 25.68 26.85 27.49 30.49
FE 21  8.00 ******************************************************** 28.50 26.60 25.58 24.91 25.99 27.69**************
FE 23  8.00 ***************************************************************** 29.22 27.38 25.95 25.28 25.97 26.35 28.49
NI 19  8.10 ***************************** 29.45 27.58 26.70 26.17 25.83 25.61 25.52 25.66 28.86**********************
NI 20  8.25 ********************************** 29.84 28.39 27.29 26.57 25.84 25.45 25.30 27.65 30.74**************
NI 19  8.30 ***************************** 29.76 27.91 27.04 26.53 26.20 25.99 25.90 26.05 29.26**********************
FE 21  8.30 ******************************************************** 28.30 26.40 25.38 24.71 25.79 27.49**************
FE 24  8.35 ***************************************************************** 30.31 28.31 26.52 24.96 25.16 25.32 26.63
MG 12  8.42 ***************************** 30.87 29.07 27.65 26.54 25.74 25.23 25.02 25.03 25.57 26.02**************
FE 19  8.60 ****************************************** 29.02 27.79 26.58 25.70 25.27 25.22 27.82 30.54**************
NI 22  8.60 ************************************************ 31.04 29.35 27.80 26.69 25.85 26.47 28.64 29.77********
NI 21  8.60 ***************************************** 30.64 28.92 27.78 26.69 25.99 25.54 27.09 29.76**************
NI 21  8.83 ***************************************** 30.72 28.97 27.82 26.72 26.01 25.55 27.08 29.75**************
FE 23  8.86 ***************************************************************** 29.16 27.34 25.92 25.28 25.99 26.37 28.52
FE 21  8.95 ******************************************************** 28.40 26.53 25.54 24.88 26.00 27.71**************
NI 19  9.00 ***************************** 29.10 27.31 26.49 26.01 25.72 25.53 25.47 25.63 28.86**********************
NI 19  9.10 ***************************** 29.08 27.29 26.48 26.00 25.71 25.53 25.46 25.63 28.86**********************
FE 18  9.15 ********************** 33.98 30.56 28.50 27.28 26.41 25.73 25.26 25.15 25.45 28.90**********************
MG 11  9.17   33.39 30.45 28.65 27.45 26.58 25.92 25.41 25.04 24.83 24.80 24.99 25.35******************************
FE 20  9.20 ********************************************** 29.03 27.41 26.16 25.41 25.09 26.89 29.18**************
NI 26  9.20 ************************************************************************ 31.00 28.85 25.81 25.97 26.16 27.44
MG 11  9.23   33.84 30.92 29.13 27.93 27.07 26.41 25.91 25.54 25.33 25.30 25.49 25.86******************************
NI 22  9.25 ********************************************** 30.91 29.29 27.78 26.70 25.89 26.57 28.76 29.90********
MG 11  9.31   33.39 30.47 28.69 27.51 26.65 26.00 25.50 25.13 24.93 24.90 25.09 25.46******************************
NI 24  9.32 ***************************************************************** 30.25 28.28 26.92 25.79 26.99 27.65 30.68
NI 23  9.35 ******************************************************** 30.74 28.64 27.40 26.36 26.11 27.83 28.73********
FE 22  9.45 ************************************************************** 27.17 25.68 24.70 24.93 26.13 26.74********
```

```
FE 19  9.50 ****************************************  28.86  27.67  26.49  25.64  25.23  25.20  27.83  30.56**************
NI 25  9.50 ************************************************************************  30.02  28.25  26.19  26.89  27.31  29.46
NE 10  9.50 ********************  31.03  29.29  28.00  27.04  26.46  26.24  26.26  26.40  26.58  27.17**********************
NI 26  9.52 ************************************************************************  30.91  28.76  25.72  25.88  26.07  27.35
FE 20  9.60 *********************************************  29.03  27.41  26.16  25.41  25.09  26.89  29.18**************
NI 23  9.60 ******************************************************  39.17  35.01  32.14  29.82  27.07  27.86  28.44********
NI 22  9.65 ************************************************  30.53  28.92  27.43  26.36  25.56  26.25  28.45  29.59********
FE 20  9.70 *********************************************  28.98  27.37  26.13  25.39  25.08  26.90  29.19**************
FE 19  9.70 ****************************************  28.56  27.37  26.19  25.34  24.93  24.90  27.53  30.26**************
FE 19  9.70 ****************************************  28.77  27.60  26.44  25.60  25.21  25.19  27.84  30.57**************
NE 10  9.70 ********************  31.16  29.42  28.12  27.17  26.59  26.36  26.39  26.53  26.70  27.30**********************
NI 26  9.70 ************************************************************************  31.04  28.89  25.86  26.02  26.21  27.50
NI 23  9.[illegible] ******************************************************  30.63  28.48  27.21  26.16  25.87  27.57  28.46********
NI 21  9.70 ****************************************  30.57  28.80  27.62  26.49  25.76  25.29  26.80  29.45**************
NI 25  9.75 ************************************************************************  30.05  28.28  26.21  26.90  27.32  29.46
FE 21  9.81 ******************************************************  28.37  26.46  25.42  24.73  25.79  27.48**************
NI 21  9.86 ****************************************  30.58  28.87  27.74  26.66  25.96  25.52  27.07  29.75**************
FE 17  9.90 **************  33.56  29.91  27.41  26.04  25.37  24.96  24.71  24.64  24.83  25.44  29.64**********************
FE 19 10.00 ****************************************  28.77  27.60  26.44  25.60  25.21  25.19  27.84  30.57**************
NI 19 10.00 ****************************  29.21  27.49  26.73  26.29  26.03  25.87  25.83  26.00  29.27**********************
NI 25 10.00 ************************************************************************  30.04  28.27  26.21  26.91  27.32  29.47
NI 24 10.00 ************************************************************  29.91  27.96  26.61  25.49  26.71  27.37  30.40
NI 19 10.00 ****************************  28.73  27.01  26.25  25.81  25.55  25.39  25.35  25.53  28.80**********************
NI 22 10.04 ************************************************  30.48  28.89  27.41  26.35  25.55  26.26  28.46  29.60********
FE 17 10.10 **************  33.79  30.16  27.66  26.30  25.65  25.24  25.00  24.93  25.13  25.74  29.95**********************
FE 20 10.20 *********************************************  29.09  27.46  26.22  25.47  25.15  26.95  29.24**************
FE 18 10.20 ********************  33.38  30.04  28.05  26.88  26.06  25.41  24.97  24.88  25.19  28.68**********************
NE 10 10.20 ********************  30.50  28.81  27.54  26.61  26.05  25.85  25.89  26.04  26.22  26.83**********************
NI 25 10.20 ************************************************************************  30.04  28.27  26.21  26.91  27.33  29.48
NI 19 10.30 ****************************  27.84  26.19  25.49  25.10  24.88  24.75  24.74  24.93  28.24**********************
FE 19 10.40 ****************************************  28.47  27.30  26.14  25.30  24.91  24.89  27.54  30.27**************
FE 18 10.40 ********************  33.26  29.92  27.93  26.76  25.93  25.29  24.85  24.76  25.07  28.55**********************
NI 24 10.40 ************************************************************  30.49  28.55  27.20  26.10  27.32  27.98  31.02
```

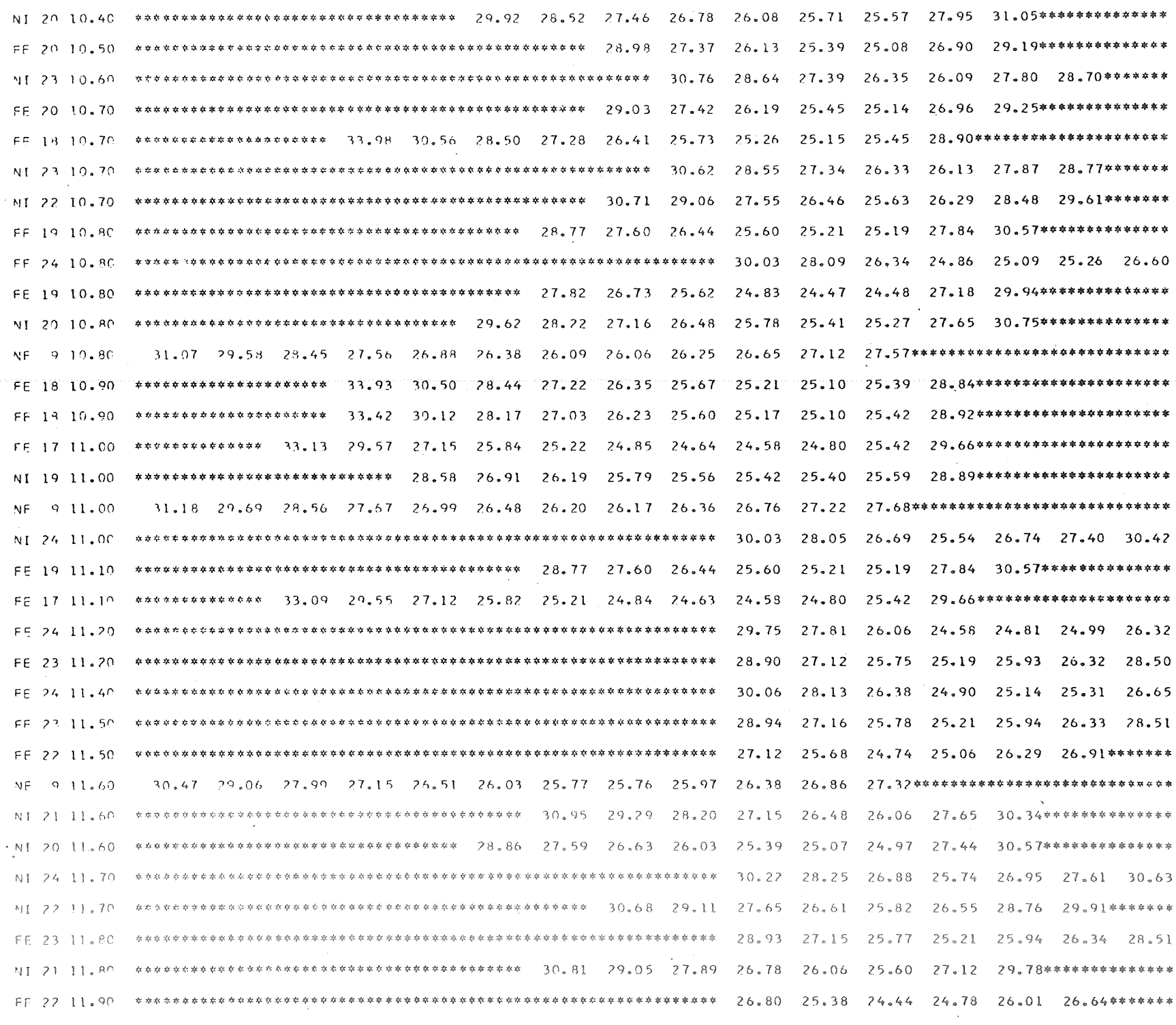
NI 20 10.40 ********** 29.92 28.52 27.46 26.78 26.08 25.71 25.57 27.95 31.05**********
FE 20 10.50 ********** 28.98 27.37 26.13 25.39 25.08 26.90 29.19**********
NI 23 10.60 ********** 30.76 28.64 27.39 26.35 26.09 27.80 28.70*******
FE 20 10.70 ********** 29.03 27.42 26.19 25.45 25.14 26.96 29.25**********
FE 18 10.70 ********** 33.98 30.56 28.50 27.28 26.41 25.73 25.26 25.15 25.45 28.90**********
NI 23 10.70 ********** 30.62 28.55 27.34 26.33 26.13 27.87 28.77*******
NI 22 10.70 ********** 30.71 29.06 27.55 26.46 25.63 26.29 28.48 29.61*******
FE 19 10.80 ********** 28.77 27.60 26.44 25.60 25.21 25.19 27.84 30.57**********
FE 24 10.80 ********** 30.03 28.09 26.34 24.86 25.09 25.26 26.60
FE 19 10.80 ********** 27.82 26.73 25.62 24.83 24.47 24.48 27.18 29.94**********
NI 20 10.80 ********** 29.62 28.22 27.16 26.48 25.78 25.41 25.27 27.65 30.75**********
NF 9 10.80 31.07 29.58 28.45 27.56 26.88 26.38 26.09 26.06 26.25 26.65 27.12 27.57**********
FE 18 10.90 ********** 33.93 30.50 28.44 27.22 26.35 25.67 25.21 25.10 25.39 28.84**********
FE 18 10.90 ********** 33.42 30.12 28.17 27.03 26.23 25.60 25.17 25.10 25.42 28.92**********
FE 17 11.00 ********** 33.13 29.57 27.15 25.84 25.22 24.85 24.64 24.58 24.80 25.42 29.66**********
NI 19 11.00 ********** 28.58 26.91 26.19 25.79 25.56 25.42 25.40 25.59 28.89**********
NF 9 11.00 31.18 29.69 28.56 27.67 26.99 26.48 26.20 26.17 26.36 26.76 27.22 27.68**********
NI 24 11.00 ********** 30.03 28.05 26.69 25.54 26.74 27.40 30.42
FE 19 11.10 ********** 28.77 27.60 26.44 25.60 25.21 25.19 27.84 30.57**********
FE 17 11.10 ********** 33.09 29.55 27.12 25.82 25.21 24.84 24.63 24.58 24.80 25.42 29.66**********
FE 24 11.20 ********** 29.75 27.81 26.06 24.58 24.81 24.99 26.32
FE 23 11.20 ********** 28.90 27.12 25.75 25.19 25.93 26.32 28.50
FE 24 11.40 ********** 30.06 28.13 26.38 24.90 25.14 25.31 26.65
FE 23 11.50 ********** 28.94 27.16 25.78 25.21 25.94 26.33 28.51
FE 22 11.50 ********** 27.12 25.68 24.74 25.06 26.29 26.91*******
NF 9 11.60 30.47 29.06 27.99 27.15 26.51 26.03 25.77 25.76 25.97 26.38 26.86 27.32**********
NI 21 11.60 ********** 30.95 29.29 28.20 27.15 26.48 26.06 27.65 30.34**********
NI 20 11.60 ********** 28.86 27.59 26.63 26.03 25.39 25.07 24.97 27.44 30.57**********
NI 24 11.70 ********** 30.27 28.25 26.88 25.74 26.95 27.61 30.63
NI 22 11.70 ********** 30.68 29.11 27.65 26.61 25.82 26.55 28.76 29.91*******
FE 23 11.80 ********** 28.93 27.15 25.77 25.21 25.94 26.34 28.51
NI 21 11.80 ********** 30.81 29.05 27.89 26.78 26.06 25.60 27.12 29.78**********
FE 22 11.90 ********** 26.80 25.38 24.44 24.78 26.01 26.64*******

```
CA 18 12.00 ********************************************************* 28.10 26.66 25.92 25.71*****************************
FE 21 12.00 ********************************************************* 27.93 26.11 25.14 24.52 25.68 27.42**************
FE 23 12.00 ************************************************************** 28.92 27.15 25.77 25.21 25.95 26.34 28.52
NI 22 12.00 ********************************************** 30.89 29.27 27.78 26.71 25.90 26.59 28.79 29.93*******
FE 18 12.20 ********************* 32.85 29.63 27.74 26.65 25.89 25.29 24.89 24.84 25.17 28.71**********************
NE 10 12.20 ********************* 29.16 27.59 26.43 25.58 25.09 24.93 25.01 25.19 25.40 26.06**********************
FE 21 12.30 ********************************************************* 27.77 25.92 24.93 24.29 25.42 27.14**************
FE 18 12.40 ********************* 32.73 29.51 27.62 26.53 25.76 25.17 24.77 24.71 25.05 28.58**********************
FE 22 12.40 ************************************************************** 27.38 25.96 25.03 25.38 26.62 27.24********
NI 19 12.40 ***************************** 29.67 28.06 27.40 27.04 26.83 26.72 26.72 26.93 30.25**********************
NI 20 12.60 ********************************** 29.06 27.78 26.82 26.22 25.57 25.26 25.15 27.61 30.74**************
NI 19 12.60 ***************************** 27.98 26.38 25.73 25.38 25.18 25.08 25.08 25.29 28.62**********************
FE 21 12.7[illegible] ********************************************************* 27.26 25.45 24.50 23.88 25.07 26.81**************
FE 17 12.70 ************ 32.41 29.02 26.73 25.52 24.99 24.68 24.52 24.51 24.76 25.40 29.69**********************
FE 20 12.70 ********************************************** 28.30 26.73 25.53 24.82 24.53 26.39 28.70**************
NI 19 12.80 ***************************** 29.54 27.96 27.31 26.96 26.76 26.66 26.66 26.88 30.21**********************
FE 21 12.90 ********************************************************* 27.92 26.09 25.12 24.49 25.65 27.38**************
NI 20 12.90 ********************************** 28.58 27.34 26.41 25.83 25.21 24.91 24.82 27.30 30.44**************
FE 18 13.00 ********************* 33.36 30.07 28.11 26.97 26.17 25.54 25.12 25.04 25.36 28.86**********************
CA 17 13.00 ********************************************************* 27.63 26.53 26.14 26.26*****************************
CA 16 13.00 ********************************************** 28.31 26.98 26.13 26.21 26.57*****************************
FE 22 13.10 ************************************************************** 26.89 25.45 24.50 24.81 26.03 26.66********
NI 20 13.10 ********************************** 28.96 27.73 26.80 26.22 25.60 25.30 25.22 27.70 30.84**************
FE 20 13.40 ********************************************** 27.93 26.38 25.19 24.49 24.20 26.08 28.40**************
FE 18 13.40 ********************* 32.78 29.51 27.57 26.44 25.65 25.03 24.61 24.54 24.86 28.37**********************
NE 9 13.40 28.82 27.61 26.69 25.97 25.42 25.02 24.82 24.86 25.10 25.54 26.04 26.52*****************************
FE 21 13.50 ********************************************************* 27.83 26.04 25.11 24.50 25.71 27.46**************
NE 9 13.60 29.31 28.11 27.21 26.50 25.96 25.57 25.37 25.41 25.67 26.11 26.61 27.09*****************************
NI 17 13.60 ********** 32.30 29.20 26.86 25.97 25.91 26.07 26.10 26.37 26.75 27.34*****************************
FE 18 13.70 ********** 33.42 30.12 28.17 27.03 26.23 25.60 25.17 25.10 25.42 28.92**********************
NE 9 13.70 28.79 27.60 26.70 26.00 25.47 25.08 24.88 24.93 25.18 25.62 26.13 26.61*****************************
NI 19 13.70 ********************* 30.20 27.28 25.91 25.42 25.21 25.02 25.04 25.15 25.51 29.25**********************
NI 19 13.80 ************************** 27.69 26.14 25.52 25.20 25.03 24.94 24.95 25.18 28.53**********************
```

```
FE 17 13.80  ************** 31.47 28.12 25.84 24.66 24.14 23.84 23.69 23.68 23.94 24.59 28.89**********************
FE 22 13.90  ************************************************************ 27.09 25.65 24.71 25.02 26.25 26.87********
FE 19 14.00  ************************************** 27.77 26.61 25.46 24.63 24.24 24.22 26.88 29.62***************
FE 19 14.20  ************************************** 27.78 26.69 25.59 24.81 24.45 24.46 27.17 29.93***************
NI 19 14.30  ************************** 27.58 26.04 25.43 25.11 24.94 24.86 24.87 25.10 28.46**********************
FE 18 14.40  ******************** 31.56 28.44 26.64 25.61 24.90 24.34 23.97 23.94 24.30 27.87**********************
FE 20 14.40  ********************************************** 27.89 26.35 25.18 24.48 24.20 26.09 28.41***************
NI 17 14.40  ************** 32.61 29.50 27.14 26.25 26.18 26.33 26.36 26.63 27.01 27.60******************************
NI 19 14.50  ********************** 30.54 27.60 26.22 25.72 25.51 25.31 25.33 25.44 25.79 29.52**********************
FE 20 14.70  ********************************************** 28.08 26.50 25.29 24.57 24.27 26.12 28.42***************
 0  8 14.80    31.68 29.54 27.86 26.66 25.86 25.46 25.39 25.48 25.64 25.84 26.05 26.24******************************
FE 19 15.00  ************************************** 28.19 27.15 26.08 25.32 24.99 25.02 27.76 30.53***************
CA 18 15.00  ************************************************************ 28.06 26.63 25.91 25.71******************************
FE 17 15.00  ************** 33.16 29.86 27.64 26.49 26.00 25.73 25.59 25.60 25.87 26.53 30.84**********************
CA 16 15.00  ********************************************** 28.26 26.95 26.11 26.20 26.57******************************
CA 15 15.10  ********************************************** 27.32 26.42 25.95 26.40 27.10******************************
FE 20 15.20  ********************************************** 28.43 26.91 25.75 25.07 24.80 26.71 29.03***************
FE 19 15.20  ************************************** 27.95 26.83 25.70 24.89 24.52 24.52 27.20 29.95***************
 0  8 15.20    31.80 29.67 27.98 26.78 25.99 25.58 25.52 25.61 25.77 25.97 26.17 26.37******************************
FE 17 15.30  ************** 31.60 28.32 26.10 24.96 24.48 24.22 24.09 24.10 24.37 25.03 29.35**********************
FE 16 15.40  ******* 33.12 30.89 27.83 25.77 24.79 24.40 24.26 24.25 24.40 24.80 25.62******************************
FE 18 15.40  ********************** 31.76 28.64 26.83 25.80 25.09 24.53 24.16 24.12 24.48 28.05**********************
FE 17 15.50  ************** 33.16 29.89 27.68 26.54 26.06 25.80 25.68 25.69 25.96 26.63 30.95**********************
 0  8 16.00    31.12 29.04 27.39 26.22 25.46 25.08 25.03 25.13 25.30 25.51 25.72 25.92******************************
CA 17 16.00  ************************************************************ 27.60 26.51 26.14 26.26******************************
FE 19 16.00  ********************** 31.22 28.15 26.37 25.38 24.69 24.15 23.79 23.77 24.14 27.73**********************
FE 19 16.20  ********************** 31.60 28.53 26.77 25.77 25.09 24.55 24.20 24.18 24.55 28.14**********************
FE 20 16.30  ********************************************** 28.42 26.91 25.75 25.07 24.80 26.71 29.04***************
CA 15 16.30  ********************************************** 27.50 26.51 25.98 26.38 27.04******************************
FE 20 16.60  ********************************************** 28.29 26.74 25.55 24.84 24.56 26.43 28.74***************
FE 17 16.80  ************** 31.25 28.03 25.86 24.76 24.30 24.06 23.95 23.98 24.26 24.93 29.27**********************
FE 15 17.00  ******* 30.89 28.09 26.14 25.22 25.16 25.30 25.02 25.27 25.66 26.29 27.30******************************
FE 16 17.10  ******* 33.09 30.96 27.97 25.97 25.04 24.68 24.57 24.59 24.75 25.17 26.00******************************
```

```
FE 17 17.10 ************** 31.14 27.93 25.77 24.67 24.22 23.99 23.88 23.91 24.19 24.87 29.20**********************
CA 14 17.20 ****************************************** 27.46 26.53 25.84 25.64 26.27 27.21******************************
 O  7 17.40   27.35 26.49 25.85 25.42 25.23 25.32 25.62 26.05 26.50 26.98 27.42 27.84******************************
FE 16 17.50 ******* 32.34 30.28 27.36 25.40 24.51 24.19 24.10 24.14 24.32 24.75 25.59******************************
 O  7 17.80   27.46 26.60 25.96 25.52 25.34 25.43 25.73 26.16 26.61 27.08 27.53 27.95******************************
CA 19 18.00 ************************************************** 27.99 26.60 25.90 25.73******************************
FE 15 18.00 ******* 31.20 28.38 26.43 25.49 25.42 25.56 25.28 25.52 25.91 26.54 27.55******************************
 O  7 18.20   26.57 25.76 25.15 24.74 24.58 24.69 25.00 25.44 25.90 26.38 26.84 27.26******************************
 O  8 18.00   29.52 27.70 26.18 25.12 24.43 24.11 24.11 24.26 24.46 24.69 24.92 25.14******************************
CA 13 18.20 ************************** 28.77 27.51 26.61 26.06 25.70 25.87 26.65 27.93******************************
 N  7 18.40   29.55 28.00 26.96 26.38 26.19 26.28 26.44 26.64 26.83 27.04 27.25 27.46******************************
CA 16 18.50 ********************************************** 27.37 26.11 25.31 25.43 25.83******************************
 N  7 18.80   29.67 28.12 27.08 26.51 26.32 26.40 26.57 26.76 26.96 27.17 27.38 27.58******************************
CA 19 19.00 ************************************************** 27.52 26.12 25.43 25.25******************************
CA 15 19.40 ********************************************** 27.47 26.54 26.05 26.48 27.17******************************
CA 14 19.40 ****************************************** 27.40 26.49 25.82 25.63 26.26 27.22******************************
CA 12 19.80 ********************* 28.76 27.69 26.83 26.24 25.88 25.89 26.41 27.29**********************************
 N  7 19.90   29.03 27.53 26.53 25.98 25.81 25.91 26.09 26.29 26.50 26.72 26.93 27.14******************************
CA 15 19.90 ********************************************** 26.63 25.71 25.22 25.66 26.36******************************
CA 19 20.00 ************************************************** 27.99 26.60 25.90 25.73******************************
 S 13 20.00 ******* 31.30 28.62 26.79 25.71 25.21 25.35 25.83 26.28 26.65 26.97 27.32******************************
CA 15 20.10 ********************************************** 27.06 26.11 25.60 26.02 26.71******************************
CA 13 20.60 ************************** 28.65 27.43 26.55 26.03 25.69 25.87 26.66 27.95******************************
 O  7 20.60   25.64 24.96 24.44 24.11 24.00 24.15 24.50 24.98 25.46 25.96 26.42 26.86******************************
 O  7 20.80   26.24 25.55 25.04 24.71 24.61 24.76 25.12 25.59 26.07 26.57 27.04 27.48******************************
 S 14 21.00 ************** 30.83 28.36 26.75 25.81 25.54 25.71 25.84 25.94 26.01 26.10******************************
CA 17 21.00 ************************************************** 26.90 25.84 25.49 25.63******************************
CA 14 21.00 ****************************************** 27.59 26.71 26.06 25.90 26.55 27.51******************************
 O  7 21.10   25.64 24.96 24.46 24.14 24.05 24.20 24.56 25.04 25.52 26.03 26.50 26.93******************************
CA 13 21.20 ************************** 28.69 27.45 26.57 26.04 25.69 25.87 26.65 27.95******************************
CA 12 21.00 ********************* 28.62 27.59 26.76 26.20 25.85 25.88 26.41 27.30**********************************
CA 15 21.20 ********************************************** 26.95 26.03 25.54 25.98 26.68******************************
 N  6 21.30   26.99 26.42 26.13 26.23 26.40 26.84 27.32 27.80 28.26 28.67 29.15 29.59******************************
```

N	6	23.80	27.11	26.54	26.25	26.35	26.52	26.96	27.45	27.93	28.38	28.79	29.28	29.72
S	12	23.90	31.42	28.70	26.76	25.56	24.91	24.81	25.32	26.09	26.82	27.46	28.03	28.62
CA	12	23.90	**********	**********	28.62	27.59	26.76	26.20	25.85	25.88	26.41	27.30	**********	**********
CA	11	24.00	**********	**********	26.70	26.08	25.67	25.37	25.28	25.57	26.27	27.56	**********	**********
S	14	24.20	**********	30.67	28.24	26.67	25.76	25.51	25.69	25.83	25.94	26.02	26.11	**********
CA	13	24.50	**********	**********	28.34	27.07	26.15	25.60	25.23	25.40	26.17	27.45	**********	**********
N	7	24.80	27.72	26.34	25.43	24.96	24.85	25.01	25.22	25.46	25.68	25.92	26.15	26.37
N	6	25.00	26.61	26.07	25.81	25.93	26.12	26.57	27.06	27.55	28.01	28.43	28.92	29.36
CA	14	25.00	**********	**********	**********	**********	**********	**********	26.64	25.78	25.15	24.99	25.64	26.61
CA	14	25.80	**********	**********	**********	**********	**********	**********	27.15	26.26	25.61	25.44	26.08	27.04
CA	13	25.80	**********	**********	**********	**********	28.33	27.12	26.24	25.72	25.38	25.57	26.36	27.66
S	13	26.00	*******	31.18	28.53	26.72	25.66	25.17	25.33	25.82	26.27	26.65	26.98	27.33
C	6	26.40	26.38	25.65	25.38	25.41	25.58	25.77	25.98	26.18	26.40	26.60	26.80	27.01
CA	11	26.70	**********	**********	26.60	26.01	25.63	25.34	25.26	25.57	26.27	27.57	**********	**********
S	11	26.80	29.01	27.10	25.82	25.16	24.96	25.28	26.08	27.15	28.14	29.03	**********	**********
CA	11	27.00	**********	**********	26.42	25.85	25.47	25.19	25.12	25.43	26.14	27.44	**********	**********
C	6	27.00	26.50	25.77	25.51	25.54	25.71	25.90	26.10	26.31	26.52	26.73	26.93	27.14
CA	12	27.30	**********	**********	27.64	26.66	25.87	25.34	25.02	25.07	25.62	26.52	**********	**********
CA	14	27.80	**********	**********	**********	**********	**********	**********	27.20	26.36	25.73	25.59	26.25	27.23
C	6	28.50	25.92	25.22	24.98	25.04	25.22	25.43	25.64	25.85	26.07	26.28	26.49	26.70
CA	14	28.50	**********	**********	**********	**********	**********	**********	27.43	26.56	25.92	25.76	26.41	27.38
S	12	28.70	31.21	28.54	26.65	25.47	24.85	24.77	25.30	26.08	26.82	27.46	28.04	28.64
S	11	28.80	29.06	27.13	25.85	25.18	24.97	25.29	26.08	27.15	28.14	29.02	**********	**********
N	6	28.80	25.48	25.03	24.83	25.01	25.24	25.73	26.25	26.76	27.24	27.67	28.17	28.62
N	6	29.10	26.20	25.76	25.57	25.75	25.98	26.47	26.99	27.50	27.98	28.42	28.92	29.37
CA	12	29.20	**********	**********	27.86	26.91	26.14	25.62	25.31	25.37	25.92	26.83	**********	**********
CA	13	29.40	**********	**********	**********	28.71	27.53	26.68	26.18	25.86	26.06	26.86	28.17	**********
N	6	29.50	25.38	24.94	24.75	24.94	25.17	25.66	26.19	26.70	27.18	27.62	28.12	28.57
SI	12	29.80	30.96	28.33	26.52	25.45	25.08	25.15	25.37	25.56	25.72	25.90	26.17	26.47
CA	13	29.80	**********	**********	**********	**********	28.63	27.39	26.50	25.96	25.61	25.79	26.57	27.86
S	14	30.20	**********	30.36	28.02	26.51	25.65	25.44	25.66	25.82	25.96	26.05	26.16	**********
S	13	31.00	*******	30.72	28.18	26.45	25.46	25.03	25.23	25.75	26.23	26.63	26.98	27.34
CA	11	31.20	**********	**********	26.43	25.90	25.55	25.29	25.24	25.57	26.28	27.60	**********	**********

C	5	40.70	25.01	25.11	25.44	25.90	26.37							
SI	12	40.90	30.33	27.86	26.16	25.19	24.89	25.01	25.28	25.51	25.70	25.90	26.18	26.50
SI	10	41.00	26.21	25.07	24.43	24.33	24.77	25.57	26.45	27.21	27.92			
S	11	41.00	27.96	26.21	25.06	24.50	24.38	24.77	25.62	26.73	27.75	28.67		
FF	15	41.00	*******	28.80	26.49	24.93	24.32	24.50	24.85	24.72	25.09	25.58	26.29	27.36
C	5	41.50	23.94	24.05	24.38	24.85	25.33							
S	9	41.50	25.67	25.11	24.99	25.23	25.75	26.72	28.12					
S	8	41.60	25.52	25.39	25.66	26.18	26.98	28.22	29.90					
NI	17	42.20	**********	30.13	27.58	25.66	25.12	25.33	25.70	25.90	26.32	26.80	27.48	
S	12	42.40	30.83	28.28	26.49	25.39	24.84	24.80	25.37	26.18	26.95	27.62	28.21	28.82
FF	16	42.50	*******	31.81	30.17	27.58	25.89	25.21	25.06	25.10	25.25	25.51	26.01	26.89
S	10	42.50	26.05	24.99	24.42	24.31	24.59	25.28	26.42	27.82				
S	9	42.[illegible]	25.58	25.04	24.94	25.20	25.74	26.71	28.12					
MG	10	43.00	26.45	25.50	25.26	25.41	25.62	25.86	25.97	26.08	26.26	26.54		
SI	9	43.00	25.64	25.01	24.86	25.14	25.91	27.05	28.12					
NI	16	43.00	*******	32.10	29.21	27.05	25.46	25.27	25.72	26.36	26.63	27.27	27.99	28.89
NI	19	43.70	**********	29.28	26.82	25.82	25.62	25.64	25.63	25.80	26.03	26.48	30.39	
SI	11	43.80	27.86	26.13	25.04	24.55	24.66	25.16	25.75	26.25	26.74	27.19	27.71	
NI	16	44.00	*******	32.46	29.57	27.41	25.83	25.64	26.09	26.73	27.00	27.64	28.36	29.27
SI	12	44.20	29.99	27.51	25.82	24.84	24.54	24.66	24.93	25.15	25.35	25.55	25.83	26.15
SI	9	44.20	25.17	24.60	24.51	24.83	25.64	26.80	27.88					
NI	18	44.20	**********	28.96	26.49	25.46	25.26	25.27	25.25	25.42	25.64	26.09	30.00	
NI	15	45.00	*******	30.39	28.09	26.45	25.41	25.51	26.31	27.25	27.64	28.54	29.53	
NI	14	45.50	*******	32.38	29.41	27.19	25.55	25.32	25.74	26.35	26.60	27.22	27.93	28.83
SI	12	45.60	30.24	27.78	26.09	25.12	24.82	24.95	25.23	25.45	25.64	25.85	26.13	26.46
NI	17	45.60	**********	30.60	28.03	26.10	25.55	25.75	26.12	26.31	26.72	27.20	27.88	
S	10	45.80	25.99	24.95	24.39	24.29	24.57	25.28	26.42	27.82				
S	8	46.00	25.38	25.29	25.59	26.14	26.95	28.21	29.90					
SI	11	46.30	27.91	26.15	25.03	24.52	24.61	25.10	25.67	26.17	26.65	27.09	27.61	
NI	15	46.60	*******	30.48	28.09	26.39	25.30	25.36	26.12	27.04	27.40	28.29	29.26	
MG	9	47.00	25.34	24.96	25.16	25.72	26.27	26.81	27.19	27.72				
S	10	47.00	26.37	25.26	24.66	24.52	24.77	25.45	26.53	27.96				
S	9	47.00	25.28	24.69	24.56	24.78	25.30	26.25	27.65					

NI	16	47.00	*******	31.88	29.00	26.86	25.29	25.10	25.56	26.21	26.48	27.12	27.85	28.76
MG	10	47.30		26.30	25.39	25.18	25.36	25.59	25.84	25.97	26.09	26.27	26.56	
FF	16	47.40	*******	31.55	29.89	27.28	25.57	24.88	24.72	24.75	24.89	25.15	25.64	26.53
SI	8	47.60		25.27	25.21	25.54	26.14	27.24	28.69					
SI	9	47.70		25.62	25.52	25.81	26.37	27.45	28.88					
S	10	47.70		26.50	25.48	24.94	24.86	25.16	25.87	27.02	28.43			
S	8	47.80		25.38	25.29	25.59	26.14	26.95	28.21	29.90				
SI	10	48.00		26.04	25.01	24.44	24.41	24.90	25.74	26.65	27.43	28.16		
SI	11	49.20		27.83	26.09	24.98	24.49	24.59	25.09	25.67	26.17	26.66	27.11	27.63
S	9	49.30		25.20	24.68	24.60	24.87	25.42	26.40	27.82				
S	7	50.00		24.95	25.29	25.84	26.69	27.87						
NI	15	50.00	*******	29.71	27.44	25.81	24.79	24.91	25.71	26.66	27.06	27.97	28.96	
SI	10	50.[illegible]		25.52	24.51	23.95	23.93	24.43	25.29	26.19	26.98	27.72		
S	10	50.60		26.46	25.45	24.92	24.85	25.15	25.87	27.03	28.43			
NI	18	51.70	**********		29.13	26.68	25.68	25.49	25.52	25.51	25.68	25.92	26.37	30.28
MG	9	52.00		25.22	24.87	25.10	25.68	26.25	26.81	27.20	27.73			
S	10	52.00		26.55	25.48	24.90	24.79	25.07	25.76	26.90	28.29			
SI	11	52.30		27.82	26.09	24.99	24.50	24.60	25.10	25.68	26.19	26.68	27.13	27.65
SI	8	52.40		25.37	25.33	25.68	26.29	27.40	28.86					
SI	9	52.50		25.34	25.27	25.58	26.16	27.25	28.69					
FF	15	52.90	*******	28.49	26.28	24.81	24.25	24.49	24.87	24.78	25.18	25.69	26.41	27.50
MG	8	53.50		24.42	24.54	25.16	26.09	26.96	27.78	28.44	29.15			
NI	18	53.50	**********		28.78	26.30	25.27	25.06	25.07	25.05	25.21	25.44	25.88	29.79
SI	8	53.80		25.31	25.29	25.65	26.27	27.39	28.85					
FF	15	53.90	*******	28.96	26.73	25.25	24.68	24.91	25.29	25.18	25.58	26.09	26.80	27.89
SI	10	54.00		26.01	25.01	24.47	24.46	24.97	25.83	26.75	27.54	28.28		
SI	9	54.00		25.06	24.55	24.50	24.96	25.70	26.88	27.99				
NI	15	54.00	*******	30.61	28.27	26.59	25.53	25.61	26.39	27.32	27.70	28.59	29.57	
FF	16	54.20	*******	30.88	29.32	26.90	25.16	24.53	24.41	24.48	24.64	24.92	25.43	26.33
SI	8	54.50		25.78	25.71	26.04	26.63	27.72	29.16					
S	8	54.60		24.42	24.37	24.71	25.29	26.12	27.40	29.10				
FF	16	54.70	*******	30.59	29.02	26.48	24.83	24.18	24.05	24.11	24.28	24.55	25.06	25.95
S	7	54.90		24.89	25.23	25.81	26.67	27.86						

S	7	55.00	24.73	25.08	25.67	26.53	27.73						
NI	16	55.00	*******	32.44	29.51	27.33	25.73	25.51	25.96	26.58	26.84	27.48	28.20	29.10
SI	9	55.30	24.18	23.69	23.66	24.03	24.87	26.07	27.18					
SI	9	55.70	24.75	24.21	24.13	24.46	25.28	26.45	27.54					
NI	16	55.70	*******	32.32	29.49	27.38	25.83	25.67	26.15	26.80	27.09	27.74	28.47	29.39
FE	14	56.00	29.44	26.92	25.22	24.24	24.11	24.70	25.41	25.44	26.13	26.90	27.93	29.21
NI	17	56.00	**********	30.51	28.01	26.14	25.63	25.86	26.26	26.47	26.90	27.40	28.08	
FE	14	56.20	29.80	27.29	25.59	24.61	24.47	25.07	25.78	25.81	26.50	27.26	28.30	29.58
S	9	56.30	25.52	25.04	25.00	25.30	25.87	26.87	28.30					
SI	7	56.50	24.95	25.39	26.11	27.01								
SI	10	56.80	25.71	24.66	24.08	24.04	24.52	25.36	26.26	27.04	27.77			
S	9	57.00	25.53	24.98	24.88	25.12	25.66	26.63	28.03					
MG	10	57.[illegible]	26.13	25.28	25.12	25.33	25.59	25.87	26.01	26.15	26.35	26.64		
FE	14	58.00	29.72	27.13	25.36	24.33	24.16	24.72	25.40	25.41	26.09	26.84	27.86	29.14
S	8	58.50	24.64	24.62	24.98	25.58	26.43	27.72	29.43					
SI	8	58.90	24.57	24.58	24.96	25.60	26.73	28.20						
FE	13	59.00	27.73	25.82	24.61	24.05	24.31	25.24	26.26	26.38	27.35	28.40		
NI	15	59.00	*******	30.16	27.92	26.33	25.33	25.46	26.28	27.25	27.65	28.57	29.56	
NI	17	59.50	**********	30.21	27.69	25.81	25.29	25.52	25.90	26.11	26.54	27.03	27.71	
FE	14	60.00	29.22	26.72	25.03	24.06	23.94	24.54	25.26	25.29	25.99	26.75	27.79	29.07
FE	13	60.00	27.80	25.81	24.54	23.92	24.15	25.05	26.04	26.15	27.09	28.13		
SI	10	60.50	26.02	24.96	24.38	24.34	24.82	25.66	26.56	27.34	28.07			
S	7	60.80	24.76	25.14	25.75	26.64	27.94							
SI	8	61.00	23.94	23.95	24.34	24.99	26.12	27.60						
SI	9	61.20	24.96	24.44	24.38	24.73	25.56	26.75	27.85					
SI	9	61.70	24.66	24.20	24.19	24.58	25.43	26.64	27.76					
MG	9	62.80	25.04	24.74	25.01	25.63	26.22	26.80	27.21	27.75				
MG	10	63.30	25.75	24.90	24.73	24.95	25.21	25.48	25.63	25.76	25.96	26.25		
MG	7	63.40	25.51	26.06	27.06	28.34	29.49							
FE	16	63.70	*******	30.74	29.20	26.69	25.06	24.43	24.31	24.38	24.55	24.84	25.35	26.25
SI	7	64.00	24.84	25.31	26.06	26.98								
MG	9	64.30	24.25	24.42	25.08	26.04	26.94	27.79	28.46	29.18				
S	9	64.30	24.12	24.12	24.49	25.10	25.96	27.25	28.97					

S	8	65.00	24.92	24.93	25.31	25.93	26.79	28.09	29.81				
FF	13	65.00	27.04	25.15	23.96	23.42	23.69	24.63	25.66	25.79	26.76	27.81	
SI	7	65.60	24.88	25.34	26.08	26.99							
SI	8	65.80	23.91	23.93	24.33	24.98	26.12	27.60					
NF	9	65.90	25.38	25.59	25.83	26.06	26.25	26.43	26.66	27.04	27.61		
MG	10	65.90	24.02	25.18	25.02	25.24	25.50	25.79	25.93	26.07	26.27	26.56	
FE	16	66.40	*******	30.45	28.87	26.33	24.67	24.02	23.89	23.95	24.11	24.39	24.89	25.79
MG	7	66.80	24.55	25.12	26.13	27.41	28.57							
MG	9	67.20	25.00	24.68	24.93	25.53	26.11	26.68	27.08	27.62				
SI	8	67.30	24.17	24.16	24.53	25.15	26.28	27.74						
SI	8	69.80	24.39	24.44	24.86	25.52	26.67	28.16						
FE	14	70.00	29.77	27.22	25.50	24.50	24.35	24.93	25.63	25.65	26.33	27.09	28.12	29.40
FE	13	70.00	27.93	25.97	24.73	24.15	24.39	25.30	26.31	26.42	27.38	28.42		
FF	15	70.00	*******	28.84	26.68	25.26	24.74	25.01	25.42	25.34	25.75	26.28	27.01	28.10
FF	14	71.00	29.66	27.20	25.55	24.61	24.50	25.12	25.85	25.89	26.60	27.37	28.41	29.70
MG	8	71.70	24.67	24.85	25.52	26.49	27.39	28.25	28.93	29.66				
MG	7	71.80	24.81	25.40	26.42	27.72	28.88							
MG	9	72.30	24.94	24.64	24.90	25.52	26.10	26.68	27.09	27.63				
S	7	72.40	24.21	24.63	25.28	26.19	27.41							
SI	7	72.50	24.50	24.92	25.64	26.53								
MG	7	72.90	25.18	25.73	26.72	27.99	29.14							
SI	7	73.40	24.46	24.95	25.71	26.65								
SI	8	74.20	24.37	24.43	24.85	25.52	26.67	28.17						
FE	15	74.50	*******	28.54	26.36	24.92	24.39	24.65	25.05	24.97	25.38	25.89	26.62	27.72
NE	8	74.60	25.29	25.53	25.80	26.04	26.25	26.44	26.68	27.06	27.64			
MG	8	75.00	24.05	24.26	24.95	25.93	26.84	27.71	28.39	29.13				
SI	8	76.00	24.38	24.39	24.79	25.43	26.57	28.04						
FE	13	76.00	27.49	25.63	24.48	23.95	24.24	25.20	26.24	26.38	27.36	28.41		
MG	8	77.40	24.24	24.41	25.07	26.03	26.92	27.77	28.44	29.17				
MG	9	77.70	24.93	24.64	24.92	25.54	26.14	26.72	27.13	27.68				
SI	7	79.50	24.84	25.36	26.14	27.10								
MG	7	81.00	25.03	25.60	26.60	27.89	29.05							

Table 3. Edges in Recombination Sum S as a Function of Temperature (^{o}K) and Wavelength (Å)

		Log T =									
λ	Ion	6.0	6.2	6.4	6.6	6.8	7.0	7.2	7.4	7.6	8.0
2050.00	HeII	0.25	0.15	0.10	0.06	0.04	0.02	0.02	0.01	0.01	....
912.00	HI	0.37	0.23	0.14	0.09	0.06	0.04	....	....	....	....
225.00	OVI	2.01	1.21	0.74	0.46	0.28	0.18	0.11	0.07	0.04	0.02
141.00	CV	8.06	4.22	2.38	1.40	0.84	0.52	0.32	0.20	0.13	0.05
100.00	SiIX	8.18	4.33	2.43	1.43	0.86	0.53	....	....	....	....
93.20	FeX	8.37	4.40	....	....	....	....	....	....	....	....
86.70	FeXVI	8.47	4.42	....	....	....	....	....	....	....	....
74.20	NVII	8.52	4.45	2.46	1.44	....	....	....	....	....	....
71.25	SiXI	....	4.51	2.52	1.45	0.87	....	....	....	....	....
56.60	SiXII	....	....	2.58	1.52	0.91	0.55	....	....	....	....
47.30	FeX	9.08	4.63	2.64	1.54	....	....	....	....	....	....
46.60	MgVIII	9.26	4.65	....	....	....	....	....	....	....	....
40.80	SiVIII	9.42	4.66	....	....	....	....	....	....	....	....
38.50	MgIX	9.79	4.67	....	....	....	....	....	....	....	....
37.70	SVIII	10.11	4.68	....	....	....	....	....	....	....	....
37.00	FeXII	10.22	4.70	....	....	....	....	....	....	....	....
35.70	MgX	10.25	4.86	....	....	....	....	....	....	....	....
35.20	SiIX	10.68	5.09	2.70	1.56	0.92	....	....	....	....	....
33.80	MgX	11.14	5.20	2.71	....	....	....	....	....	....	....
33.40	FeXV	11.33	5.29	2.73	1.57	....	....	....	....	....	....
31.60	CV	11.53	5.34	2.77	1.58	....	....	....	....	....	....
30.60	FeXVI	23.73	5.77	2.79	....	....	....	....	....	....	....

27.55	FeXVII	.....	....	2.86	1.62	0.93	....	....	....	....	....
25.35	FeXVI	.....	....	2.92	1.66	....	....	....	....	....	....
24.90	SiXII	55.55	17.83	5.38	2.35	1.21	0.67	....	....	....	....
22.50	NVI	.....	18.12	5.70	2.46	1.25	0.68	....	....	....	....
18.60	NVII	60.24	19.11	5.75	....	....	....	....	....	....	....
17.60	SXIV	60.87	21.93	6.84	2.72	1.33	0.71	0.32	0.20	0.13	0.05
16.80	OVII	.....	21.94	7.10	2.91	1.39	0.74	0.33	....	....	....
14.20	OVIII	79.90	36.96	9.92	3.06	1.40	....	....	....	....	....
10.40	NeIX	80.00	40.62	19.02	6.46	2.36	1.09	....	....	....	....
9.16	FeXVIII	.....	41.99	20.49	7.06	2.42	....	....	....	....	....
9.12	NeX	.....	.....	.....	7.08	2.50	1.12	....	....	....	....
8.55	FeXIX	.....	.....	20.63	8.00	3.06	1.30	0.40	....	....	....
7.85	FeXX	.....	.....	.....	....	3.10	1.36	....	....	....	....
7.36	FeXXI	.....	.....	.....	....	3.12	1.45	0.41	....	....	....
7.04	MgXI	.....	.....	.....	....	....	1.55	0.45	....	....	....
6.92	FeXXII	.....	.....	21.45	8.89	3.58	1.61	0.46	....	....	....
6.36	FeXXIII	.....	.....	.....	....	....	1.65	0.52	0.21	....	....
6.33	MgXII	.....	.....	.....	....	....	1.66	0.57	0.23	....	....
6.06	FeXXIV	.....	.....	.....	8.89	4.02	2.07	0.73	0.29	....	....
5.09	SiXIII	.....	.....	.....	....	....	2.08	0.97	0.47	0.22	0.06
4.65	SiXIV	.....	.....	22.10	8.99	5.04	2.63	1.07	0.48	....	....
3.85	SXV	.....	.....	.....	....	5.14	3.15	1.58	0.71	0.32	....
3.56	SXVI	.....	.....	.....	9.22	5.37	3.32	1.67	0.74	....	....

2.42	CaXIX	.....	.....	.....	....	....	3.35	1.78	0.88	0.40	0.08
1.35	FeXXVI	.....	.....	.....	....	....	....	....	1.10	0.69	0.19
1.24	NiXXVII	.....	.....	.....	....	....	....	....	....	....	0.21
1.01	NiXXVIII	.....	.....	.....	....	....	....	....	1.13	0.74	0.24

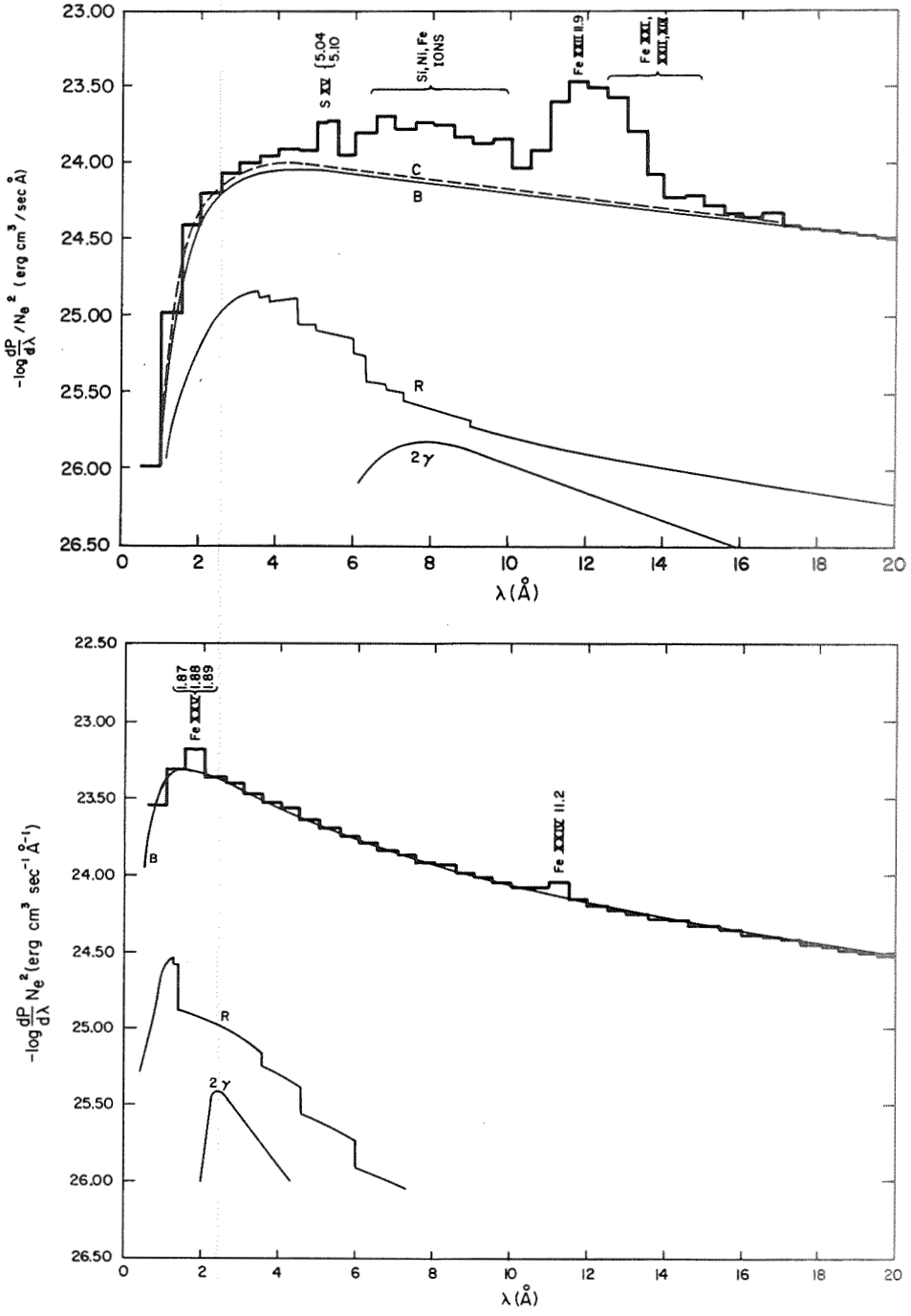
S XV {5.04 5.10
Si, Ni, Fe IONS
Fe XXIII 11.9
Fe XXI, XXII, XIII
C
B
R
2γ
$-\log \frac{dP}{d\lambda} / N_e^2$ (erg cm^3 / sec Å)
λ (Å)
Fe XXV {1.87 1.88 1.89
Fe XXIV 11.2
B
R
2γ
$-\log \frac{dP}{d\lambda} N_e^2$ (erg cm^3 sec^{-1} Å^{-1})
λ (Å)

Figure 1

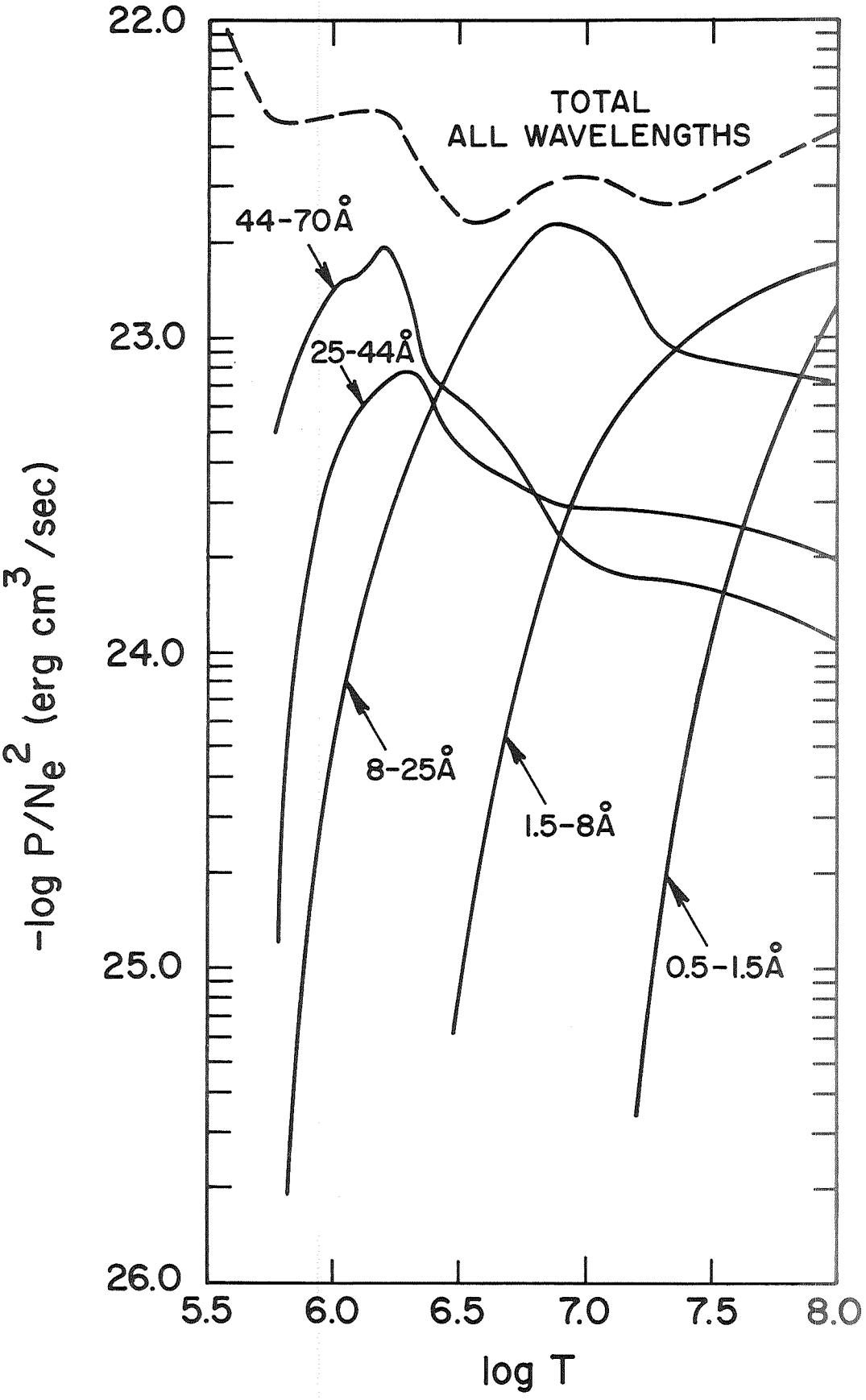
22.0
23.0
24.0
25.0
26.0
5.5
6.0
6.5
7.0
7.5
8.0
log T
-log P/Ne2 (erg cm3/sec)
TOTAL
ALL WAVELENGTHS
44-70Å
25-44Å
8-25Å
1.5-8Å
0.5-1.5Å

Figure 2

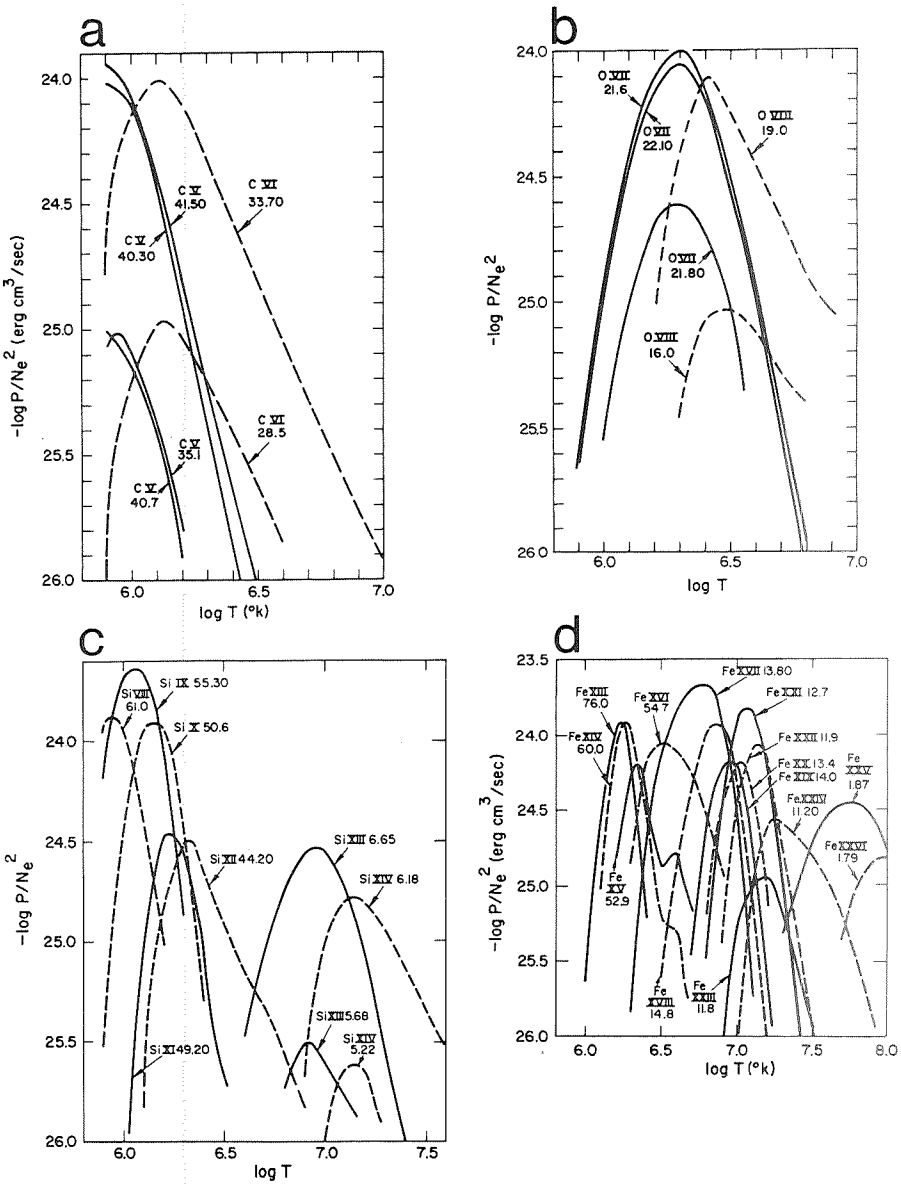
a
b
c
d
-log P/Ne2 (erg cm3/sec)
log T (°k)
log T
C VI 41.50
C V 40.30
C VI 33.70
C V 35.1
C V 40.7
C VI 28.5
O VIII 21.6
O VII 22.10
O VIII 19.0
O VII 21.80
O VIII 16.0
Si IX 55.30
Si VIII 61.0
Si X 50.6
Si XII 44.20
Si XIII 6.65
Si XIV 6.18
Si XIII 5.68
Si XIV 5.22
Si XI 49.20
Fe XVII 13.80
Fe XIII 76.0
Fe XVI 54.7
Fe XII 12.7
Fe XIV 60.0
Fe XXII 11.9
Fe XX 13.4
Fe XIX 14.0
Fe XXV 1.87
Fe XXIV 11.20
Fe XXVI 1.79
Fe XV 52.9
Fe XVIII 14.8
Fe XVIII 11.8

Figure 3

APPENDIX D

```
      C  MKOREN
      C
      C  INPUT
      C       NUMT :  NUMBER OF TEMPERATURES OF INTEREST STARTING FROM TEMP
      C       TEMP :  THE INITIAL TEMPERATURE OF INTEREST
      C     FOR SOLAR TEMP RANGE IS 5.8 TO 8.0
      C     FOR STELLAR TEMP RANGE IS 5.5 TO 8.0
      C       ISTELL = 1 : STELLAR  RUN
      C       ISTELL = 0 : SOLAR RUN
      C  IOUT = 1 RESONANCE LINES
      C  IOUT = 2  DIELECTRIC RECOMBINATION
      C  IOUT = 3  RADIATIVE RECOMBINATION
0001            COMMON /STELL/ ISTELL, XLLIM, XLLIMN
0002            COMMON/ ALIEZE/ ALAM, IELTAY, ZETA, NUMCNT, IONAY, NARRAY
0003            COMMON /SETIT/ ITINIT , KT
0004            COMMON/ MAONLP/ JPL, NUMT, NZONH, EDELT, ELTION, IZ, ION
               1  , OMEGA, F, G , IECODE, IPLOT, REFWVL, IELT,IOUT, IFILL,
               1   TRANS  , RFWVLO
0005            COMMON /FXXX/ FX,FXLAM, IXCNT
0006            DIMENSION FX(190),FXLAM(190)
0007            INTEGER END
0008            INTEGER CONVRT
0009            DIMENSION IELTAY(77), ALAM(77), ZETA(77)
0010            DIMENSION TRANS(6)
0011            INTEGER * 2  IONAY(77), NARRAY(77)
0012            REAL * 4  NZONH(12)
0013            DIMENSION DATUM(10)
0014            DIMENSION ELTION (10,30,26)
0015                DATA                    NOHHE / 'NOHH' /, END /' END'/
0016            READ(1, 500) NUMT , TEMP, IOUT, ISTELL, DATUM
0017            IF ( ISTELL .EQ. 1 ) GO TO 905
      C  SOLAR   ABUNDANCES FOLLOW
      C   C , N , NE , O , MG , SI , S , FE , NI , CA , HE
0018            NZONH(1) = 5E-04
0019            NZONH(2) = 6.3E-05
0020            NZONH(3) =4E-05
0021            NZONH(4) =3.1E-04
0022            NZONH(5) =3.2E-05
0023            NZONH(6) =5E-05
0024            NZONH(7) =2E-05
0025            NZONH(8) =5E-05
0026            NZONH(9) =5E-06
0027            NZONH(10)= 2E-06
0028            NZONH(11)=.2
0029            GO TO 906
0030     905    CONTINUE
      C  STELLAR ABUNDANCES FOLLOW
      C   C , N , NE , O , MG , SI , S , FE , NI , CA , HE
0031            NZONH(1) = 4E-04
0032            NZONH(2) =1.1E-04
0033            NZONH(3) =1E-04
0034            NZONH(4) =8.9E-04
0035            NZONH(5) =2.5E-05
0036            NZONH(6) =3.2E-05
```

```
0037              NZONH(7) =2.2E-05
0038              NZONH(8) =3.7E-06
0039              NZONH(9) =8.9E-07
0040              NZONH(10)= 1.5E-06
0041              NZONH(11)=.1
0042          906  CONTINUE
0043              PRINT 500,   NUMT , TEMP, IOUT, ISTELL, DATUM
0044          500    FORMAT (I5, F5.0, 2I5, 10A4 )
0045              IPLOT = 2
0046              ITINIT = (TEMP + .00001 - 5.5) * 10.
0047              IDEX = 3
0048              I= -2
0049          902 CONTINUE
0050              I= I + IDEX
0051              READ(1,900)IELTAY(I  ),IONAY(I  ),ALAM(I  ),NARRAY(I  ),ZETA(I  )
                 1,          IELTAY(I+1),IONAY(I+1),ALAM(I+1),NARRAY(I+1),ZETA(I+1)
                 1  ,        IELTAY(I+2),IONAY(I+2),ALAM(I+2),NARRAY(I+2),ZETA(I+2)
0052          900 FORMAT ( 3 (A4,I2, 1X, F5.2, I2,    F4.2 ) )
0053          901 FORMAT (    A4,I2, 1X, F7.2, 2X, I2, 2X, F4.2 )
0054              WRITE (3, 901)
                 1           IELTAY(I  ),IONAY(I  ),ALAM(I  ),NARRAY(I  ),ZETA(I  )
                 1,          IELTAY(I+1),IONAY(I+1),ALAM(I+1),NARRAY(I+1),ZETA(I+1)
                 1  ,        IELTAY(I+2),IONAY(I+2),ALAM(I+2),NARRAY(I+2),ZETA(I+2)
0055              I2 = I + 1
0056              I3 = I + 2
0057              WRITE ( 3, 904)  I , I2, I3
0058          904       FORMAT ( 70X, 3I7 )
0059              IDEX = 3
0060              IF ( IONAY(I+2) .EQ. -1) IDEX = 2
0061              IF ( IONAY(I+1) ) 902, 903, 902
0062          903 CONTINUE
0063              NUMCNT = I
0064              KT = 54
0065              DO 10 J = 1, 1000
0066              READ(1,100) IELT,ION,IT,IF,N,(ELTION(CONVRT(IELT), ION + I - 1 ,
                 1IT*10+IF     -KT  ),  I = 1, N )
0067              IF ( ION .EQ. 30) GO TO 12
0068              TLOG = IT + .1 * IF
0069              ITEMP = ION + N    - 1
0070              WRITE(3,107) IELT,ION,TLOG,N,(ELTION(CONVRT(IELT),I,
                 1IT * 10 +IF  -KT  ),  I = ION, ITEMP )
0071          10  CONTINUE
0072          12    CONTINUE
0073          100   FORMAT ( A4, I2, I2, 1X, I1, I5, 13F5.2 )
0074          107   FORMAT ( A4, I2, F5.1,       I5, 13F5.2 )
0075              IF ( IPLOT .NE. 2)
                 1WRITE (3, 102)
0076          102   FORMAT ( '1 SEQUENCE   TRANSITION  ELEMENT   ION  DELTA E   F
                 1 G      TEMP    P(L) / N(E) N(H)   LAMBDA (A)  P(L)/N(E)**2   R')
0077              PRINT 140
0078          140   FORMAT ( '1ELT ION LAMBDA    -LOG POWER IN LINES '
                 1              /'    LOG T=     5.9    6.0    6.1    6.2    6.3
                 16.4    6.5    6.6    6.7    6.8    6.9    7.0    7.3    7.5    7.6
                 1    8.0')
```

```
0079                JPL = 0
0080          31        CONTINUE
0081                READ( 1, 130) IELT, ION, TRANS, REFWVL, EDELT, F, G, IECODE, IFILL
                   1    , RFWVLO
0082          130       FORMAT( A4, I2, 6A4, F8.3, F7.4, F6.2, F5.2, A4, I2 ,
                   1  F5.2 )
0083                WRITE(11)          IELT, ION, TRANS, REFWVL, EDELT, F, G
                   1  ,RFWVLO
0084                IZ = CONVRT(IELT)
0085                IF ( IZ .EQ. 99 ) GO TO 40
0086                IF ( G     ) 34, 34, 35
0087          34      CONTINUE
0088                OMEGA = F
0089                CALL          MAINSB ( ITINIT, 1)
0090                GO TO 31
0091          35      CONTINUE
0092                CALL          MAINSB ( ITINIT, 0)
0093                GO TO 31
0094           40   CONTINUE
0095                END FILE 7
0096                PRINT 151
0097          151     FORMAT ( '1 LAMBDA            RECOMBINATION SUMS      '
                   1                 /'     LOG T=          5.9   6.0   6.1   6.2   6.3
                   16.4   6.5   6.6   6.7   6.8   6.9   7.0   7.1   7.2   7.3   7.4
                   17.5   7.6   8.0')
0098                DO 41 JI = 1, NUMCNT
0099                IT = ITINIT
0100                DO 42 I = 1, NUMT
0101                IT = IT + 1
0102                TEMP =  (IT + KT ) / 10.
0103                T  = 10.**TEMP
0104                T6 =  T /1.E06
0105                CALL SUMSUB( IT, JI, SUM , T6 )
0106                FX (I) = SUM   / T6
0107          42      CONTINUE
0108                NUMT4 = NUMT - 4
0109                PRINT  150, ALAM(JI), IELTAY(JI), IONAY(JI),
                   1                            (FX(IJI), IJI=2, NUMT4)
                   1  ,    FX(NUMT)
0110          150     FORMAT ( / F8.2, A4, I3, 2X, F6.2, 1X, 18F6.2 )
0111          41      CONTINUE
0112                END FILE 11
0113                IF ( IPLOT .EQ. 2) CALL PLTXWV ( NUMT, JPL )
0114                IF ( IPLOT .EQ. 1 .OR. IPLOT .EQ. 2 )
                   1                      CALL PLOT( 0., 0., 999)
0115                RETURN
0116                END
```

```
0001                BLOCK DATA
0002                COMMON/ MAONLP/ JPL, NUMT, NZONH, EDELT, ELTION, IZ, ION
                   1  , OMEGA, F, G , IECODE, IPLOT, REFWVL, IELT,IOUT, IFILL,
                   1   TRANS , RFWVLO
0003                COMMON/XLAMLO/ XLMLO, XLMHI
0004                DIMENSION XLMLO(5), XLMHI(5)
0005                REAL * 4  NZONH(12)
0006                DIMENSION ELTION (10,30,26)
0007                DIMENSION TRANS(6)
0008                DATA ELTION / 7800*99./
0009                DATA TRANS /'    ', '    ', '    ', '    ', '    ', '    ' /
0010                DATA XLMLO/ 0.1, 1.5, 8.0, 25. , 44./,
                   1  XLMHI / 1.5, 8., 25., 44., 70. /
0011                END
```

```
0001              SUBROUTINE  MAINSB ( ITINIT,IOMEGA )
0002              COMMON /SETIT/ IDUMMY , KT
0003              COMMON/ MAONLP/ JPL, NUMT, NZONH, EDELT, ELTION, IZ, ION
                 1  , OMEGA, F, G , IECODE, IPLOT, REFWVL, IELT,IOUT, IFILL,
                 1    XRANS, RFWVLO
0004              COMMON /PL2WVL/ PL2, XWVL
0005              COMMON /STELL/ ISTELL, XLLIM, XLLIMN
0006              COMMON /FXXX/ FX,FXLAM, IXCNT
0007              DIMENSION FX(190),FXLAM(190)
0008              DIMENSION                                    PL2(280), XWVL(280)
0009              DIMENSION XRANS(6)
0010              DIMENSION TRANS(6)
0011              DIMENSION ELTION (10,30,26)
0012              REAL * 4  NZONH(12)  , I158T
0013              DIMENSION PL1(30), TT(30)
0014              EQUIVALENCE (FXLAM(1), PL1(1) ), (FXLAM(31), TT(1) )
0015              DATA TRANSO /'    '/
0016                  DATA                  NOHHE / 'NOHH' /, END /' END'/
0017              DATA IHYG /'H   '/, IHE/'HE  '/
0018              IF ( XRANS(1) .NE. TRANSO ) GO TO 60
0019              GO TO 61
0020         60   DO 62 I = 1, 6
0021         62   TRANS(I) = XRANS(I)
0022         61    CONTINUE
0023              ZRO = 0.
0024              IFUDGE = 1
0025              IF ( IFILL .EQ. 3 )  IFUDGE = 2
0026              IF ( IFILL .EQ. 1 ) IWT = 1
0027              IF ( IFILL .EQ. 2 ) IRD = 1
0028              IF ( IFILL .EQ. 2 ) REWIND 5
0029              IF ( IFILL .EQ. 1 ) REWIND 5
0030              IF ( ISTELL .EQ. 1) FACTOR = .714 * 1.17
0031              FACTOR = .714 * 1.08
0032              XUPLIM = -22.
0033              XLOLIM = -26.5
0034              IPL = 0
0035              SUMINT = 0.
0036              INTSUM = 0
0037              IT = ITINIT
0038              JPL = JPL + 1
0039              DO 50 I = 1,NUMT
0040              IT = IT + 1
0041              TLOG = (KT  + IT) / 10.
0042              T = 10. **TLOG
0043              R = 1.
0044              IF ( IOUT .EQ. 3 )  GO TO 13
0045              IF ( IOMEGA ) 10, 11, 10
0046          10     CONTINUE
0047              CZ = -16. + ALOG10(1.86) + ALOG10(NZONH(IZ))
0048              XLOGPL = CZ + ALOG10 (OMEGA) + ALOG10 ( EDELT / 13.53 )
                 1         -ELTION( IZ, ION, IT )  - 5040. * EDELT / T
                 1   -.5 * TLOG
0049              GO TO 12
0050         11     CONTINUE
```

```
0051              CZ = -15. + ALOG10(2.71) + ALOG10(NZONH(IZ))
0052              XLOGPL = CZ + ALOG10(F*G) - ELTION(IZ,ION,IT) - .5*TLOG
                 1         - 5040. * EDELT / T
0053              GO TO 12
0054           13   I12 = (ION  ) **2
0055              IF ( IECODE .EQ. IHYG) JHY = 1
0056              IF ( IECODE .EQ. IHE ) JHY = 2
0057              IF ( IOMEGA .EQ. 1 ) JHY = 0
0058              I158T = I12 * 158000. / T
0059              XLOGPL = -100.
0060              IF ( ELTION( IZ, ION, IT) .EQ. 99. .OR. ELTION(IZ,ION+1,IT) .EQ.
                 1   99.) GO TO 12
0061              IF ( JHY .EQ. 2 ) GO TO 15
0062              IF ( JHY .EQ. 1 ) GO TO 14
0063              IF ( IWT .EQ. 1 ) GO TO 17
0064              IF ( IRD .EQ. 1 ) GO TO 18
0065              GO TO 12
0066           14   PLQ   = 6.1E-23 * SQRT(T) * EXP(-I158T )
                 1      * 10.**(- ELTION(IZ, ION, IT )  )
                 1  * NZONH( IZ ) * EDELT * F / I12**2
0067           108    FORMAT ( ' AT 14 ' )
0068              GO TO 44
0069           17     F = .7
0070              GO TO 15
0071           18     F = .3
0072              GO TO 15
0073           15     PLQ = 1.6E-23 * T**(-.5) * I12 * F * EDELT
                 1   * NZONH(IZ ) * 10.** (- ELTION( IZ, ION+1, IT ) )
                 1   *(.4288 + .5 * ALOG( I158T) + .47 * I158T**(-.3333333) )
0074           107    FORMAT ( ' AT 15 ' )
0075              GO TO 44
0076           12     CONTINUE
0077              FX(I) =  99999.
0078              PL2(I) = 0.
0079              IF (XLOGPL + 99.) 55,55,45
0080            55 CONTINUE
0081              PLQ = 0.
0082              IF ( IRD .EQ. 1 .AND. IOUT .EQ. 2) READ(5) PLQ
0083              GO TO 43
0084            45 PL = 10. ** XLOGPL
0085              A = 1.
0086              IF ( IOMEGA .EQ. 0 ) A = 1./( 1. + .075*ION + .0085*(ION  )**2)
0087              RN = 10. * EDELT * (ION  )**2.5 * 2. * A * (ION-1)
                 1   / ( T * (ION**2 -2.*ION + 14.4 ) **.5   )
0088              IF ( IOUT .EQ. 2 ) R = 10. * ION**2 *(EDELT / T  ) * IFUDGE
0089              PLQ = PL * R * FACTOR
0090              IF ( IRD .EQ. 1 .AND. IOUT .EQ. 2) READ(5) PLQ
0091           44   CONTINUE
0092              IF ( PLQ .EQ. 0. ) GO TO 43
0093              TEST      = ALOG10( PLQ )
0094              FX(I) =  ABS( TEST )
0095              IF ( TEST .LE.XLOLIM ) GO TO 43
0096               IPL = IPL + 1
0097              PL1( IPL) = TEST
```

```
0098                PL2(I) = PL1(IPL)
0099                TT(IPL) = ALOG10( T)
0100          43      CONTINUE
0101                IF ( IWT .EQ. 1 .AND. IOUT .EQ. 2 ) WRITE(5) PLQ
0102                SUMINT = SUMINT + INTSUM * (PLQ+PO)*.5 * (T-TO)
                   1    *( ( T+TO) *.5)**( -2.833333)
0103                INTSUM = 1
0104                PO = PLQ
0105                TO = T
0106          70     CONTINUE
0107                IF (    IOMEGA .EQ. 1 .AND. IPLOT .NE. 2 )
                   1   WRITE( 3, 103) IELT, ION, TRANS, REFWVL, EDELT, OMEGA, ZRO,
                   1   T, XLAM, RN, PLQ, R
0108                IF (    IOMEGA .EQ. 0 .AND. IPLOT .NE. 2 )
                   1   WRITE( 3, 103) IELT, ION, TRANS, REFWVL, EDELT, F,     G,
                   1   T, XLAM, RN, PLQ, R
0109          103     FORMAT ( A4, 1X, I2, 1X, 6A4, 1X, 2F9.2, 1X, 2F8.3, 1X, E10.2,
                   1   1X, F8.2, 1X, 3E13.5 )
0110           50   CONTINUE
0111                XLAM = 12400. / EDELT
0112                IF ( IFILL .EQ.-1 ) IWT = 0
0113                IF ( IFILL .EQ.-2 ) IRD = 0
0114                A =(KT + ITINIT + 1 )/10.
0115                B = ( KT + ITINIT + NUMT) / 10.
0116                INTESG = 0
0117                IF ( INTESG .EQ. 1) WRITE(3, 100)  A, B,
                   1                                   SUMINT, IELT, ION, TRANS, REFWVL
0118          100     FORMAT(     ' INTEGRAL FROM 10** ', F4.1, ' TO ', F4.1,
                   1   E13.5 ,
                   1   A4, 1X, I2, 1X, 6A4, F13.3 )
0119                 WRITE (7) SUMINT, IELT, ION, TRANS, REFWVL
0120                 WRITE (4)  XLAM    ,(PL2(I), I= 1, NUMT),IELT, ION, TRANS, REFWVL
                   1 , RN    , RFWVLO
0121                 PRINT 101, IELT, ION, REFWVL, (FX(I), I=2, 13),FX(16),   FX(18),
                   1   FX(19), FX(23)
0122          101    FORMAT (/A4, 1X, I2, F6.2,  2X, 16F7.2 )
0123                 RETURN
0124                 END
```

```
0001              SUBROUTINE                PLTXWV ( NUMT, JPL )
0002              COMMON/ MAONLP/ IDUM, JDUM,NZONH, EDELT, ELTION, IZ, ION
                 1  , OMEGA, F, G , IECODE, IPLOT, REFWVL, IELT,IOUT, IFILL,
                 1   TRANS  , RFWVLO
0003              COMMON /EORWVL/ ISTELL
0004              COMMON /PL3WVL/ PL3, XWVLK
0005              COMMON /PL2WVL/ PL2, XWVL
0006              COMMON /SETIT/ ITINIT , KT
0007              COMMON /FXXX/ FX, XLAM, IXCNT
0008              COMMON/ FYYY/  FY, YLAM, IYCNT
0009              COMMON/XLAMLO/ XLMLO, XLMHI
0010              DIMENSION FX(190), XLAM(190)
0011              DIMENSION   FY(110),YLAM(110)
0012              REAL * 4  NZONH(12)
0013              DIMENSION PL3(190), XWVLK(190)
0014              DIMENSION                                   PL2(280), XWVL(280)
0015              DIMENSION WVL(20), POW(20)
0016              DIMENSION ELTION (10,30,26)
0017              INTEGER CONVRT
0018              DIMENSION XLMLO(5), XLMHI(5)
0019              DIMENSION SU(5)
0020              DIMENSION        ONES(2), ONES2(3)
0021              DIMENSION TRANS(6)
0022              DATA ONES/'1S-2', 'P   ' /, ONES2/ '1S2-','1S2P' ,'(1P)' /
0023              PRINT 783
0024        783     FORMAT ( 'ELEMENT  ION TRANSITION              WAVELENGTH DELTA
                 *E F OR OMEGA   G    WVLENGTH LO')
0025              REWIND 11
0026         787      CONTINUE
0027              READ(11, END=786) IELT, ION, TRANS, REFWVL, EDELT, F, G
                 1  ,RFWVLO
0028              PRINT 785,        IELT, ION, TRANS, REFWVL, EDELT, F, G
                 1  ,RFWVLO
0029         785   FORMAT ( 1X, A4, 2X,I3,2X, 6A4,5F10.3 )
0030              GO TO 787
0031         786     CONTINUE
0032              ISTELL = 0
                C   ISTELL = 0 : PLT VS WAVELENGTH
                C   ISTELL = 1 : PLT VS ENERGY
0033              JNTTMP = 1
                C     JNTTMP = 0     : NO INTEGRAL OVER TEMPERATURE
0034              IF ( INIT .NE. 123456) GO TO 11
0035              GO TO 13
0036         11    INIT = 123456
0037              CALL PLOTS
0038              CALL PLOT( 0., -.5, 3)
0039              IF ( ISTELL ) 14, 14, 15
0040         15    XMIN = -1.
0041              XDEL = .05
0042              XDST = 40.
0043              GO TO 16
0044         14     CONTINUE
0045              XDST = 35.
0046              XDEL = 2.
```

```
0047                XMIN = 0.
0048          16      CONTINUE
0049                YDST = 8.
0050                YDEL = 4. / YDST
0051                YMIN = -26.5
0052                IT = ITINIT
0053          13     CONTINUE
0054                DO 20 ITEMP = 1, NUMT
0055                IT = IT + 1
0056                CALL AXIS( 0., 0., 'LOG(P/NE**2)',12, YDST, 90., YMIN, YDEL)
0057                IF ( ISTELL .EQ. 0 )
                   1CALL AXIS( 0., 0., 'WAVELENGTH',      -10, XDST, 0., XMIN, XDEL)
0058                IF ( ISTELL .EQ. 1 )
                   1CALL AXIS( 0., 0., 'LOG W KEV ',      -10, XDST, 0., XMIN, XDEL)
0059                HENZ = .2
0060                TEMP =  (IT + KT ) / 10.
0061                T  = 10.**TEMP
0062                CALL SYMBOL( 0., 9., .12, 'LOG(T)=', 0., 7)
0063                CALL NUMBER( .96, 9., .12, TEMP, 0., 1)
0064                WRITE ( 3, 108) TEMP
0065          108    FORMAT (  /////' LOG(T) = ', F10.3 /
                     1    '     TRANSITION                                  LOG(W)  POWER IN LI
                     1NE  CHECK        12400/E DELTA    R             WAVELENGTH')
0066                REWIND 4
0067                JSU = 5
0068                DO 3456 I = 1, JSU
0069          3456    SU(I) = 0.
0070                SUMP = 0.
0071                IND = 0
0072                DO 10 J = 1, JPL
0073                READ  (4) XLAM1    ,(PL2(I), I= 1, NUMT),IELT, ION, TRANS, REFWVL
                    1   ,RN   , RFWVLO
0074                IF ( PL2(ITEMP) .EQ. 0.) GO TO   10
0075                XWVL(ITEMP) = XLAM1
0076                                    TEMP1 = ALOG10( 12.4 / REFWVL )
0077                WRITE (3,106)          TRANS,          IELT, ION, TEMP1
                    1, PL2(ITEMP)  , TEMP      , XWVL(ITEMP)
                    1 , RN   , REFWVL   , RFWVLO
0078           106 FORMAT (7X, 6A4,              A4, 6X, I2, F7.2, E14.6 ,2F12.2 ,E14.6
                    1, F12.2 , F7.2 )
0079                IF ( TRANS(1) .EQ. ONES(1) .AND. TRANS(2) .EQ. ONES(2) ) GO TO 31
0080                IF ( TRANS(1) .EQ. ONES2(1).AND. TRANS(2) .EQ. ONES2(2)
                    1                          .AND. TRANS(3) .EQ. ONES2(3) )GO TO 32
0081                GO TO 33
0082          31       CONTINUE
0083                TEMP = 4.
0084                GO TO 34
0085          32      CONTINUE
0086                TEMP = 2.
0087          34      CONTINUE
0088                IND = IND + 1
0089                WVL( IND) = XWVL( ITEMP)
0090                POW( IND) = 10.**PL2( ITEMP) * TEMP
0091          33       CONTINUE
```

```
0092                ILINP = 1
0093                IF ( ILINP .EQ. 0) GO TO 10
0094                XWVL(ITEMP ) = REFWVL
0095                IF ( ISTELL .EQ. 1) XWVL(ITEMP) = ALOG10( 12.4 / REFWVL )
0096                IF ( XWVL(ITEMP) .GT. XMIN+XDST*XDEL ) GO TO 10
0097                DO 35 I = 1, JSU
0098                IF ( REFWVL .GT. XLMLO(I) .AND.REFWVL .LE. XLMHI(I) )
                   1SU(I)= SU(I)+ 10.**PL2(ITEMP)
0099          35      CONTINUE
0100                SUMP = SUMP + 10.**PL2(ITEMP)
0101                WRITE (12) XWVL(ITEMP)  , PL2(ITEMP)   , REFWVLO
0102                CALL          PLTLIN( XWVL(ITEMP), PL2(ITEMP), XMIN, XDEL,
                   1   YMIN, YDEL, IELT, ION, REFWVL, TRANS )
0103          10      CONTINUE
0104                WRITE ( 3, 107) SUMP
                   1  ,SU
0105          107    FORMAT ( '  SUM OF LINES = ' , E14.6  / 5E14.6 )
0106                END1 = 123456.
0107                WRITE( 12) END1, END1, END1
0108                ICONT = 1
0109                IF ( ICONT .EQ. 1 )
                   1CALL TWOPHO( WVL, XWVL, PL2, POW, IND, II )
0110                XWVL (II+1) = XMIN
0111                XWVL (II+2) = XDEL
0112                PL2(II+1) = YMIN
0113                PL2(II+2) = YDEL
0114                IF ( ISTELL .EQ. 1 ) CALL LAMTOW( XWVL, II )
0115                IF ( II .GT. 0 )
                   1CALL LINE  ( XWVL,  PL2, II, 1, 0,1 )
0116                IF ( ICONT .EQ. 1 )
                   1CALL CONT( II, IT, T , KK)
0117                XWVL (II+1) = XMIN
0118                XWVLK(KK+1) = XMIN
0119                XWVL (II+2) = XDEL
0120                XWVLK(KK+2) = XDEL
0121                PL2(II+1) = YMIN
0122                PL3(KK+1) = YMIN
0123                PL2(II+2) = YDEL
0124                PL3(KK+2) = YDEL
0125                IF ( ISTELL .EQ. 1 ) CALL LAMTOW( XWVL, II )
0126                IF ( II .GT. 0 )
                   1CALL LINE  ( XWVL,  PL2, II, 1, 0,1 )
0127                IF ( ISTELL .EQ. 1 ) CALL LAMTOW( XWVLK, KK )
0128                IF ( KK .GT. 0 )
                   1CALL LINE  ( XWVLK, PL3, KK, 1, 0,1 )
0129                IJ = 0
0130                DO 12    I = 1, IYCNT
0131                FIY = TRPLIN( YLAM(I), IXCNT, XLAM, FX )
0132                TEMP     = FIY + FY(I)
0133                IF ( TEMP .LE. 0.) GO TO 12
0134                IJ = IJ + 1
0135                PL2(IJ) = ALOG10( TEMP)
0136                XWVL(IJ) = YLAM(I)
0137          12      CONTINUE
```

```
0138                DO 40 I = 1, IXCNT
0139                FIX = TRPLIN( XLAM(I), IYCNT, YLAM, FY )
0140                TEMP = FIX + FX(I)
0141                IF ( TEMP .LE. 0.) GO TO 40
0142                IJ = IJ + 1
0143                PL2(IJ) = ALOG10( TEMP)
0144                XWVL(IJ) = XLAM(I)
0145          40       CONTINUE
0146                CALL SORTP( IJ, XWVL, PL2 )
0147                WRITE(12)T, IJ, (XWVL(IIJ), PL2(IIJ), IIJ=1, IJ)
0148                JI = 0
0149                DO 41 IIJ = 1, IJ
0150                IF ( PL2( IIJ) .LT. YMIN) GO TO 41
0151                JI = JI + 1
0152                PL2(JI) = PL2( IIJ)
0153                XWVL(JI) = XWVL( IIJ)
0154           41     CONTINUE
0155                IJ = JI
0156                IF (  IJ .EQ. 0 ) GO TO 21
0157                PL2(IJ+2) = YDEL
0158                PL2(IJ+1) = YMIN
0159                XWVL (IJ+2) = XDEL
0160                XWVL (IJ+1) = XMIN
0161                WRITE(8) T, IJ, (XWVL(IIJ), PL2(IIJ), IIJ=1, IJ)
0162                IF ( ISTELL .EQ. 1 ) CALL LAMTOW( XWVL, IJ )
0163                CALL LINE  ( XWVL,  PL2, IJ, 1, 0,1 )
0164          21      CONTINUE
0165                X = XDST+ 1.2
0166                CALL PLOT( X,         0., -3 )
0167          20      CONTINUE
0168                IF ( JNTTMP .EQ. 1 ) CALL INTTMP
0169                END FILE 12
0170                RETURN
0171                END
```

```
0001              FUNCTION  CONVRT (I    )
0002              INTEGER CONVRT
0003              INTEGER
                 1       C, N, NE, O, MG, SI, S, FE, NI  , CA
0004              DATA  C, N, NE, O, MG, SI, S, FE, NI /'   C','   N','  NE',
                 1     '   O','  MG','  SI','   S', '  FE', '  NI' /
0005              DATA CA /'  CA' /
0006              CONVRT= 99
0007              IF ( I . EQ. C) CONVRT = 1
0008              IF ( I . EQ. N) CONVRT = 2
0009              IF ( I . EQ.NE) CONVRT = 3
0010              IF ( I . EQ. O) CONVRT = 4
0011              IF ( I . EQ.MG) CONVRT = 5
0012              IF ( I . EQ.SI) CONVRT = 6
0013              IF ( I . EQ. S) CONVRT = 7
0014              IF ( I . EQ.FE) CONVRT = 8
0015              IF ( I . EQ.NI) CONVRT = 9
0016              IF ( I . EQ.CA) CONVRT = 10
0017               TEMP = CONVRT
0018              IF ( TEMP .EQ. 99. ) WRITE ( 3, 100) I    , CONVRT
0019          100   FORMAT ( /// ' ERROR IN ELMT CONVERSION , ELMT = ' , A4 , I5 )
0020              RETURN
0021              END
```

```
0001              SUBROUTINE CONT( II, IT, T , KK)
0002              COMMON /EORWVL/ JSTELL
0003              COMMON /STELL/ ISTELL, XLLIM, XLLIMN
0004              COMMON/ ALIEZE/ ALAM, IELTAY, ZETA, NUMCNT, IONAY, NARRAY
0005              COMMON /PL2WVL/ PL2, XWVL
0006              COMMON /PL3WVL/ PL3, XWVLK
0007              COMMON /FXXX/ FXLAM, XXLAM, JX
0008              COMMON/XLAMLO/ XLMLO, XLMHI
0009              DIMENSION SU(5)     , SM(5)
0010              DIMENSION XLMLO(5), XLMHI(5)
0011              DIMENSION SZETA(77)
0012              INTEGER * 2  IONAY(77), NARRAY(77)
0013              DIMENSION IELTAY(77), ALAM(77), ZETA(77)
0014              DIMENSION XXLAM(190), FXLAM(190)
0015              DIMENSION PL3(190), XWVLK(190)
0016              DIMENSION                                    PL2(280), XWVL(280)
0017           951  FORMAT ('  WAVELENGTH BREMSTRAHLUNG   RECOMBINATION   S LAMBDA
                 1   INDEX    ' )
0018              WRITE (3, 951)
0019              T6 =  T /1.E06
0020              SUM08 =                          (1.58 / T6) **.08
                 1        + (6.32 /T6 )**.08
0021              SQT6 = SQRT( T6 )
0022              KK = 0
0023              JX = 0
0024              II= 0
0025              SLAM= -1.5
0026              IF ( JSTELL .EQ. 1) SLAM = -.75
0027              JSU = 5
0028              DO 3456 I = 1, JSU
0029              SM(I) = 0.
0030           3456   SU(I) = 0.
0031              SUMI = 0.
0032              SUMK = 0.
0033              INDEX = 2
0034              DELTA = 1.E-03
                C
0035              DO 916 JI = 1, NUMCNT
0036              CALL SUMSUB( IT, JI, SUM , T6 )
0037              SZETA(JI) = SUM
0038           916       CONTINUE
                C
0039           922  CONTINUE
0040              SLAM = SLAM + 2.
0041              IF (ALAM(INDEX-1) - SLAM ) 910, 911, 911
0042           910  XLAM =  ALAM(INDEX-1) - DELTA
0043              SLAM =  SLAM - 2.
0044              IDO  =  2
0045              GO TO  912
0046           911  XLAM =  SLAM
0047              IDO  =  1
0048           912  CONTINUE
0049              E143 =  EXP (-143.89 /(XLAM * T6))
0050              DO  920 JJ = 1, IDO
```

```
0051              IF (JJ  .EQ. 2)XLAM = XLAM + 2. * DELTA
0052              DO 904  I = 1, NUMCNT
0053              IF ( ALAM(I) .LE. XLAM ) GO TO 905
0054          904 CONTINUE
0055              INDEX = NUMCNT + 1
0056              SUM = SZETA( NUMCNT)
0057              GO TO 906
0058          905 CONTINUE
0059              SUM = SZETA( I )
0060              INDEX = I
0061          906 CONTINUE
0062              SUM = SUM * .142 /T6
0063              IF ( JSTELL ) 20, 20, 21
0064          21    CONTINUE
0065              W = 12.4 / XLAM
0066              E116 = EXP( -11.6 * W / T6 )
0067              TEMPK =(2.64E-23 * E116 / SQT6  ) * 1.17
0068              GO TO 22
0069          20    CONTINUE
0070              TEMPK   = (3.28E-22 / (SQT6 * XLAM**2 ) )  * E143     * 1.08
0071          22   CONTINUE
0072              PL2I    = TEMPK
                 1        * (.59 *((1.+ 143.89 / (XLAM * T6) ) * E143
                 1        * (.81 + ALOG ( XLAM * T6 / 143.89 )        )
                 1        + 1.81 * (1.- E143)) * ( SUM08
                 1  )  )
0073              PL2K = TEMPK * SUM
0074              JX = JX + 1
0075              XXLAM(JX) = XLAM
0076              FXLAM(JX) = PL2I + PL2K
0077              IF ( JX .EQ. 1) GO TO 954
0078                              SUMI = SUMI + (PL2IO + PL2I) * .5 *
                 1  ( XXLAM(JX) - XXLAM(JX-1) )
                 1   * ( 12.4 /(XXLAM(JX)*XXLAM(JX-1) ) )**JSTELL
0079                              SUMK = SUMK + (PL2KO + PL2K) * .5 *
                 1  ( XXLAM(JX) - XXLAM(JX-1) )
                 1   * ( 12.4 /(XXLAM(JX)*XXLAM(JX-1) ) )**JSTELL
0080              DO 955 I = 1, JSU
0081              IF ( XXLAM(JX-1) .GT. XLMLO(I) .AND. XXLAM(JX) .LE. XLMHI(I)  )
                 1                SU(I)= SU(I)+ (PL2IO + PL2I) * .5 *
                 1  ( XXLAM(JX) - XXLAM(JX-1) )
0082              IF ( XXLAM(JX-1) .GT. XLMLO(I) .AND. XXLAM(JX) .LE. XLMHI(I)  )
                 1                SM(I)= SM(I)+ (PL2KO + PL2K) * .5 *
                 1  ( XXLAM(JX) - XXLAM(JX-1) )
0083          955   CONTINUE
0084          954    CONTINUE
0085              PL2IO = PL2I
0086              PL2KO = PL2K
0087              IF ( PL2I .GT. 1.E-22 .OR. PL2I .LT. .3E-26 ) GO TO 952
0088              II = II +1
0089              XWVL(II) =  XLAM
0090              PL2(II) = ALOG10( PL2I )
0091          952   CONTINUE
0092              IF ( PL2K .GT. 1.E-22 .OR. PL2K .LT. .3E-26 ) GO TO 953
```

```
0093                KK = KK + 1
0094                XWVLK(KK) = XLAM
0095                PL3(KK) = ALOG10( PL2K )
0096          953       CONTINUE
0097                TEMP2 = ALOG10( 12.4 / XLAM )
0098                WRITE (3,950) XLAM, PL2I,PL2K, SLAM, INDEX
                   1    , TEMP2
0099          950   FORMAT (  F14.3,2E14.6 ,  F12.1, I10  , F10.2 )
0100          920   CONTINUE
0101                IF(XLAM .GE. XLLIM .OR. XLAM .LE. XLLIMN) GO TO 921
0102                GO TO 922
0103          921   CONTINUE
0104                WRITE ( 3, 103) SUMI, SUMK    , SM, SU
0105          103      FORMAT ( // ' AREA UNDER BREMSTRAHLUNG AND RECOMBINATION = ',
                  1   2E14.6  / 5E14.6 / 5E14.6 ////)
0106                RETURN
0107                END
```

```
0001                SUBROUTINE TWOPHO( ALAM, XWVL, PL2, POW, NUMCNT, II )
0002                COMMON /EORWVL/ JSTELL
0003                COMMON/ FYYY/ FYLAM, YYLAM, JY
0004                COMMON /STELL/ ISTELL, XLLIM, XLLIMN
0005                COMMON/XLAMLO/ XLMLO, XLMHI
0006                DIMENSION SU(5)
0007                DIMENSION XLMLO(5), XLMHI(5)
0008                DIMENSION     FYLAM(110),  YYLAM(110)
0009                DIMENSION ALAM(1), XWVL(1), PL2(1), POW(1)
0010                WRITE (3, 951)
0011             951  FORMAT ('  WAVELENGTH  TWO PHOTON          SUM          S LAMBDA
                    1   INDEX     ' )
0012                XLLIM = 70.
0013                IF ( JSTELL .EQ. 1) XLLIM = 124.
0014                XLLIMN = -1.
0015                IF ( NUMCNT .EQ. 0 ) GO TO 666
0016                CALL SORTP( NUMCNT, ALAM, POW )
0017                JY = 0
0018                II= 0
0019                SLAM= -1.5
0020                IF ( JSTELL .EQ. 1) SLAM = -.75
0021                INDEX = 2
0022                JSU = 5
0023                DO 3456 I = 1, JSU
0024             3456   SU(I) = 0.
0025                SUMI = 0.
0026                DELTA = 1.E-03
0027             922  CONTINUE
0028                SLAM = SLAM + 2.
0029                IF (ALAM(INDEX-1) - SLAM ) 910, 911, 911
0030             910  XLAM =  ALAM(INDEX-1) - DELTA
0031                SLAM =  SLAM - 2.
0032                IDO  =  2
0033                GO TO  912
0034             911  XLAM =  SLAM
0035                IDO  =  1
0036             912  CONTINUE
0037                DO  920 JJ = 1, IDO
0038                IF (JJ  .EQ. 2)XLAM = XLAM + 2. * DELTA
0039                SUM = 0.
0040                DO 904  I = 1, NUMCNT
0041                IF ( ALAM(I) .GT. XLAM ) GO TO 905
0042                TEMP = ALAM(I) / XLAM
0043                GO TO 10
0044             11     SUM = SUM + POW(I) * TEMP**2 * (1- TEMP) * ALAM(I) / 12.4
0045                GO TO 12
0046             10    CONTINUE
0047                SUM = SUM + POW(I) * (TEMP          )**3 *(1.-TEMP         )/XLAM
0048             12     CONTINUE
0049             904  CONTINUE
0050                INDEX = NUMCNT + 2
0051                ALAM( INDEX-1) = XLLIM + .5
0052                GO TO 906
0053             905  CONTINUE
```

```
0054                INDEX = I    + 1
0055           906  CONTINUE
0056                JY = JY + 1
0057                FYLAM(JY) = SUM
0058                YYLAM(JY) = XLAM
0059                IF ( JY .EQ. 1 ) GO TO 954
0060                                 SUMI = SUMI + (SUM + SUMO ) * .5 *
                   1    (YYLAM(JY) - YYLAM(JY-1 )      )
                   1  *( 12.4 / (YYLAM(JY) * YYLAM(JY-1) ) ) **JSTELL
0061                DO 955 I = 1, JSU
0062                IF ( YYLAM(JY-1) .GT. XLMLO(I) .AND.YYLAM(JY) .LE. XLMHI(I) )
                   1                 SU(I)= SU(I)+ (SUM + SUMO ) * .5 *
                   1    (YYLAM(JY) - YYLAM(JY-1 )      )
0063           955     CONTINUE
0064           954    CONTINUE
0065                SUMO = SUM
0066                IF ( SUM  .GT. 1.E-22 .OR. SUM  .LT. .3E-26 ) GO TO 952
0067                II = II +1
0068                XWVL(II) =  XLAM
0069                PL2(II) = ALOG10( SUM  )
0070           952     CONTINUE
0071                TEMP2 = ALOG10( 12.4 / XLAM )
0072                WRITE (3,950) XLAM, PL2I, SUM, SLAM, INDEX
                   1    , TEMP2
0073           950  FORMAT (  F14.3,2E14.6 ,  F12.1, I10  , F10.2 )
0074           920  CONTINUE
0075                IF(XLAM .GE. XLLIM .OR. XLAM .LE. XLLIMN) GO TO 921
0076                GO TO 922
0077           921  CONTINUE
0078                WRITE ( 3, 100) SUMI
                   1  , SU
0079           100    FORMAT ( // ' AREA UNDER THE TWO PHOTON CONTINUM = ', E14.6 ,
                   1 / 5E14.6 )
0080                RETURN
0081           666    II = 1
0082                FYLAM(1) = .3E-26
0083                JY = 2
0084                FYLAM(2) = FYLAM(1)
0085                YYLAM(2) = XLLIM - .0001
0086                YYLAM(1) = XLLIM
0087                XWVL(1) = XLLIM
0088                PL2(1) = ALOG10( FYLAM(1) )
0089                RETURN
0090                END
```

```
0001                SUBROUTINE LAMTOW( X, I )
0002                DIMENSION X(1)
0003                IF ( I .LE. 0 ) RETURN
0004                DO 10 K = 1, I
0005          10      X(K) = ALOG10( 12.4 / X(K) )
0006                RETURN
0007                END
```

```
0001              SUBROUTINE PLTLIN( X1, Y1, XMIN, XDEL, YMIN, YDEL, IELT, ION,
                 1   REFWVL, TRANS )
0002              DIMENSION TRANS(6)
0003              X =       (X1          - XMIN) / XDEL
0004              Y =(Y1         - YMIN) / YDEL
0005              CALL PLOT( X, 0., 3)
0006              CALL PLOT( X, Y, 2)
0007              HLT = .07
0008              CALL SYMBOL( X, Y, HLT, IELT, 90., 4)
0009              YYY = 4.5 * HLT      + Y
0010              CALL NUMBER( X, YYY   , HLT, FLOAT( ION), 90., -1)
0011              CALL NUMBER( X, Y+ 8.*HLT , HLT, REFWVL, 90., 1 )
0012              CALL SYMBOL( X, Y +13.*HLT, HLT, TRANS, 90., 24 )
0013              RETURN
0014              END
```

```
0001                SUBROUTINE INTTMP
0002                COMMON /PL2WVL/ PL2, XWVL
0003                COMMON/ MAONLP/ IDUM, JDUM,NZONH, EDELT, ELTION, IZ, ION
                   1  , OMEGA, F, G , IECODE, IPLOT, REFWVL, IELT,IOUT, IFILL,
                   1   TRANS  , RFWVLO
0004                DIMENSION ELTION(7800)
0005                REAL * 4  NZONH(12)
0006                DIMENSION PL(300), WL(300)
0007                DIMENSION SPL(300), WVLO(300), PLO(300)
0008                DIMENSION     TRANS(6),                          PL2(280), XWVL(280)
0009                DIMENSION EPL(300), DUTUTP(300), ANS(300), WV(300)
0010                EQUIVALENCE(ELTION(1), SPL(1) ), (ELTION(301), WVLO(1) ),
                   1  (ELTION(601), PLO(1) )
                   1  , (ELTION(901), PL(1))  ,(ELTION(1201), WL(1) )
                   1  ,(ELTION(1501),EPL(1)),(ELTION(1801), DUTUTP(1) )
                   1  ,(ELTION(2101), ANS(1) ), (ELTION(2401), WV(1) )
0011                BACKSPACE 8
0012                READ( 8, END=91)
                   1         TO, IJ, (WVLO(I), PLO(I), I=1, IJ)
0013                DO 20 I = 1, IJ
0014                PLO(I) = 10. **PLO(I)
0015          20      SPL(I) =0.
0016          33      CONTINUE
0017                BACKSPACE 8
0018                BACKSPACE 8
0019                READ(8, END=50) T, NUM, (XWVL(I), PL2(I), I=1, NUM)
0020                IF ( T .EQ. TO) GO TO 50
0021                IF ( PL2(1) .GT. PL2(2) ) PL2(1) = PL2(2)
0022                IF ( PL2(1) .GT. PL2(2) ) XWVL(1) = XWVL(2)
0023                DO 30 K= 1, IJ
0024                I = IJ - K + 1
0025                PPP = TRPLIN( WVLO(I), NUM, XWVL, PL2 )
0026          34      PPP = 10. **PPP
0027                  SPL(I) = SPL(I) + (PPP + PLO(I) )*.5 * ABS( T-TO) *
                   1  ((T+ TO)* .5) **(-2.833333)
0028                PLO(I) = PPP
0029                L = I
0030          100     FORMAT ( ' PPP, P, WVLO(I), XWVL(L),  L, I ', 4E13.5, 2I5 )
0031          30       CONTINUE
0032          36      CONTINUE
0033                TO = T
0034                GO TO 33
0035          50        CONTINUE
0036                YDST = 8.
0037                YDEL = 4. / YDST
0038                YMIN = -37.5
0039                J = 0
0040                DO 51 I = 1, IJ
0041                IF ( SPL(I) .LT. 10.**YMIN ) GO TO 51
0042                IF ( SPL(I) .EQ. 0. ) GO TO 51
0043                J = J + 1
0044                WVLO(J) = WVLO(I)
0045                 SPL(J) = ALOG10( SPL(I) )
0046          51    CONTINUE
```

```
0047                IJ = J
0048                XMIN = 0.
0049                XDEL = 2.
0050                XDST = 35.
0051                SPL( IJ+1) = YMIN
0052                SPL( IJ+2 ) = YDEL
0053                CALL AXIS( 0., 0., 'WAVELENGTH',     -10, XDST, 0., XMIN, XDEL)
0054                CALL AXIS( 0., 0.,  'INTEGRAL',8,YDST, 90., SPL(IJ+1), SPL(IJ+2))
0055                WVLO(IJ+1) = XMIN
0056                WVLO(IJ+2) = XDEL
0057                CALL LINE  ( WVLO, SPL , IJ, 1, 0,1 )
0058                REWIND 7
0059                IC = 0
0060          10       CONTINUE
0061                READ(7,END=90)
                   1          SUMINT, IELT, ION, TRANS, REFWVL
0062                IF ( SUMINT .LE. 0.) GO TO 10
0063                IC = IC + 1
0064                PL(IC) = SUMINT
0065                WL(IC) = REFWVL
0066                SUMINT = ALOG10( SUMINT )
0067                IF ( SUMINT .LT. SPL(IJ+1) ) GO TO 10
0068                IF ( SUMINT .GT. SPL(IJ+1) +YDST*SPL(IJ+2) ) SUMINT =
                   1                SPL(IJ+1) +YDST*SPL(IJ+2)
0069                IF ( REFWVL       .GT. XMIN+XDST*XDEL ) GO TO 10
0070                X = REFWVL
0071                CALL PLTLIN( X      , SUMINT, XMIN, XDEL,  SPL(IJ+1), SPL(IJ+2),
                   1  IELT, ION, REFWVL, TRANS )
0072                GO TO 10
0073          90       CONTINUE
0074                CALL PLOT( XDST+1.5, 0., -3 )
0075                CALL PBOX( PL, WL, IC, SPL, WVLO, IJ, ANS, WV, FPL, OUTPTP )
0076                RETURN
0077          91       CONTINUE
0078                PRINT 4,TO, IJ, (WVLO(I), PLO(I), I=1, IJ)
0079          4       FORMAT ( F8.2, I8, /( 10E13.5 ) )
0080                RETURN
0081                END
```

```
0001              SUBROUTINE PBOX( PL, WL, IT, PC, WC, IJ, ANS, WV, EP, DUTUTP )
0002              DIMENSION PL(1), WL(1), PC(1), WC(1), ANS(1), WV(1), EP(1),
                 1  DUTUTP(1)
0003               XLAM = 0.
0004               II = 0
0005               DLAM = .5
0006          53    XLAM = XLAM + DLAM
0007               IF ( XLAM .GT. 70.) GO TO 333
0008               PC1 = TRPLIN( XLAM, IJ, WC, PC )
0009               PC1 = 10 **PC1
0010               XLAM2 = XLAM + DLAM
0011               PC2 = TRPLIN( XLAM2,IJ, WC, PC )
0012               PC2 = 10 **PC2
0013               SUM = 0.
0014               DO 51 I = 1, IT
0015               IF ( WL(I) .LT. XLAM) GO TO 51
0016               IF ( WL(I) .GT. XLAM2)GO TO 52
0017               SUM = SUM + PL(I)
0018          51     CONTINUE
0019          52     CONTINUE
0020               II = II + 1
0021               ANS(II) = (DLAM *(( PC1+PC2) / 2.) + SUM ) / DLAM
0022               ANS(II) = ALOG10( ANS(II) )
0023               WV(II) = XLAM + DLAM / 2.
0024               IF ( IPRINT .EQ. 1 )
                  1PRINT 102, ANS(II), WV(II), XLAM, PC1, XLAM2, PC2, SUM
0025          102      FORMAT ( E14.6, 2F10.2, E14.6, F10.2,2E14.6     )
0026               GO TO 53
0027          333      CONTINUE
                 C   PLOT
0028               CALL PLOTT( WV, ANS, II,  EP, DUTUTP , DLAM )
0029               RETURN
0030               END
```

```
0001                SUBROUTINE PLOTT( E, DUTUT, INUG, EP, DUTUTP , DEL )
0002                DIMENSION E(1), DUTUT(1), DUTUTP(1), EP(1)
0003                CALL SCALE( DUTUT, 9.00, INUG, 1 )
0004                 E(INUG+1) = 0.
0005                 E(INUG+2) = 4.
0006                XL = 18.
0007                CALL AXIS(0.,0., 'WAVELENTH , (A)          ',
                   1                        -24,XL   ,0.,E(INUG+1),E(INUG+2))
0008                CALL AXIS(0.,0., 'LOG( INTEGRAL)',
                   1                         14,9.,90.,DUTUT(INUG+1),DUTUT(INUG+2))
0009                N = 0
0010                DO 9000 I = 1, INUG
0011                N = N + 1
0012                EP (N) = E(I) - DEL / 2.
0013                DUTUTP(N) = DUTUT(I)
0014                N = N + 1
0015                EP (N) = E(I) + DEL / 2.
0016           9000 DUTUTP(N) = DUTUT(I)
0017                DUTUTP (N+1) = DUTUT( INUG+1)
0018                DUTUTP (N+2) = DUTUT( INUG+2)
0019                EP(N+1) =E(INUG+1)
0020                EP(N+2) =E(INUG+2)
0021                CALL LINE( EP, DUTUTP, N, 1, 0, 1, 1 )
0022                RETURN
0023                END
```

```
0001                SUBROUTINE SUMSUB( IT, JI, SUM , T6 )
0002               COMMON/ MAONLP/ IDUM, JDUM,NZONH, EDELT, ELTION, IZ, ION
                  1  , OMEGA, F, G , IECODE, IPLOT, REFWVL, IELT,IOUT, IFILL,
                  1   TRANS  , RFWVLO
0003               COMMON/ ALIEZE/ ALAM, IELTAY, ZETA, NUMCNT, IONAY, NARRAY
0004               INTEGER * 2  IONAY(77), NARRAY(77)
0005               DIMENSION IELTAY(77), ALAM(77), ZETA(77)
0006               DIMENSION ELTION (10,30,26)
0007               REAL * 4  NZONH(12)
0008               DIMENSION TRANS(6)
0009               INTEGER CONVRT
0010               DATA IHE /'  HE' /  , IHHY/'   H'/
0011               SUM = 0.
0012               DO 914  I = 1, NUMCNT
0013               IF ( ALAM(I) .LE. ALAM(JI) ) GO TO 915
0014               IF(IELTAY(I).EQ. IHE ) GO TO 960
0015               IF(IELTAY(I).EQ. IHHY) GO TO 963
0016               GO TO 961
0017          960    CONTINUE
0018               SELTIN = 1.
0019               SNZONH = NZONH(11)
0020               GO TO 962
0021          963     CONTINUE
0022               SELTIN = 1.
0023               SNZONH = 1.
0024               GO TO 962
0025          961    CONTINUE
0026               SNZONH =     NZONH  ( CONVRT (IELTAY(I)) )
0027               SELTIN=        ELTION(CONVRT (IELTAY(I)) , IONAY(I)+1,  IT )
0028               IF ( SELTIN .EQ. 99.) GO TO 914
0029               SELTIN=10.**(- SELTIN )
0030          962     CONTINUE
0031               TEMP2 =           143.89 / (ALAM(I) * T6 )
0032               IF ( TEMP2 .GT. 174.) TEMP2 = 174.
0033               SUM = SUM + EXP( TEMP2 )
                  1  * SELTIN * SNZONH
                  1           * ZETA(I)  *  NARRAY(I)  *(912. / ALAM(I)) **2
0034          914  CONTINUE
0035          915     CONTINUE
0036               RETURN
0037               END
```

```
C
C   FILGEN
C
C   THIS PROGRAM CALCULATES X-RAY FILTER TRANSMISSIONS FOR 3-60 ANGS.
C
0001          DIMENSION FILNAM(35),IATNUM(10),DENSTY(10),THICK(10),NEG(10,70)
0002          DIMENSION IATNO(10),NCDS(10),WVLHE(10,70),ABSCOF(10,70)
0003          DIMENSION IAT(10), THK(10), DEN(10), HEAD(10)
0004          DOUBLE PRECISION HEAD, HEADER
C
C   READ HENKE'S ELEMENT CARDS, WHICH LIST X/RAY MASS ABSORPTIONS AT EACH
C    WAVELENGTH FOR GIVEN ELEMENTS.
C   999 SIGNALS END OF HENKE'S ELEMENT CARDS.
C
0005          I=1
0006    40    READ 3,IATNO(I),NCDS(I)
0007          IF (IATNO(I) .EQ. 999) GO TO 30
0008          NLP1=NCDS(I)
0009          DO 100 II=1,NLP1
0010    100   READ 1,NEG(I,II),WVLHE(I,II),ABSCOF(I,II)
0011          I=I+1
0012          IELEM=I-1
0013          GO TO 40
C
0014     30     CONTINUE
0015          I = 0
0016    1005     CONTINUE
0017          I = I + 1
C
C   READ INITIAL FILTER CARDS AND INCLUDE THESE CARDS IN EACH SUBSEQUENT FILTER.
C    THERE DO NOT HAVE TO BE ANY INITIAL FILTER CARDS IF DESIRED.
C    A GREEN 999 CARD SIGNALS END OF INITIAL FILTER CARDS.
C
0018          READ 1, IAT(I), THK(I), DEN(I), HEAD(I)
0019          IF ( IAT(I) .EQ. 999) GO TO 1006
0020          GO TO 1005
0021     1006  NUMCD = I -1
0022     1000    CONTINUE
C
C       PUNCH CARDS
C
0023          IPUN=1
0024          READ(1,2, END=1007) (FILNAM(I), I=1, 35)
0025          PRINT 8,(FILNAM(I),I=1,35)
0026          IFIL = 0
0027          I=1
C
C   READ SUBSEQUENT  INPUT FILTER CARDS TO WHICH INITIAL FILTER CARDS MAY BE
C    ADDED.  999 SIGNALS END OF EACH FILTER GROUPING.
C
0028    10    READ 1,IATNUM(I),THICK(I),DENSTY(I) , HEADER
0029          IF (IATNUM(I) .EQ. 999) GO TO 20
0030          PRINT 1111,IATNUM(I),THICK(I),DENSTY(I) , HEADER
0031          I=I+1
```

```
0032              IFIL=I-1
0033              GO TO 10
0034           20   CONTINUE
0035              NCARD=0
0036              IF ( NUMCD .EQ. 0 ) GO TO 1003
0037              DO 1002 JLP = 1, NUMCD
                C
0038              IFIL = IFIL + 1
0039              IATNUM(IFIL) = IAT(JLP)
0040              THICK(IFIL) = THK(JLP)
0041              DENSTY(IFIL) = DEN(JLP)
0042              HEADER = HEAD(JLP)
0043              I = IFIL
0044              PRINT 1,IATNUM(I),THICK(I),DENSTY(I) , HEADER
                C
0045           1002     CONTINUE
0046            1003  CONTINUE
0047              WVL=0.
0048              PRINT 9
0049           45   WVL=WVL+1.
0050              ICONT=0
0051              SUMEXP=0.
0052              DO 200 I=1,IELEM
0053              NLP3=NCDS(I)
0054              DO 300 II=1,NLP3
0055              IF (NEG(I,II) .NE. 0 .AND. WVL .GE. WVLHE(I,II) .AND. WVL-1. .LT.
                 * WVLHE(I,II)) GO TO 50
0056              IF (WVLHE(I,II) .NE. WVL) GO TO 300
0057              ICONT=ICONT+1
0058              DO 400 N=1,IFIL
0059              IF (IATNUM(N) .NE. IATNO(I)) GO TO 400
0060              SUMEXP=SUMEXP+THICK(N)*DENSTY(N)*ABSCOF(I,II)
0061           400  CONTINUE
0062              GO TO 200
0063           50   IF (WVL .EQ. WVLHE(I,II)) ICONT=ICONT+1
0064              IF (NEG(I,II) .NE. 1) GO TO 300
0065              SEXPLO=0.
0066              SEXPHI=0.
0067              DO 500 N=1,IELEM
0068              IF (N .EQ. I) GO TO 500
0069              NLP6=NCDS(N)
0070              DO 600 NN=1,NLP6
0071              NNN=NN-1
0072              IF (WVLHE(I,II) .LE. WVLHE(N,NN) .AND. WVLHE(I,II) .GT. WVLHE(N,
                 *NNN)) GO TO 70
0073              GO TO 600
0074           70   ALPHA=ALOG(ABSCOF(N,NN)/ABSCOF(N,NNN))/(WVLHE(N,NN)-WVLHE(N,NNN))
0075              CONS=ABSCOF(N,NN)/EXP(ALPHA*WVLHE(N,NN))
0076              AC=CONS*EXP(ALPHA*WVLHE(I,II))
0077           600  CONTINUE
0078              DO 700 NN=1,IFIL
0079              IF (IATNO(N) .NE. IATNUM(NN)) GO TO 700
0080              SEXPLO=SEXPLO+AC*THICK(NN)*DENSTY(NN)
0081              SEXPHI=SEXPLO
```

```
0082         700   CONTINUE
0083         500   CONTINUE
0084               III=II+1
0085               DO 800 N=1,IFIL
0086               IF (IATNO(I) .NE. IATNUM(N)) GO TO 800
0087               SEXPLO=SEXPLO+ABSCOF(I,II)*DENSTY(N)*THICK(N)
0088               SEXPHI=SEXPHI+ABSCOF(I,III)*DENSTY(N)*THICK(N)
0089         800   CONTINUE
0090               TRAN=EXP(-SEXPLO)
0091               N=1
0092               PRINT 4,WVLHE(I,II),TRAN,N
0093               IF (IPUN .EQ. 1) PUNCH 5,WVLHE(I,II),TRAN,N
0094               NCARD=NCARD+2
0095               TRAN=EXP(-SEXPHI)
0096               N=2
0097               PRINT 4,WVLHE(I,III),TRAN,N
0098               IF (IPUN .EQ. 1) PUNCH 5,WVLHE(I,III),TRAN,N
0099         300   CONTINUE
0100         200   CONTINUE
0101               IF (ICONT .NE. IELEM) GO TO 60
0102               N=0
0103               TRAN=EXP(-SUMEXP)
0104               PRINT 4,WVL,TRAN,N
0105               NCARD=NCARD+1
0106               IF (IPUN .EQ. 1) PUNCH 5,WVL,TRAN,N
0107               IF (WVL .LT. 59.5) GO TO 45
0108               IF (IPUN .EQ. 1) PUNCH 7,(FILNAM(I),I=1,35),NCARD
0109               GO TO 80
0110         60    PRINT 6,WVL
0111               IF (WVL .LT. 59.5) GO TO 45
0112               IF (IPUN .EQ. 1) PUNCH 7,(FILNAM(I),I=1,35),NCARD
0113         80    CONTINUE
0114         1111   FORMAT( ' ', I3, 2E12.4, 9X, A8 )
0115         1     FORMAT(I3,2E12.4, 9X, A8 )
0116         2     FORMAT(35A2)
0117         3     FORMAT(I3,I7)
0118         4     FORMAT(' ',F7.2,F12.6,I3)
0119         5     FORMAT(2F10.6,I2)
0120         6     FORMAT(' ','INSUFICIENT DATA AT',F7.2)
0121         7     FORMAT(35A2,I5)
0122         8     FORMAT('1',35A2)
0123         9     FORMAT(' ',/////)
0124         1001      CONTINUE
0125               GO TO 1000
0126          1007   CONTINUE
0127               END
```

```
      C
      C   OSOINT
      C
      C   THIS PROGRAM CALCULATES A THEORETICAL FILTERED SOLAR SPECTRUM . IT IS A
      C    MODIFIED VERSION OF TEMPINT, MAKING CALCULATIONS IN COUNTS INSTEAD OF
      C    POWER.
      C
0001            DIMENSION STORET(20)
0002             DIMENSION SPEC(400,2),SPCLIN(400,2),FILNAM(35)
0003            DIMENSION SIMB(6),SIMBL(14),SIMP(35)
0004            DATA END/ 'END'/
0005            DIMENSION WVL2(50), COEF2(50)
               1  ,MEDGE(50) , COEI(100)
0006            COMMON /COMM/ TLOGA,  IP , INTEG
0007            COMMON WVL(100),COEF(100),NEDGE(100),NCDS
0008            CALL PLOTS
0009            CALL PLOT(0.0,-.5, 3)
0010            ISW = 1
0011            I = 0
0012     81      I = I + 1
0013            READ 987, STORET(I)
      C
      C READ TEMPERATURES    999 SIGNALS THE END OF TEMPERATURES.   IF THERE ARE NO
      C    TEMPERATURE CARDS IT IS ASSUMED THAT ALL TEMPERATURES ARE REQUESTED : LOG T
      C     = 5.8 TO LOG T = 8.0.
      C
0014     987    FORMAT(F20.2)
0015            IF ( STORET(I) .EQ. 999. ) GO TO 80
0016            GO TO 81
0017     80     NUMTP = I -1
0018            IF ( NUMTP .EQ. 0 ) ISW = 2
0019            IF ( NUMTP .EQ. 0 ) NUMTP = 23
0020            READ(1,3333) SIMB
      C  X AXIS LABEL
0021     3333   FORMAT(6A4)
0022            READ(1,4444) SIMBL
      C    Y AXIS LABEL
0023     4444   FORMAT(14A4)
0024     30     READ 2,(FILNAM(I),I=1,17),NCDS
0025     2      FORMAT(17A4, 2X, I5 )
0026            PRINT 5,(FILNAM(I),I=1,17),NCDS
0027     5      FORMAT('0',///,17A4,I10)
0028            IF ( NCDS .EQ. 9999) GO TO 51
0029            DO 100 I=1,NCDS
      C
      C   READ FIRST FILTER . AS MANY FILTERS MAY BE INSERTED AS DESIRED  WITH
      C    AN END CARD FOLLOWING EACH ONE UNLESS THERE ARE TWO FILTERS TO
      C      BE MULTIPLIED TOGETHER.
      C
0030            READ 3,WVL(I),COEF(I),NEDGE(I)
0031            PRINT 3,WVL(I),COEF(I),NEDGE(I)
0032     3      FORMAT(2F10.6,I2)
0033     100    CONTINUE
0034            NCDS=NCDS-1
```

```
0035              READ 74, DUM1, DUM2, DUMMY
0036              IF ( DUMMY .EQ. END) GO TO 71
0037              I = 1
0038           72  READ 74, WVL2(I),COEF2(I), DUMMY
                  1  ,MEDGE(I)
               C
               C   READS ANOTHER FILTER WHICH WILL BE MULTIPLIED BY THE FIRST FILTER AT
               C    EACH WAVELENGTH.  LINEAR INTERPOLATION IS MADE IF WAVELENGTHS OF FIRST AND
               C     SECOND FILTER AREN'T THE SAME.   PUT AN END CARD AFTER THIS FILTER.
               C
0039              PRINT 74, WVL2(I),COEF2(I), DUMMY
                  1  ,MEDGE(I)
0040           74  FORMAT ( 2F10.4, A3, I1 )
0041              IF ( DUMMY .EQ. END ) GO TO 73
0042              I = I + 1
0043              GO TO 72
0044           73   ISV = I - 1
0045              NCDS1 = NCDS + 1
0046              DO 75 I = 1, NCDS1
0047              Y = TRPLIN( WVL(I), ISV, WVL2, COEF2 )
0048                COEI(I) = COEF(I) * Y
0049              PRINT 3,WVL(I),COEI(I),NEDGE(I)
0050           75    CONTINUE
0051              J = NCDS1
0052              DO 76 I = 1, ISV
0053              IF ( MEDGE(I) .EQ. 0 ) GO TO 76
0054              Y = TRPLIN( WVL2(I), NCDS1, WVL, COEF )
0055              J = J + 1
0056              COEI(J) = Y * COEF2(I)
0057              NEDGE(J) = MEDGE(I)
0058              WVL(J) = WVL2(I)
0059              PRINT 3,WVL(J),COEI(J),NEDGE(J)
0060           76   CONTINUE
0061              NCDS = J -1
0062               CALL SORTP( J, WVL, COEI, NEDGE )
0063              DO 77 I = 1, J
0064              COEF(I) = COEI(I)
0065           77 PRINT 3,WVL(I),COEF(I),NEDGE(I)
0066           71    CONTINUE
               C
               C   READS A TEMPERATURE AND PERFORMS CALCULATIONS FOR ALL WAVELENGTHS
               C    BEFORE RETURNING FOR NEXT TEMPERATURE IN SEQUENCE.
               C
0067              READ(11) XMRK,TLOG
0068              DO 500 ITCY = 1, NUMTP
0069              TLOGT = STORET(ITCY)
0070              IF (ISW .EQ.  2)  TLOG = TLOGT
0071              IF ( ABS(TLOGT-TLOG) .LT. .00001 ) GO TO 989
0072           986  CONTINUE
0073              READ(11) XMRK,TLOG
0074              IF ( XMRK . NE. 9999. ) GO TO 986
0075              IF ( ABS(TLOGT-TLOG) .LT. .00001 ) GO TO 989
0076              GO TO 986
0077           989   CONTINUE
```

```
0078          10    NSPEC=0
0079          20    NSPEC=NSPEC+1
0080                READ(11, END=51) SPEC(NSPEC,1), SPEC(NSPEC,2)
0081                IF (SPEC(NSPEC,2) .GE. 0.) GO TO 20
0082                SPCLIN(1,1)=SPEC(NSPEC,1)
0083                SPCLIN(1,2)=SPEC(NSPEC,2)
0084                 NSPEC=NSPEC-1
0085                NLIN=1
0086          60    NLIN=NLIN+1
0087                READ(11) SPCLIN(NLIN,1),SPCLIN(NLIN,2)
0088                IF (SPCLIN(NLIN,1) .NE. 9999.) GO TO 60
0089                 TLOG=SPCLIN(NLIN,2)-.1
0090                NLIN=NLIN-1
0091                TLOGA = TLOG
0092                PRINT 1,TLOG
0093          1     FORMAT('1','LOG T=',F5.2)
0094                TLOG = TLOG + .1
0095          988     CONTINUE
0096                PRINT 4
0097          4     FORMAT('0',//,' WAVELENGTH',5X,'FILTERED SPECTRUM', T39,
                   1   ' TRANS.', T52, 'INPUT SPECTRUM')
              C
              C   CALCULATES FILTERED POWER IN 0.2 ANGS WAVELENGTH BINS.
              C
0098                 IP = 0
0099                FILIN=0.
0100                FILI =0.
0101                WAVEL=1.
0102                II=0
0103          40    WAVEL=WAVEL+0.2
0104                II=II+1
0105                DO 200 III=1,NCDS
0106                IF (NEDGE(III) .NE. 1) GO TO 200
0107                IF (WVL(III) .GE. WAVEL .OR. WVL(III) .LE. WAVEL-.2) GO TO 200
0108                WSAVE=WAVEL
0109                WAVEL=.5*(WAVEL-.2+WVL(III))
0110                VAL=VALIN(WAVEL)
0111                FUNVAL=VAL*SPEC(II,2)*((WVL(III)-WSAVE+.2)/.2)
0112                FUNVA =1. *SPEC(II,2)*((WVL(III)-WSAVE+.2)/.2)
              C
              C   FUNVAL IS THE CALCULATED BIN POWER FOR THE FILTERED SPECTRUM. FUNVA IS
              C    THE CALCULATED BIN POWER OF THE INPUT SPECTRUM.
              C
0113                 CALL FLIN (SPCLIN,NLIN,WVL(III),WSAVE-.2,FUNVAL)
0114                 CALL FLINO(SPCLIN,NLIN,WVL(III),WSAVE-.2,FUNVA )
0115                 WAVEL=.5*(WVL(III)+WSAVE)
0116                 III=III+1
0117                 VAL=VALIN(WAVEL)
0118                  FUNVAL=FUNVAL+VAL*SPEC(II,2)*((WSAVE-WVL(III))/.2)
0119                  FUNVA =FUNVA +1. *SPEC(II,2)*((WSAVE-WVL(III))/.2)
0120                  CALL FLIN (SPCLIN,NLIN,WSAVE,WVL(III),FUNVAL)
0121                  CALL FLINO(SPCLIN,NLIN,WSAVE,WVL(III),FUNVA )
              C
              C   CONVERTS FILTERED POWER TO COUNTS FOR EACH WAVELENGTH BIN.
```

```
C
      WAL = WAVEL * 1E-8
      FUNVAL = FUNVAL *(WAL/((6.6256E-27)*(2.997925E10)))
      WAVEL = WAL * 1E8
      PRINT 6,WSAVE,FUNVAL,VAL
     1 , FUNVA
      CALL PLTSPT( WSAVE, FUNVAL )
      FILI =FILI +FUNVA
      FILIN=FILIN+FUNVAL
      WAVEL=WSAVE
      GO TO 50
200   CONTINUE
C
C   CALCULATES FILTERED POWER ACROSS ABSORPTION EDGES.
C
      VAL=0.
      WAVEL=WAVEL-0.1
      DO 300 III=1,NCDS
      N=III+1
      IF (WAVEL .GT. WVL(III) .AND. WAVEL .LE. WVL(N))
     * VAL=VALIN(WAVEL)
300   CONTINUE
      WAVEL=WAVEL+0.1
      FUNVAL=VAL*SPEC(II,2)
      FUNVA =1. *SPEC(II,2)
       CALL FLIN (SPCLIN,NLIN,WAVEL,WAVEL-.2,FUNVAL)
       CALL FLINO(SPCLIN,NLIN,WAVEL,WAVEL-.2,FUNVA )
      WAL = WAVEL * 1E-8
      FUNVAL = FUNVAL *(WAL/((6.6256E-27)*(2.997925E10)))
      WAVEL = WAL * 1E8
      PRINT 6,WAVEL,FUNVAL,VAL
     1 , FUNVA
      CALL PLTSPT( WAVEL, FUNVAL )
 6      FORMAT ( F8.2, 9X, E13.6, 7X, F8.6, 7X, E13.6)
      FILIN=FILIN+FUNVAL
      FILI =FILI +FUNVA
50    IF (WAVEL .LT. 69.9) GO TO 40
      INTEG = ALOG10( FILIN )
      CALL       PLOTT(                    SIMB, SIMBL, FILNAM )
      PRINT 7,FILIN   , FILI
7     FORMAT('0','FILTERED SPECTRUM INTEGRAL(3-60A)=',E13.6 /
     1       '0','   INPUT SPECTRUM INTEGRAL(0-70A)=',E13.6 )
 500    CONTINUE
      REWIND 11
      GO TO 30
 51     CONTINUE
      CALL PLOT(15.0,0.0,999)
      END
```

```
0001                FUNCTION VALIN (WAVEL)
                C
                C   THIS SUBROUTINE CALCULATES THE FILTER TRANSMISSION BY A LOG INTERPOLATION
                C    BETWEEN INPUT POINTS.
                C
0002                COMMON WVL(100),COEF(100),NEDGE(100),NCDS
0003                 DO 100 I=1,NCDS
0004                II=I+1
0005                 IF (WAVEL .GT. WVL(I) .AND. WAVEL .LE. WVL(II)) GO TO 10
0006          100   CONTINUE
0007          30    VALIN=0.
0008                RETURN
0009          10    I=II-1
0010                IF (COEF(I) .GT. .0001 .AND. COEF(II) .GT. .0001) GO TO 20
              C**** IF (COEF(I) .LE. .0001 .AND. COEF(II) .LE. .0001) GO TO 30
0011                VALIN=COEF(I)*((WAVEL-WVL(I))/(WVL(II)-WVL(I)))*(COEF(II)
                   *-COEF(I))
0012                 RETURN
0013          20    ALPHA=ALOG(COEF(I)/COEF(II))/(WVL(I)-WVL(II))
0014                CONS=COEF(I)/EXP(ALPHA*WVL(I))
0015                VALIN=CONS*EXP(ALPHA*WAVEL)
0016                 RETURN
0017                END
```

```
0001                SUBROUTINE FLIN (SPCLIN,NLIN,WLHI,WLLO,FUNVAL)
                C
                C   THIS SUBROUTINE USES THE FILTER TRANSMISSION FROM VALIN TO CALCULATE THE
                C    BIN POWER CONTRIBUTED BY LINES AND ADDS IT TO EACH BIN'S TOTAL POWER
                C
0002                 DIMENSION SPCLIN(400,2)
0003                DO 100 I=1,NLIN
0004                 IF (SPCLIN(I,1) .GT. WLLO .AND. SPCLIN(I,1) .LE. WLHI)
                    *FUNVAL=FUNVAL+VALIN(SPCLIN(I,1))*(10.**SPCLIN(I,2))
0005            100  CONTINUE
0006                 RETURN
0007                 END
```

```
FORTRAN IV G LEVEL  19                  FLINO               DATE = 71142          04/33/02

0001                  SUBROUTINE FLINO(SPCLIN,NLIN,WLHI,WLLO,FUNVAL)
                C
                C    THIS SUBROUTINE ADDS THE BIN POWER CONTRIBUTED BY LINES TO EACH BIN'S
                C     TOTAL POWER.
                C
0002                   DIMENSION SPCLIN(400,2)
0003                  DO 100 I=1,NLIN
0004                   IF (SPCLIN(I,1) .GT. WLLO .AND. SPCLIN(I,1) .LE. WLHI)
                      *FUNVAL=FUNVAL+ 1.                *(10.**SPCLIN(I,2))
0005            100   CONTINUE
0006                  RETURN
0007                   END
```

```
0001                SUBROUTINE PLOTT(                    SIMB, SIMBL, SIMP )
                C
                C   THIS SUBROUTINE PLOTS FILTERED COUNTS VS WAVELENGTH FOR EACH
                C    TEMPERATURE ON THE CALCOMP PLOTTER.
                C
                C  SIMB IS X AXIS LABEL    SIMBL IS Y AXIS LABEL   SIMP IS A LABEL
0002                DIMENSION IBUF(1000),ELLM(300),QJEN(300),DUTUT(400)
0003                DIMENSION DATUM (10)
0004                DIMENSION SIMB(6),SIMBL(14),SIMP(35),ESUM(350),E(400)
0005                DIMENSION DUTUTP(800),EP(800)     , LABEL(12)
0006                COMMON /COMM/ TEMP, IP , INTEG
0007                DATA BLANK /'    '/
0008                PI=3.1415927
0009                YMIN = INTEG - 5
0010                DUTUT(INUG+1) = YMIN
0011                DUTUT(INUG+2) = .5
0012                 E(INUG+1) = 0.
0013                 E(INUG+2) = 4.
0014                CALL SYMBOL( 1., 9., .12, 'LOG(T)=', 0., 7)
0015                CALL NUMBER(1.96, 9., .12, TEMP, 0., 1)
0016                CALL SYMBOL(1.,8.5,.1,SIMP,0.,68)
0017                XL = 18.
0018                CALL AXIS(0.,0.,SIMB,-23,XL   ,0.,E(INUG+1),E(INUG+2))
0019                CALL AXIS(0.,0.,SIMBL,56,9.,90.,DUTUT(INUG+1),DUTUT(INUG+2))
0020                CALL AXIS( 0., 10., BLANK, -4, XL, 0., E(INUG+1), E(INUG+2))
0021                EP(1) = E(1)
0022                IF ( DUTUT(1) .LT. YMIN) DUTUT(1) = YMIN
0023                DUTUTP(1) = DUTUT(1)
0024                N = 1
0025                DO 9000 I = 2, INUG
0026                IF ( DUTUT(I) .LT. YMIN) DUTUT(I) = YMIN
0027                IF ( E(I) - E(I-1) .LT. .25 ) GO TO 9001
0028                N = N + 1
0029                EP(N) = E(I-1)
0030                DUTUTP(N)=YMIN
0031                N = N + 1
0032                EP(N) = E(I) - .2
0033                DUTUTP(N)=YMIN
0034          9001   CONTINUE
0035                N = N + 1
0036                EP (N) = E(I)      - .2
0037                DUTUTP(N) = DUTUT(I)
0038                N = N + 1
0039                EP (N) = E(I)
0040                DUTUTP(N) = DUTUT(I)
0041          9000   CONTINUE
0042                DUTUTP (N+1) = DUTUT( INUG+1)
0043                DUTUTP (N+2) = DUTUT( INUG+2)
0044                EP(N+1) =E(INUG+1)
0045                EP(N+2) =E(INUG+2)
0046                CALL LINE( EP, DUTUTP, N, 1, 0, 1, 1 )
0047                CALL PLOT ( XL + 1.5, 0., -3 )
0048                RETURN
0049                ENTRY PLTSPT( WSAVE, FUNVAL )
```